united nations
educational, scientific
and cultural
organization

international atomic
energy agency

the
abdus salam
international centre for theoretical physics

H4.SMR/1228-10

"Workshop on Correlation Effects in
Electronic Structure Calculations"

12 - 23 June 2000

Introduction to Dynamical Mean-Field Theory

A. Georges

C.N.R.S. - Laboratoire de Physique Theorique
L"Ecole Normale Superieure
Paris
France

Dynamical mean-field theory of strongly correlated fermion systems and the limit of infinite dimensions

Antoine Georges

Laboratoire de Physique Théorique de l'Ecole Normale Supérieure, 24, rue Lhomond, 75231 Paris Cedex 05, France

Gabriel Kotliar

Serin Physics Laboratory, Rutgers University, Piscataway, New Jersey 08854

Werner Krauth and Marcelo J. Rozenberg

Laboratoire de Physique Statistique de l'Ecole Normale Supérieure, 24, rue Lhomond, 75231 Paris Cedex 05, France

We review the dynamical mean-field theory of strongly correlated electron systems which is based on a mapping of lattice models onto quantum impurity models subject to a self-consistency condition. This mapping is exact for models of correlated electrons in the limit of large lattice coordination (or infinite spatial dimensions). It extends the standard mean-field construction from classical statistical mechanics to quantum problems. We discuss the physical ideas underlying this theory and its mathematical derivation. Various analytic and numerical techniques that have been developed recently in order to analyze and solve the dynamical mean-field equations are reviewed and compared to each other. The method can be used for the determination of phase diagrams (by comparing the stability of various types of long-range order), and the calculation of thermodynamic properties, one-particle Green's functions, and response functions. We review in detail the recent progress in understanding the Hubbard model and the Mott metal-insulator transition within this approach, including some comparison to experiments on three-dimensional transition-metal oxides. We present an overview of the rapidly developing field of applications of this method to other systems. The present limitations of the approach, and possible extensions of the formalism are finally discussed. Computer programs for the numerical implementation of this method are also provided with this article.

CONTENTS

 0034-6861/96/68(1)/13(113)/$23.95

I. INTRODUCTION

The discovery of the heavy fermion compounds and of the high-temperature superconductors has revived interest in strongly correlated electron systems. These are systems in which the strength of the electron-electron interactions is comparable to or larger than the kinetic energy. The investigation of this class of systems goe back to the early 1960s. The main motivations at th time came from experiments on transition metal oxides from the Mott metal-insulator transition, and from th problem of itinerant ferromagnetism.

Theoretical progress in the field has been impede however by the extreme difficulty of dealing with eve the simplest model Hamiltonians appropriate for thes systems, such as the Hubbard model and the Kondo lat tice model. Only in the one-dimensional case do w have a variety of theoretical tools at our disposal t study these models in a systematic manner. For two- an three-dimensional models, one is often unable to asses confidently whether a given physical phenomenon is in deed captured by the idealized Hamiltonian under con sideration or whether a theoretical prediction reflects true feature of this Hamiltonian, rather than an artifac of the approximation used in its solution. These difficul ties originate in the nonperturbative nature of the prob lem, and reflect the presence of several competing physi cal mechanisms for even the simplest models. Th interplay of localization and lattice coherence, of quan tum and spatial fluctuations, and of various competin types of long-range order are important examples.

Numerous approximation schemes have been em ployed to circumvent these difficulties, but many theo rists in the field have learned to consider with caution those approximations (such as arbitrary resummation of some class of diagrams) that are not based on som *controlled limit*, by which we mean that some extrem limit of the model is considered (often after some gen eralization) wherein the problem simplifies and can b solved in a controlled manner. The reason to favor thes approaches is not that of out-of-place mathematica rigor, but rather that it is often easier to identify whic of the physical aspects of the problem will be privilege by a specific limit, and thus to choose that specific limi best adapted to the physical phenomenon under consid eration. In favorable cases, the physical ingredients tha have been left out can be reintroduced by expandin around this starting point. Of course the dramatic in crease in computational power has also stimulated a di rect numerical solution of these models using exact di agonalization and quantum Monte Carlo methods, a recently reviewed by Dagotto (1994). However, the ex act diagonalization technique is limited by the exponen tial growth of the computations with system size, whil the quantum Monte Carlo method is restricted to rathe high temperatures by the minus-sign problem. Despit the interest of these numerical studies, these limitation have often prevented the extraction of reliable low energy information. Until these limitations are ove come, analytic tools remain essential for the study of th strong correlation problem.

This article reviews a new approach to the problem c strong correlations that has been developed over recer years and has led to some progress in our understandin of these systems. The essential idea is to replace a *lattic* model by a *single-site* quantum impurity problem em bedded in an effective medium determined *self*

consistently. The impurity model offers an intuitive picture of the local dynamics of a quantum many-body system. Also, a large number of techniques developed over a thirty-year period of intensive study of impurity models are available. The self-consistency condition captures the translation invariance and coherence effects of the lattice. We refer to this approach as the *local impurity self-consistent approximation* (LISA) in this article.

The LISA is the natural generalization of quantum many-body problems of the Weiss mean-field theory familiar from classical statistical mechanics. The term "mean-field theory" should be taken with caution however: the present approach *does not* assume that *all* fluctuations are frozen (this would lead to the Hartree-Fock approximation). Rather, it freezes spatial fluctuations but takes full account of *local* quantum fluctuations (i.e., of temporal fluctuations between the possible quantum states at a given lattice site). Hence the LISA method is best characterized as a "dynamical mean-field theory." The main difference with the classical case is that the on-site quantum problem remains a many-body problem (which nevertheless can be addressed with a variety of techniques).

As in classical statistical mechanics, this dynamical mean-field theory becomes *exact* in the limit of large spatial dimensions $d \to \infty$, or more appropriately in the limit of large lattice coordination (note that the coordination z is already quite large for several three-dimensional lattices: $z=6$ for a cubic lattice, $z=12$ for a face-centered-cubic lattice). This ensures the internal consistency of the approach and establishes $1/z$ as a control parameter. Indeed, it is the pioneering work of Metzner and Vollhardt (1989) on the limit of large dimensions for strongly correlated fermion models that triggered the developments leading to the LISA method in the form reviewed here. However, this approach may be viewed in a broader context, as a starting point for the investigation of many *finite-dimensional* strongly correlated systems, in the same sense that the Weiss mean-field theory is the starting point of most investigations in the classical statistical mechanics of three-dimensional systems. In particular, the method can be used as an approximation to more realistic models of actual materials, taking into account several orbitals, and specific lattice structure and density of states, as obtained, e.g., from local density approximation (LDA) calculations (cf. Sec. VIII.C). Calculations along these lines are only beginning to appear.

This article is a self-contained introduction to the LISA approach, which has only partly the character of a review. It contains (a) a discussion of the general theoretical formalism and several derivations of the dynamical mean-field equations, (b) a description of the algorithms which are useful for their solution, (c) source codes of computer programs implementing these algorithms, (d) a thorough discussion of analytic techniques developed to analyze the dynamical mean-field equations, and (e) several examples of physical problems to which the LISA approach has been successfully applied. Our hope is that making this package widely available will allow many workers to contribute in applying these techniques to the countless number of open problems in the field of strongly correlated electrons. With this idea in mind, we have indicated some possible directions for further research and pointed out the aspects of the formalism which need further improvement.

Several authors contributed in recent years to the emergence of the LISA approach in its present form starting with the pioneering work of Metzner and Vollhardt (1989). These authors pointed out the scaling of the hopping amplitude that leads to a nontrivial limit of infinite spatial dimensions for lattice models of correlated fermions. More importantly, they recognized the potential usefulness of this limit by demonstrating the local nature of perturbation theory in $d=\infty$. Müller Hartmann (1989a, 1989b, 1989c) also proved the locality of many-body Green's function perturbation theory and used it in order to derive self-consistent equations for the self-energy in terms of the (generally unknown) Luttinger-Ward functional, which he evaluated to various orders in weak-coupling perturbation theory. Following this work, self-consistent functional equations were derived and solved for the Falicov-Kimball model by Brandt and Mielsch (1989, 1990, 1991; see also, Janiš 1991). These authors also pointed out how these equations could be formally extended to the Hubbard model. A mean-field interpretation of these equations was given for the Falicov-Kimball model by van Dongen and Vollhardt (1990). This interpretation is quite different from the LISA ideas however. Functional equations for the Green's function and the self-energy of the Hubbard model in infinite dimensions were derived by Janiš (1991) following the dynamical coherent potential approximation analogy, but, in this formulation, these functional equations did not lend themselves to explicit calculations.

Further progress was made possible by the realization (Ohkawa 1991a, 1991b; Georges and Kotliar, 1992) that the functional equations can be interpreted as an Anderson impurity model subject to a self-consistent bath: this is the main content of the LISA approach [see also the subsequent work of Jarrell (1992)]. In the work of Georges and Kotliar (1992), a precise correspondence with the classical mean-field theory, and the proper identification of the quantum analog of the Weiss effective field, was carried out. This allowed an immediate extension of the LISA method to phases with broken symmetry and to a large number of models of strongly correlated electrons (Georges, Kotliar, and Si, 1992). Using general properties on the single-impurity Anderson model in conjunction with the self-consistency condition Georges and Kotliar (1992) also established that the metallic phase of the $d=\infty$ Hubbard model is a Fermi liquid for arbitrary doping and interaction strength. An important lesson of that work is that reliable techniques for treating the Anderson impurity model can be used to study correlated electrons in large dimensions. For example, the perturbative approach of Yosida and Yamada (1970, 1975) can be turned into an efficient "iterated perturbation theory" scheme in the LISA context

(Georges and Kotliar, 1992). Another example is the noncrossing approximation method first applied in the LISA context by Jarrell and Pruschke (1993a, 1993b) and Pruschke, Cox, and Jarrell (1993a, 1993b).

Many numerical methods have been recently implemented for the solution of the dynamical mean-field equations. The quantum Monte Carlo algorithm of Hirsch and Fye (1986) was first applied to this problem independently by Jarrell (1992), Rozenberg, Zhang, and Kotliar (1992), and Georges and Krauth (1992). Two different exact diagonalization algorithms were later introduced by Caffarel and Krauth (1994) and by Si *et al.* (1994). The Wilson numerical renormalization group approach to the single-impurity problem has been recently applied to the $d=\infty$ Hubbard model by Sakai and Kuramoto (1994) and Shimizu and Sakai (1995), and a projective renormalization method using in an essential way the self-consistency condition has been recently introduced by Moeller *et al.* (1995). One of the major applications of these methods and of the LISA approach has been the study of the Mott transition in the half-filled Hubbard model (Rozenberg, Zhang, and Kotliar, 1992; Georges and Krauth, 1992, 1993; Pruschke, Cox, and Jarrell, 1993a, 1993b; Zhang, Rozenberg, and Kotliar, 1993; Caffarel and Krauth, 1994; Laloux, Georges, and Krauth, 1994; Rozenberg, Kotliar, and Zhang, 1994; Rozenberg, Moeller and Kotliar, 1994; Moeller *et al.*, 1995). The important lesson learned from these studies is that no single technique stands out as the most appropriate, but a thorough understanding of the many-body phenomena associated with this problem required a combination of various numerical methods and of analytical approximations.

Having reviewed the recent history of the LISA approach, it is interesting to mention that early related ideas can be traced back in the literature, starting with the papers of Hubbard (1964, 1979) and Wang, Evenson, and Schrieffer (1969). Impurity models (without a self-consistent embedding) have been used to model the photoemission spectra of correlated solids for a long time (Zaanen and Sawatzky, 1987, 1990; Fujimori, Minami, and Sugano, 1984). The LISA method also has some relationship with the dynamical coherent potential approximation method for random alloys: indeed, a functional integral approach reduces the quantum many-body problem to averaging a free-particle problem over external fields with random variations in space and time (for recent work along those lines, see Turov and Grebenikov, 1988; Kakehashi, 1992). In this context, Schwartz and Siggia (1972) first recognized the importance of the inverse coordination number as the small parameter justifying the coherent potential approximation. In fact, the LISA equations first appeared in the literature as early as 1987, in the context of the periodic Anderson model, in an interesting but little known paper of Kuramoto and Watanabe (1987) that also emphasized the limit of large lattice coordination. Finally, the assumption of local vertices has sometimes been used as a simplifying hypothesis in many-body perturbation theory calculations (see, e.g., Treglia, Ducastelle, and Spanjaard, 1980).

The LISA dynamical mean-field approach can be compared and contrasted to other frequently used approximation schemes for lattice models of correlated fermions. In the Hartree-Fock approximation, the starting point is a mean-field theory in which *all* fluctuations, both spatial and temporal, are frozen. Fluctuations can then be treated by making random phase approximation expansions around the static and uniform saddle point. Local quantum fluctuations, however, are often nonperturbative in character (being associated, like in the Kondo problem, with tunneling events between degenerate minima), so that such expansions do not capture them correctly. The purpose of the dynamical mean-field approach is to privilege these fluctuations, by treating them from the beginning in a nonperturbative manner. Another type of approximation is based on the controlled limit of extending the spin symmetry from SU(2) to SU(N) (or some other group) and considering the large N limit (see, e.g., Newns and Read, 1987; Kotliar, 1993a, 1994 for reviews). These approaches make use of some auxiliary degrees of freedom (e.g., slave bosons) to describe the enlarged Hilbert space. The saddle point which holds at $N=\infty$ generally replaces the problem with a gas of renormalized quasiparticles. High-energy incoherent excitations are completely absent at the saddle-point level, and must be reintroduced by expanding in $1/N$. In contrast, the LISA dynamical mean-field theory treats the local aspects of both quasiparticles and incoherent high-energy excitations on the same footing. This is crucial for calculating thermodynamic properties or when considering systems having no characteristic low-energy scale. The limit of large lattice coordination is also a natural playground where one can test the different numerical techniques used in the treatment of the many-body problem in finite dimensions, without dealing with the additional complications of lattices of finite size (the thermodynamic limit is built in from the beginning in this approach).

The general organization of this article is as follows (see the Table of Contents). Section II gives a general overview of the method (without any formal justification), and introduces the reader to the dynamical mean-field equations, to the mapping onto a self-consistent impurity model, and to the connection with the limit of infinite dimensions. Sections III to V set up the theoretical framework: various useful derivations are presented in Sec. III, the calculation of response functions is considered in Sec. IV, and the extension of the formalism to phases with long-range order is described in Sec. V. Section VI reviews the various techniques available to solve the self-consistent impurity problem, including a detailed discussion and comparison of various numerical methods. This section has a deliberately technical character: the goal here is to provide sufficient information so that the reader can use these methods independently. To this aim, FORTRAN programs are provided with this article (accessible via the internet, see Appendix D).

The numerous possible applications of the dynamical mean-field approach to physical systems are only beginning to be explored, and the field is currently very active. We have chosen to discuss in detail only one of these applications. This is the purpose of Sec. VII, which reviews the recent progress made on the Hubbard model and the Mott metal-insulator transition. The LISA method has solved many open questions related to this phenomenon, which had proven intractable by previous techniques. Recently, concrete applications to the physics of transition-metal oxides have also appeared. Comparison to some experiments can be found in this section. In Sec. VIII, several other strongly correlated models are considered and a much less exhaustive approach is adopted. In each case, the associated impurity model and the self-consistency equations are given in order to illustrate the wide scope of the method, and a short summary of recent results obtained for these models is made. The purpose of this section is simply to provide a guide to the literature and to stimulate further work.

The dynamical mean-field method discussed in this paper can be applied as an approximation scheme directly to three-dimensional lattice problems (this is also true of the usual mean-field theory of classical spin systems). We have provided several derivations of the mean-field equations which, besides showing that they become exact in infinite dimensions, are aimed to give them an intuitive content. This approach is advocated throughout this article, and particularly in Sec. VIII.C. For this reason, this article is restricted to those aspects of the $d=\infty$ limit that are closely related to the idea of a dynamical mean-field approach and omitted (or briefly mentioned) other applications of this limit, such as the studies of variational wave functions in the $d\rightarrow\infty$ limit. Excellent expositions of these omitted topics already exist, and we refer the reader to the review articles of Vollhardt (1991, 1993, 1994). Earlier reviews of some of the topics treated in the present paper can be found in Kotliar (1993b), Freericks and Jarrell (1994b), and Pruschke, Jarrell, and Freericks (1995).

Finally, Sec. IX stresses the limitations of the mean-field approach in its present form and explores possible extensions of the formalism to systems where the dynamical effects of intersite interactions, the influence of long-wavelength collective modes, or certain forms of short-range order are important. This is currently one of the main theoretical challenges in the field, and the main role of Sec. IX is to outline what we perceive to be fruitful directions for further research.

II. THE LOCAL IMPURITY SELF-CONSISTENT APPROXIMATION: AN OVERVIEW

This section is devoted to a survey of the LISA method. We shall first describe the dynamical mean-field equations but, for the sake of clarity, will postpone detailed derivations to Sec. III. In order to stress the analogy with the familiar Weiss mean-field theory of classical statistical mechanics, we shall review in parallel the classical case and its quantum generalization. The connection with quantum impurity models will be explained in Sec. II.B. In Sec. II.C, the limit of infinite spatial dimensions of lattice fermion models will be presented. The dynamical mean-field equations become exact in this limit.

A. Dynamical mean-field equations

The goal of a mean-field theory is to approximate a lattice problem with many degrees of freedom by a *single-site effective problem* with less degrees of freedom. The underlying physical idea is that the dynamics at a given site can be thought of as the interaction of the degrees of freedom at this site with an external bath created by all other degrees of freedom on other sites.

The simplest illustration of this idea is the Ising model with ferromagnetic couplings $J_{ij}>0$ between nearest-neighbor sites of a lattice with coordination z:

$$H=-\sum_{\langle ij\rangle} J_{ij}S_iS_j-h\sum_i S_i. \tag{1}$$

The Weiss mean-field theory views each given site (say, o) as governed by an effective Hamiltonian:

$$H_{\rm eff}=-h_{\rm eff}S_o. \tag{2}$$

All interactions with the other degrees of freedom are lumped into the effective field $h_{\rm eff}$:

$$h_{\rm eff}=h+\sum_i J_{oi}m_i=h+zJm, \tag{3}$$

where $m_i=\langle S_i\rangle$ is the magnetization at site i, and translation invariance has been assumed ($J_{ij}=J$ for nearest-neighbor sites, $m_i=m$). Hence $h_{\rm eff}$ has been related to a local quantity which can in turn be computed from the single-site effective model $H_{\rm eff}$. For the simple case at hand, this reads $m=\tanh(\beta h_{\rm eff})$, which can be combined with (3) to yield the well-known mean-field equation for the magnetization:

$$m=\tanh(\beta h+z\beta Jm). \tag{4}$$

These mean-field equations are, in general, an approximation of the true solution of the Ising model. They become *exact* however in the limit where the *coordination of the lattice becomes large.* It is quite intuitive indeed that the neighbors of a given site can be treated globally as an external bath when their number becomes large, and that the spatial fluctuations of the local field become negligible. As is clear from Eq. (3), the coupling J must be scaled as $J=J^*/z$ to yield a sensible limit $z\rightarrow\infty$ (this scaling is such that both the entropy and internal energy per site remain finite, so as to maintain a finite T_c).

These ideas can be directly extended to quantum many-body systems. This will be illustrated here on the example of the Hubbard model:

$$H=-\sum_{\langle ij\rangle,\sigma} t_{ij}(c^+_{i\sigma}c_{j\sigma}+c^+_{j\sigma}c_{i\sigma})+U\sum_i n_{i\uparrow}n_{i\downarrow}. \tag{5}$$

It will be assumed in this section, for simplicity, that no symmetry breaking occurs, i.e., that one deals with the translation-invariant paramagnetic phase. Phases with long-range order will be dealt with in Sec. V.

Again, the mean-field description associates with this Hamiltonian a single-site effective dynamics, which is conveniently described in terms of an imaginary-time action for the fermionic degrees of freedom $(c_{o\sigma}, c^{+}_{o\sigma})$ at that site:

$$S_{\rm eff} = -\int_0^\beta d\tau \int_0^\beta d\tau' \sum_\sigma c^{+}_{o\sigma}(\tau)\mathcal{G}_0^{-1}(\tau-\tau')c_{o\sigma}(\tau') + U\int_0^\beta d\tau\, n_{o\uparrow}(\tau)n_{o\downarrow}(\tau). \quad (6)$$

$\mathcal{G}_0(\tau-\tau')$ plays the role of the Weiss effective field above. Its physical content is that of an effective amplitude for a fermion to be created on the isolated site at time τ (coming from the "external bath") and being destroyed at time τ' (going back to the bath). The main difference with the classical case is that this generalized "Weiss function" is a *function of time* instead of a single number. This, of course, is required to take into account *local quantum fluctuations*. Indeed, the mean-field theory presented here freezes spatial fluctuations but takes full account of local temporal fluctuations (hence the name "dynamical"). $\mathcal{G}_0$ plays the role of a bare Green's function for the local effective action $S_{\rm eff}$, but it should not be confused with the noninteracting local Green's function of the original lattice model.

A closed set of mean-field equations is obtained by supplementing Eq. (6) with the expression relating $\mathcal{G}_0$ to local quantities computable from $S_{\rm eff}$ itself, in complete analogy with Eq. (3) above. As will be shown below, this self-consistency condition reads

$$\mathcal{G}_0(i\omega_n)^{-1} = i\omega_n + \mu + G(i\omega_n)^{-1} - R[G(i\omega_n)]. \quad (7)$$

In this expression, $G(i\omega_n)$ denotes the on-site interacting Green's function calculated from the effective action $S_{\rm eff}$:

$$G(\tau-\tau') \equiv -\langle Tc(\tau)c^{+}(\tau')\rangle_{S_{\rm eff}}, \quad (8)$$

$$G(i\omega_n) = \int_0^\beta d\tau\, G(\tau)e^{i\omega_n\tau}, \quad \omega_n \equiv \frac{(2n+1)\pi}{\beta} \quad (9)$$

and $R(G)$ is the reciprocal function of the Hilbert transform of the density of states corresponding to the lattice at hand. Explicitly, given the noninteracting density of states $D(\epsilon)$,

$$D(\epsilon) = \sum_{\mathbf{k}} \delta(\epsilon-\epsilon_{\mathbf{k}}), \quad \epsilon_{\mathbf{k}} \equiv \sum_{ij} t_{ij}e^{i\mathbf{k}\cdot(\mathbf{R}_i-\mathbf{R}_j)}, \quad (10)$$

the Hilbert transform $\tilde{D}(\zeta)$ and its reciprocal function R are defined by

$$\tilde{D}(\zeta) \equiv \int_{-\infty}^{+\infty} d\epsilon \frac{D(\epsilon)}{\zeta-\epsilon}, \quad R[\tilde{D}(\zeta)] = \zeta. \quad (11)$$

Since G can in principle be computed as a functional of $\mathcal{G}_0$ using the impurity action $S_{\rm eff}$, Eqs. (6)–(8) form a closed system of functional equations for the on-site Green's function G and the Weiss function $\mathcal{G}_0$. These are the basic equations of the LISA method. In practice, the main difficulty lies in the solution of $S_{\rm eff}$. These equations can hardly be attributed to a single author, as detailed in the Introduction. They appeared first in an early work of Kuramoto and Watanabe (1987) for the periodic Anderson model. Following the paper of Metzner and Vollhardt (1989) that emphasized the interest of the $d\to\infty$ limit, these equations were obtained by several authors. Brandt and Mielsch (1989) derived and solved them for the Falicov-Kimball model; the case of the Hubbard model was considered by Janiš (1991), Ohkawa (1991a, 1991b), Georges and Kotliar (1992), and Jarrell (1992). The presentation followed here is closest to those of Georges and Kotliar (1992) and Georges, Kotliar, and Si (1992).

It is instructive to check these equations in two simple limits:

(i) In the *noninteracting limit* $U=0$, solving (6) yields $G(i\omega_n)=\mathcal{G}_0(i\omega_n)$ and hence, from (7), $G(i\omega_n) = \tilde{D}(i\omega_n+\mu)$ reduces to the free on-site Green's function.

(ii) In the *atomic limit* $t_{ij}=0$, one only has a collection of disconnected sites and $D(\epsilon)$ becomes a δ function, with $\tilde{D}(\zeta)=1/\zeta$. Then (7) implies $\mathcal{G}_0(i\omega_n)^{-1} = i\omega_n+\mu$ and the effective action $S_{\rm eff}$ becomes essentially local in time and describes a four-state Hamiltonian yielding $G(i\omega_n)_{\rm at} = (1-n/2)/(i\omega_n+\mu) + n/2/(i\omega_n+\mu-U)$, with $n/2 = (e^{\beta\mu}+e^{\beta(2\mu-U)})/(1+2e^{\beta\mu}+e^{\beta(2\mu-U)})$.

Solving the coupled equations above not only yields *local quantities* but also allows us to reconstruct all the **k**-dependent correlation functions of the original lattice Hubbard model. For example, the Fourier transform of the one particle Green's function $G_{ij}(\tau-\tau') \equiv -\langle Tc_{i,\sigma}(\tau)c^{+}_{j,\sigma}(\tau')\rangle$ can be shown to read

$$G(\mathbf{k},i\omega_n) = \frac{1}{i\omega_n+\mu-\epsilon_{\mathbf{k}}-\Sigma(i\omega_n)}, \quad (12$$

where the self-energy can be computed from the solution of the effective on-site problem as

$$\Sigma(i\omega_n) = \mathcal{G}_0^{-1}(i\omega_n) - G^{-1}(i\omega_n). \quad (13$$

It is therefore **k**-independent in this approach i.e., purely local in space: $\Sigma_{ij}(i\omega_n)=\delta_{ij}\Sigma(i\omega_n)$ (Metzner and Vollhardt, 1989, Müller-Hartmann, 1989a, 1989b, 1989c). From this expression one sees that the "self-consistency condition," Eq. (7), relating G and $\mathcal{G}_0$, ensures that the on-site (local) component of the Green's function, given by $G_{ii}(i\omega_n)=\Sigma_{\mathbf{k}}G(\mathbf{k},i\omega_n)$, coincides with the Green function $G(i\omega_n)$ calculated from the effective action $S_{\rm eff}$. Indeed, summing Eq. (12) over **k** yields $\tilde{D}(i\omega_n+\mu-\Sigma(i\omega_n))$. Identifying this expression with $G(i\omega_n)$ and using Eq. (13) leads to Eq. (7).

Thermodynamic quantities for the Hubbard model can all be simply related to their single-site model counterparts: the relevant expressions for the free energy and internal energy are given by Eqs. (46) and (47) in Sec. III.B. Two-particle Green's functions, dynamical response functions, and transport properties for the latti

model can also be related to vertex functions of the on-site action $S_{\rm eff}$; this will be reviewed in Sec. IV.

B. Physical content and connection with impurity models

The structure of the dynamical mean-field theory is that of a functional equation for the local Green's function $G(i\omega_n)$ and the "Weiss function" $\mathcal{G}_0(i\omega_n)$. In contrast to mean-field theory for classical systems, the on-site effective action $S_{\rm eff}$ remains a many-body problem. This is because the present approach freezes *spatial fluctuations* but fully retains local quantum fluctuations. As a function of imaginary time, each site undergoes transitions between the four possible quantum states $|0\rangle$, $|\uparrow\rangle$, $|\downarrow\rangle$, $|\uparrow,\downarrow\rangle$ by exchanging electrons with the rest of the lattice described as an external bath. The dynamics of these processes is encoded in the Weiss function $\mathcal{G}_0(\tau-\tau')$.

For these reasons, no Hamiltonian form involving *only* the on-site degrees of freedom $(c_{o\sigma},c^+_{o\sigma})$ can be found for the effective on-site model: once the bath has been eliminated, $S_{\rm eff}$ necessarily includes retardation effects. In order to gain physical intuition and to make some practical calculations with $S_{\rm eff}$, it is useful to have such a Hamiltonian formulation. This is possible upon reintroducing auxiliary degrees of freedom describing the "bath." For example, one can view $(c_{o\sigma},c^+_{o\sigma})$ as an "impurity orbital" and the bath as a "conduction band" described by operators $(a_{l\sigma},a^+_{l\sigma})$ and consider the Hamiltonian

$$H_{\rm AM}=\sum_{l\sigma}\tilde{\epsilon}_l a^+_{l\sigma}a_{l\sigma}+\sum_{l\sigma}V_l(a^+_{l\sigma}c_{o\sigma}+c^+_{o\sigma}a_{l\sigma})$$
$$-\mu\sum_{\sigma}c^+_{o\sigma}c_{o\sigma}+Un_{o\uparrow}n_{o\downarrow}, \tag{14}$$

where the subscript AM denotes the Anderson model. This Hamiltonian is quadratic in $a^+_{l\sigma},a_{l\sigma}$; integrating these out gives rise to an action of the form (6), with

$$\mathcal{G}_0^{-1}(i\omega_n)^{\rm AM}=i\omega_n+\mu-\int_{-\infty}^{+\infty}d\omega\,\frac{\Delta(\omega)}{i\omega_n-\omega},$$
$$\Delta(\omega)\equiv\sum_{l\sigma}V_l^2\delta(\omega-\tilde{\epsilon}_l). \tag{15}$$

Hence Eq. (14) can be viewed as a Hamiltonian representation of $S_{\rm eff}$ provided $\Delta(\omega)$ (i.e., the parameters $V_l,\tilde{\epsilon}_l$) is chosen such as to reproduce the actual solution $\mathcal{G}_0$ of the mean-field equations. The spectral representation Eq. (15) is general enough to permit this in all cases. Note that the $\tilde{\epsilon}_l$'s are *effective* parameters that should not be confused with the single-particle energies $\epsilon_{\mathbf{k}}$ of the original lattice model. The Hamiltonian (14) is the familiar Anderson model of a magnetic impurity coupled to a conduction bath (Anderson, 1961). Note however that the shape of the conduction bath density of states $\Delta(\omega)$ is *not* known *a priori* in the present context but must be found by solving the self-consistent problem. The isolated site o plays the role of the impurity orbital, and the conduction bath is built out of all other sites.

There is of course a degree of arbitrariness in the Hamiltonian representation of the local action $S_{\rm eff}$. Instead of viewing it as an Anderson model, we can consider the Wolff model (Wolff, 1961), in which the interaction term acts only at a single-site of a conduction-electron lattice representing the bath

$$H_{\rm WM}=\sum_{l\sigma}\tilde{\epsilon}_l a^+_{l\sigma}a_{l\sigma}+Un_{o\uparrow}n_{o\downarrow}. \tag{16}$$

If we adopt this point of view the Weiss function is given by

$$\mathcal{G}_0^{\rm WM}=\int_{-\infty}^{+\infty}d\omega\,\frac{\Delta(\omega)}{i\omega_n-\omega},\quad \Delta(\omega)\equiv\sum_l\delta(\omega-\tilde{\epsilon}_l), \tag{17}$$

and it merely corresponds to a different spectral representation of $\mathcal{G}_0$.

Hence, the LISA approach to the Hubbard model maps the lattice problem onto that of an Anderson impurity embedded in a self-consistent medium (Ohkawa 1991a, 1991b; Georges and Kotliar, 1992; Georges, Kotliar, and Si, 1992; Jarrell, 1992). The solution of the mean-field equations involves the determination of $\mathcal{G}_0$ such that, when inserted into the Anderson model, the resulting impurity Green's function obeys the self-consistency condition (7).

The reduction of a lattice problem to a single-site problem with *effective* parameters is a common feature to both the classical and quantum mean-field constructions. The two constructions parallel each other quite precisely, as summarized in the "dictionary" displayed in Table I. The main difference is that the Weiss field is a number in the classical case, and a function in the quantum case. Physically, this reflects the existence of *many* energy scales in strongly correlated fermion models. (We note in passing that this also occurs in the mean-field theory of some classical problems with many energy scales, such as spin glasses.) This points to the limitations of other "mean-field" approaches, such as the Hartree-Fock approximation or slave bosons methods, where one attempts to parametrize the whole mean-field function by a single *number* (or a few of them). This in effect amounts to freezing local quantum fluctuations by replacing the problem with a purely classical one, and can only be reasonable when a single low-energy scale is important. This is the case, for instance, for a Fermi-liquid phase. However, even in such cases, parametrizing the Weiss field by a single number can only be satisfactory at low energy, and misses the high-energy incoherent features associated with the other energy scales in the problem. When no characteristic low-energy scale is present, a single number parametrization fails completely: this is the case, for example, when correlation functions have power-law decays as a function of frequency (as in x-ray edge problems). This occurs, e.g., in the Falicov-Kimball model (Sec. VIII.B).

TABLE I. Correspondence between the mean-field theory of a classical system and the (dynamical) mean-field theory of a quantum system.

Quantum case	Classical case	
$-\Sigma_{\langle ij\rangle\sigma} t_{ij} c_{i\sigma}^{+} c_{j\sigma} + U\Sigma_i n_{i\uparrow} n_{i\downarrow}$	$H=-\Sigma_{\langle ij\rangle} J_{ij} S_i S_j - h\Sigma_i S_i$	Hamiltonian
$t_{ij} \sim (1/\sqrt{d})^{\lvert i-j\rvert}$	$J_{ij} \sim (1/d)^{\lvert i-j\rvert}$ (ferromagnet)	Scaling
$G_{ij}(i\omega_n) = -\langle c_i^{+}(i\omega_n) c_j(i\omega_n)\rangle$	$\langle S_i S_j\rangle$	Correlation function
$G_{ii}(i\omega_n) = -\langle c_i^{+}(i\omega_n) c_i(i\omega_n)\rangle$	$m_i = \langle S_i\rangle$	Local observable
$-\int\int c_\sigma^{+}(\tau)\mathcal{G}_0^{-1}(\tau-\tau') c_\sigma(\tau') + \int U n_\uparrow n_\downarrow$ $H_{\text{eff}} = \Sigma_{l\sigma}\tilde{\epsilon}_l a_{l\sigma}^{+} a_{l\sigma} + \Sigma_{l\sigma} V_l (a_{l\sigma}^{+} c_\sigma + \text{H.c.})$ $-\mu\Sigma_\sigma c_\sigma^{+} c_\sigma + U n_\uparrow n_\downarrow$	$H_{\text{eff}} = -h_{\text{eff}} S_0$	Single-site Hamiltonian
$\mathcal{G}_0(i\omega_n)$	h_{eff}	Weiss field/function
$\mathcal{G}_0^{-1}(i\omega_n) = \omega_n + \mu + G(i\omega_n)^{-1} - R[G(i\omega_n)]$	$h_{\text{eff}} = z\ J\ m + h$	Relation between Weiss field and local observable

Finally, besides its intuitive appeal, the mapping onto impurity models has proven to be useful for practical calculations. These models have been studied intensively in the last 30 years by a variety of analytical and numerical techniques, and this knowledge can be put to good use in order to understand strongly correlated lattice models in large dimensions. The crucial step is to use *reliable* tools to solve S_{eff}. Recent progress in the field came from an effort in exploiting the connection with impurity models in a qualitative and quantitative manner.

C. The limit of infinite dimensions

The above mean-field equations become exact in the limit of infinite coordination on various lattices. In this section, we discuss several such examples and in each case we give the relation (7) between the local Green's function and the Weiss function $\mathcal{G}_0$ in explicit form. Notice that, in the paramagnetic phase, the lattice enters the mean-field equations only through the noninteracting density of states $D(\epsilon)$. Since many different lattices give rise to the same density of states in the limit of large coordination, one can construct models with the same single-particle properties (i.e., the same Green's function) in the paramagnetic phases but very different properties regarding magnetic responses and transitions to phases with long-range order (Müller-Hartmann, 1989a). We refer to Sec. IV and Appendix A for a more detailed explanation of this point, and to Sec. VII.D for explicit examples.

The first case to be discussed is the d-dimensional cubic lattice with nearest-neighbor hopping (with coordination $z=2d$). In order that the kinetic and interaction energies remain of the same order of magnitude in the $d\to\infty$ limit, the hopping amplitude must be scaled appropriately (Metzner and Vollhardt, 1989). The correct scaling is easily found from the Fourier transform $\epsilon_{\mathbf{k}}$ of t_{ij}, which for a generic vector $\mathbf{k}$ involves $\Sigma_{n=1}^{d}\cos(k_n)$, a sum of d numbers with essentially random signs. Hence t_{ij} must be scaled as

$$t_{ij} = \frac{t}{\sqrt{2d}}. \tag{18}$$

More precisely, this ensures that the density of states has a well-defined $d\to\infty$ limiting form, which reads (from the central-limit theorem)

$$D(\epsilon) = \frac{1}{t\sqrt{2\pi}} \exp\left(-\frac{\epsilon^2}{2t^2}\right). \tag{19}$$

This expression, and various useful properties of tight-binding electrons on a $d\to\infty$ cubic lattice, is derived in Appendix A. The Hilbert transform of (19) reads (for $t=1/\sqrt{2}$):

$$\tilde{D}(\zeta) = -is\sqrt{\pi}\,\exp(-\zeta^2)\,\text{erfc}(-is\zeta), \tag{20}$$

where $s=\text{sgn}[\text{Im}(\zeta)]$ and erfc denotes the complementary complex error function. There is no simple explicit form for the reciprocal function $R(G)$ in this case and hence (7) must be used as an implicit relation between $\mathcal{G}_0$ and G. The Gaussian density of states (19) is also obtained for the $d\to\infty$ cubic lattice with longer-range hopping along the *coordinate axis*. As discussed by Müller-Hartmann (1989a) and reviewed in Appendix A, next-nearest-neighbor hopping along the *diagonals* does change the density of states and provides an interesting $d=\infty$ model in which magnetic order is frustrated.

A second important example is the Bethe lattice (Cayley tree) with coordination $z\to\infty$ and nearest-neighbor hopping $t_{ij}=t/\sqrt{z}$. A semicircular density of states is obtained in this case (see, e.g., Economou, 1983):

$$D(\epsilon) = \frac{1}{2\pi t^2}\sqrt{4t^2-\epsilon^2}, \quad |\epsilon|<2t. \tag{21}$$

The Hilbert transform and its reciprocal function take very simple forms

$$\tilde{D}(\zeta) = (\zeta - s\sqrt{\zeta^2-4t^2})/2t^2, \quad R(G) = t^2 G + 1/G \tag{22}$$

so that the self-consistency relation between the Weiss function and the local Green's function takes in this case the explicit form

$$\mathcal{G}_0^{-1}(i\omega_n)=i\omega_n+\mu-t^2G(i\omega_n). \tag{23}$$

The same density of states is also realized for a random Hubbard model on a fully connected lattice (all N sites pairwise connected) where the hoppings are independent random variables with variance $\overline{t_{ij}^2}=t^2/N$ (see Sec. VII).

Finally, the Lorentzian density of states

$$D(\epsilon)=\frac{t}{\pi(\epsilon^2+t^2)} \tag{24}$$

can be realized with a t_{ij} matrix involving long-range hopping (Georges, Kotliar, and Si, 1992). One possibility is to take $\epsilon_{\mathbf{k}}=t/d\sum_{i=1}^{d}\tan(k_i)\mathrm{sgn}(k_i)$ for the Fourier transform of t_{ij} on a d-dimensional lattice, with either $d=1$ or $d=\infty$. Because of the power-law tails of the density of states, this model needs a regularization to be properly defined. If one introduces a cutoff in the tails, which is like the bottom of a Fermi sea, then a $1/d$ expansion becomes well defined. Some quantities like the total energy are infinite if one removes the cutoff. Other low-energy quantities, like the difference between the energy at finite temperatures and at zero temperature, the specific heat, and the magnetic susceptibility have a finite limit when the cutoff is removed. The Hilbert transform of (24) reads $\tilde{D}(\zeta)=1/\{\zeta+it\ \mathrm{sgn}[\mathrm{Im}(\zeta)]\}$. Using this in (7), one sees that a drastic simplification arises in this model: the Weiss function no longer depends on G, and reads explicitly

$$\mathcal{G}_0(i\omega_n)^{-1}=i\omega_n+\mu+it\ \mathrm{sgn}\omega_n. \tag{25}$$

Hence the mean-field equations are no longer coupled, and the problem reduces to solving S_{eff} with (25). It turns out that (25) is precisely the form for which S_{eff} becomes solvable by Bethe ansatz, and thus many properties of this $d\to\infty$ lattice model with long-range hopping and a Lorentzian density of states can be solved for analytically (Georges, Kotliar, and Si, 1992). Some of its physical properties are nongeneric however (such as the absence of a Mott transition).

Other lattices can be considered, such as the $d=\infty$ generalization of the two-dimensional honeycomb and three-dimensional diamond lattices considered by Santoro *et al.* (1993), and are briefly reviewed in Appendix A. This lattice is bipartite but has no perfect nesting.

III. DERIVATIONS OF THE DYNAMICAL MEAN-FIELD EQUATIONS

In this section, we provide several derivations of the mean-field equations introduced above. In most instances, the simplest way to guess the correct equations for a given model with on-site interactions is to postulate that the self-energy can be computed from a single-site effective action involving (i) the original interactions and (ii) an arbitrary retarded quadratic term. The self-consistency equation is then obtained by writing that the interacting Green's function of this single-site action coincides with the site-diagonal Green's function of the lattice model, with identical self-energies. The derivations presented below prove the validity of this construction in the limit of large dimensions.

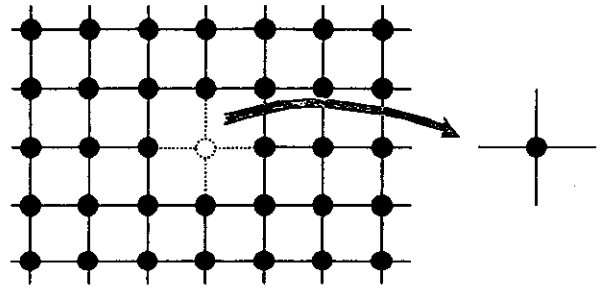

FIG. 1. Cavity created in the full lattice by removing a single site and its adjacent bonds.

A. The cavity method

The first derivation that we shall present is borrowed from classical statistical mechanics, where it is known under the name of "cavity method." It is not the first one that has historically been used in the present context, but it is both simply and easily generalized to several models. The underlying idea is to focus on a given site of the lattice, say $i=0$, and to explicitly integrate out the degrees of freedom on all other lattice sites in order to define an effective dynamics for the selected site.

Let us first illustrate this on the Ising model. The effective Hamiltonian H_{eff} for site o is defined from the partial trace over all other spins:

$$\sum_{S_i,i\neq o} e^{-\beta H}\equiv e^{-\beta H_{\mathrm{eff}}[S_o]}. \tag{26}$$

The Hamiltonian H in Eq. (1) can be split into three terms: $H=-h_oS_o-\Sigma_iJ_{io}S_oS_i+H^{(o)}$. $H^{(o)}$ is the Ising Hamiltonian for the lattice in which site o has been removed together with all the bonds connecting o to other sites, i.e., a "cavity" surrounding o has been created (Fig. 1). The first term acts at site o only, while the second term connects o to other sites. In this term, $J_{io}S_o\equiv\eta_i$ plays the role of a field acting on site i. Hence summing over the S_i's produces the generating functional of the connected correlation functions of the cavity Hamiltonian $H^{(o)}$ and a formal expression for H_{eff} can be obtained as

$$H_{\mathrm{eff}}=\mathrm{const}+\sum_{n=1}^{\infty}\sum_{i_1\cdots i_n}\frac{1}{n!}\eta_{i_1}\cdots\eta_{i_n}\langle S_{i_1}\cdots S_{i_n}\rangle_c^{(o)} \tag{27}$$

For a ferromagnetic system, with $J_{ij}>0$ scaled as $1/d^{|i-j|}$ ($|i-j|$ is the Manhattan distance between i and j), only the first ($n=1$) term survives in this expression in the $d\to\infty$ limit. Hence H_{eff} reduces to $H_{\mathrm{eff}}=-h_{\mathrm{eff}}S_o$, where the effective field reads

$$h_{\mathrm{eff}}=h+\sum_i J_{oi}\langle S_i\rangle^{(o)}. \tag{28}$$

$\langle S_i\rangle^{(o)}$ is the magnetization at site i once site o has been removed. The limit of large coordination brings in a fur-

ther simplification to this expression: because each site has of the order of d neighbors, removing a single site produces an effect of order $1/d$ in local quantities, which can be neglected. Hence the magnetization $\langle S_i\rangle^{(o)}$ calculated for the cavity Hamiltonian equals the magnetization $\langle S_i\rangle$ for the full Hamiltonian. Furthermore, translation invariance implies $\langle S_i\rangle=\langle S_o\rangle\equiv m$, so that $h_{\rm eff}=h+zJm$. On the other hand, the single-site effective Hamiltonian $H_{\rm eff}$ is easily solved to yield $m=\tanh\beta h_{\rm eff}$. Hence, a closed set of mean-field equations is found.

Let us mention that the relation between the magnetizations with and without the cavity is more involved for Ising models with nonuniform signs of J_{ij}. For spin-glass models with $J_{ij}=+1,-1$ at random, one is forced to scale the couplings as $1/\sqrt{d}$ so that a correction term must be retained in the difference $\langle S_i\rangle-\langle S_i\rangle^{(o)}$ (Thouless, Anderson, and Palmer, 1977; see also Mezard, Parisi, and Virasoro, 1987). This correction term, first discovered by Onsager (1936) in his studies on dielectrics, accounts for local-field effects created by the removal of one site ("reaction terms").

This derivation extends in a straightforward manner to quantum many-body models. It is convenient to write the partition function of the Hubbard model (5) as a functional integral over Grassmann variables:

$$Z=\int\prod_i Dc_{i\sigma}^{+}Dc_{i\sigma}e^{-S}, \tag{29}$$

$$S=\int_o^\beta d\tau\left(\sum_{i\sigma}c_{i\sigma}^{+}\partial_\tau c_{i\sigma}-\sum_{ij,\sigma}t_{ij}c_{i\sigma}^{+}c_{j\sigma}-\mu\sum_{i\sigma}c_{i\sigma}^{+}c_{i\sigma}+U\sum_i n_{i\uparrow}n_{i\downarrow}\right). \tag{30}$$

We follow closely the Ising analogy: all fermions are traced out except for site o in order to obtain an effective action:

$$\frac{1}{Z_{\rm eff}}e^{-S_{\rm eff}[c_{o\sigma}^{+},c_{o\sigma}]}\equiv\frac{1}{Z}\int\prod_{i\neq o,\sigma}Dc_{i\sigma}^{+}Dc_{i\sigma}e^{-S}. \tag{31}$$

Note that the knowledge of $S_{\rm eff}$ allows us to calculate *all the local* correlation functions of the original Hubbard model, since we can couple sources to degrees of freedom at site o. This observation is valid in any number of dimensions. In order to obtain a formal expression for $S_{\rm eff}$, the original action is again split into three parts: $S=S^{(o)}+S_o+\Delta S$, where $S^{(o)}$ is the lattice action in the presence of the "cavity," and

$$S_o=\int_0^\beta d\tau\left(\sum_\sigma c_{o\sigma}^{+}(\partial_\tau-\mu)c_{o\sigma}+Un_{o\uparrow}n_{o\downarrow}\right), \tag{32}$$

$$\Delta S=-\int_0^\beta d\tau\sum_{i\sigma}t_{io}(c_{i\sigma}^{+}c_{o\sigma}+c_{o\sigma}^{+}c_{i\sigma}). \tag{33}$$

Again, $\eta_i\equiv t_{io}c_{o\sigma}$ plays the role of a source coupled to $c_{i\sigma}^{+}$, and the integration over fermions for $i\neq o$ brings in the generating functional of the connected Green's functions $G^{(o)}$ of the cavity Hamiltonian:

$$S_{\rm eff}=\sum_{n=1}^{\infty}\sum_{i_1\cdots j_n}\int\eta_{i_1}^{+}(\tau_{i_1})\cdots\eta_{i_n}^{+}(\tau_{i_n})\eta_{j_1}(\tau_{j_1})\times\cdots\eta_{j_n}(\tau_{j_n})G^{(o)}_{i_1\cdots j_n}(\tau_{i_1}\cdots\tau_{i_n},\tau_{j_1}\cdots\tau_{j_n})+S_o+\text{const.} \tag{34}$$

As before, the large d limit (with a scaling $1/\sqrt{d}^{|i-j|}$ of the hopping t_{ij}) brings in a crucial simplification: the nth order term is of order $(1/d)^{n-2}$ so that only $n=2$ survives the $d\to\infty$ limit. This is easily seen by considering the first few terms. The scaling of t_{ij} ensures that $G_{ij}^{(o)}\sim(1/\sqrt{d})^{|i-j|}$ and so the first term is of order 1. The second-order term involves a connected four-point function $G_{ijkl}^{(o)}$ which falls off as $(1/\sqrt{d})^{|i-j|}(1/\sqrt{d})^{|i-k|}(1/\sqrt{d})^{|i-l|}$. When i,j,k,l are all different, there are four sums which give d^4 and four factors of t giving $1/d^2$. The net result is, since $|i-j|$, $|i-l|$, and $|i-k|$ are at least 2, of order $1/d$. Similarly, the terms where $i=j$ (distinct from k and l with $k\neq l$) contain three sums, which give d^3, four factors of t giving $1/d^2$, and a factor $1/d^2$ from $G^{(o)}$ since $|i-l|$ and $|k-i|$ are at least two. The result is again of order $1/d$. The effective action therefore reduces to Eq. (6) as $d\to\infty$, with

$$\mathcal{G}_0^{-1}(i\omega_n)=i\omega_n+\mu-\sum_{ij}t_{oi}t_{oj}G_{ij}^{(o)}(i\omega_n). \tag{35}$$

Expression (35) is important because it relates the Weiss function $\mathcal{G}_0$ to the Green's function $G_{ij}^{(o)}$ of a Hubbard model *with one site removed*. In order to obtain a closed set of equations, one still needs to relate the latter to the Green's function of the original lattice. Again, the $d\to\infty$ limit makes this possible here, but this relation takes, in general, a slightly more complicated form than for the classical Ising case discussed above. On the Bethe lattice, however, it remains very simple. In this case, the summation in (35) can be restricted to $i=j$ (since neighbors of o are completely disconnected on this lattice once the cavity has been introduced), and again, in the limit of infinite connectivity, removing one site does not change the Green's function so that $G_{ii}^{(o)}=G_{ii}$. Using translation invariance, one finally obtains Eq. (23) for the Weiss function on this lattice: $\mathcal{G}_0^{-1}=i\omega_n+\mu-t^2G(i\omega_n)$.

For a general lattice, the relation between the cavity and full Green's functions reads

$$G_{ij}^{(o)}=G_{ij}-\frac{G_{io}G_{oj}}{G_{oo}}. \tag{36}$$

This equation is most easily proven by using the expansion of Green's functions in the hopping matrix elements t_{kl}, which is described in Sec. III.C. First, we note that the additional paths contributing to G_{ij} and not to $G_{ij}^{(o)}$ are those which connect sites i and j through site o. Then, one observes that, in the $d=\infty$ limit, only those paths that go *once* through site o need to be considered. This is true provided we allow an arbitrary dressing of each site in a path by the irreducible cumulant M_1 defined in Sec. III.C. Because of this property, the contri-

bution of these additional paths is obviously proportional to $G_{io}G_{oj}$, but this quantity has to be divided by G_{oo} in order to count *only once* the contribution of paths leaving and returning to the intermediate site o. Interestingly, Eq. (36), which is essential to the whole formalism, already appears in early works of Hubbard himself: this is Eq. (36) of the so-called "Hubbard III" paper (Hubbard, 1964).

Inserting (36) into (35) we have to compute $\Sigma_{ij}t_{io}t_{jo}G_{ij}-(\Sigma_i t_{io}G_{io})^2/G_{oo}$. To proceed, let us use Fourier transforms and insert the form (12) of the lattice Green's function, assuming a local self-energy (this has to be justified independently by power counting in $1/d$). The above expression reads

$$\int_{-\infty}^{+\infty} d\epsilon D(\epsilon)\frac{\epsilon^2}{\zeta-\epsilon} - \left(\int_{-\infty}^{+\infty} d\epsilon D(\epsilon)\frac{\epsilon}{\zeta-\epsilon}\right)^2 \Bigg/ \int_{-\infty}^{+\infty} d\epsilon D(\epsilon)\frac{1}{\zeta-\epsilon}$$

with $\zeta \equiv i\omega_n+\mu-\Sigma(i\omega_n)$. This can be simplified further using the following relations:

$$\int_{-\infty}^{+\infty}\frac{D(\epsilon)\epsilon^2}{\zeta-\epsilon}=\zeta\int_{-\infty}^{+\infty}\frac{D(\epsilon)\epsilon}{\zeta-\epsilon},$$

$$\int_{-\infty}^{+\infty}\frac{D(\epsilon)}{\zeta-\epsilon}\epsilon=-1+\zeta\int_{-\infty}^{+\infty}\frac{D(\epsilon)}{\zeta-\epsilon}. \tag{37}$$

We have used $t_{oo}=\Sigma_{\mathbf{k}}t_{\mathbf{k}}=\int D(\epsilon)\epsilon=0$. Finally, inserting (36) into (35) yields

$$\mathcal{G}_0^{-1}=\Sigma+1/\tilde{D}(i\omega_n+\mu-\Sigma), \tag{38}$$

which coincides with (7) and (13).

B. Local nature of perturbation theory in infinite dimensions

From a historical perspective, the notion that in infinite dimensions the local Green's function obeys a closed set of functional equations was derived by various authors from considerations on perturbation theory in the interaction strength U.

Indeed, remarkable simplifications in the many-body diagrammatics occur in this limit, as first noticed by Metzner and Vollhardt (1989; see also Metzner, 1989; Müller-Hartmann, 1989a). Consider a given diagram (Fig. 2), in which the interaction term $Un_{i\uparrow}n_{i\downarrow}$ is depicted as a four-leg vertex at site i, and in which each line stands for a free-fermion propagator between two sites (it is easier to proceed in real space). The crucial observation is that whenever two internal vertices (i,j) can be connected by at least three paths, they must correspond to identical sites $i=j$. This property is of course only true for $d=\infty$, and can be shown by simple power counting. Since the hopping has been scaled by $1/\sqrt{d}$, each path made of fermion propagators connecting i to j will involve at least a factor $(1/\sqrt{d})^{|i-j|}$. On the other hand, i being held fixed, the eventual summation to be performed on the internal vertex j will bring in a factor

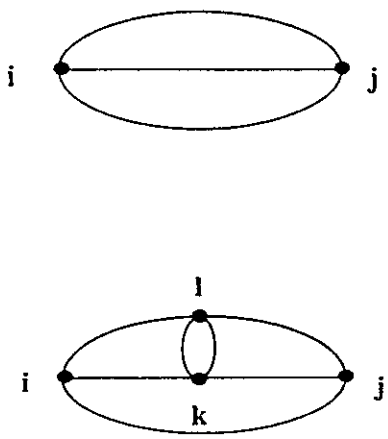

FIG. 2. Example of diagrams contributing to the self-energy at second and fourth order which can be "collapsed" to a single site.

of order d^R. Indeed, this is the number of sites j located at a (Manhattan) distance $|i-j|\equiv R$ from i (R can be summed over afterwards). Hence, one obtains an overall factor of $d^R(1/\sqrt{d})^{R\mathcal{P}_{ij}}$ where $\mathcal{P}_{ij}$ is the number of (independent) paths joining i to j in the diagram. Thus, if $\mathcal{P}_{ij}>2$, only those contributions with $i=j$ ($R=0$) will survive the $d\to\infty$ limit. (Notice that this argument compares the contribution with $i=j$ to that with $i\neq j$, for a given value of the external vertices of the Green's function). Alternatively, in the perhaps more familiar momentum-space formulation of perturbation theory, this property means that whenever two vertices can be "collapsed" according to the rule above, the fermion propagators $G^{(0)}(\mathbf{k},i\omega_n)$ connecting them can be replaced by their local, $\mathbf{k}$-independent counterpart $\Sigma_k G^{(0)}(\mathbf{k},i\omega_n)$, ignoring momentum conservation at the vertices. Frequency conservation is retained however as $d\to\infty$. Figure 2 illustrates these considerations with two diagrams contributing to the self-energy at second and fourth orders.

This simplification of weak-coupling expansions is of course very useful in practice, since evaluating momentum sums is the main practical obstacle in going to high orders. In fact, discarding momentum conservation at some vertices has sometimes been used in perturbative calculations as a simplifying "local approximation" (see, e.g., Treglia, Ducastelle, and Spanjaard, 1980). The $d=\infty$ limit provides a framework in which this approximation can be justified. Various authors have exploited this simplification to perform weak-coupling studies of various models much beyond what is commonly feasible if one attempts to perform Brillouin-zone summations. Müller-Hartmann (1989b, 1989c) and Menge and Müller-Hartmann (1991) have studied self-consistent perturbation theory schemes for the Hubbard model. Similar schemes were applied to the periodic Anderson model by Schweitzer and Czycholl (1989, 1990a, 1991b). Schweitzer and Czycholl (1990b, 1991a) also used the $d=\infty$ simplifications in order to facilitate the weak-coupling studies of *finite-dimensional* models. The main idea is to

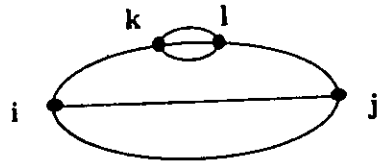

FIG. 3. Example of a diagram that cannot be "collapsed" to a single-site, because only two independent paths connect site i to site k (or j to l). Note that this is not a skeleton diagram, since it contains a correction to the ij propagator.

perform a summation over successive shells of neighbors in real space, rather than momentum summations.

Besides this practical use, these properties of perturbation theory in $d=\infty$ can also be used to formally derive the dynamical mean-field equations. Consider the real-space self-energy $\Sigma_{ij}(i\omega_n)$. It is clear that not all diagrams of a standard weak-coupling expansion for this quantity can be fully collapsed to a local form. An example of a diagram which cannot be collapsed is provided by Fig. 3. We can consider making, however, a "skeleton" expansion of Σ rather than a direct expansion: this amounts to grouping together all corrections to internal propagators, so that all lines of a skeleton diagram stand for the full *interacting* fermion propagator G_{ij}. The diagrams in Fig. 2 are skeleton diagrams, but the one in Fig. 3 is not. In this way, the self-energy can be viewed as a functional of the interacting Green's functions:

$$\Sigma_{ij}=\Sigma_{ij}^{\text{skel}}[\{G_{kl}\}]. \tag{39}$$

It is easily seen that two internal vertices of a *skeleton* diagram can always be connected by more than two paths, so that all diagrams contributing to Σ in a skeleton perturbation expansion can be fully collapsed to a single-site. More generally, this is true of the Luttinger-Ward free-energy functional $\Phi[\{G_{ij}\}]$, which is the sum of all vacuum-to-vacuum skeleton graphs (Fig. 4). This functional is such that (see, e.g., Abrikosov *et al.*, 1965):

$$\Sigma_{ij}(i\omega_n)=\frac{\delta\Phi}{\delta G_{ij}(i\omega_n)}. \tag{40}$$

Hence, as $d\to\infty$, Φ and $\Sigma_{ij}^{\text{skel}}$ depend *only* on the local (site-diagonal) Green's functions G_{ii}:

$$\Phi=\sum_i \phi[G_{ii}], \quad d\to\infty, \tag{41}$$

in which ϕ is a functional of the local Green's function at site i *only*. An obvious consequence is that the self-energy is site diagonal:

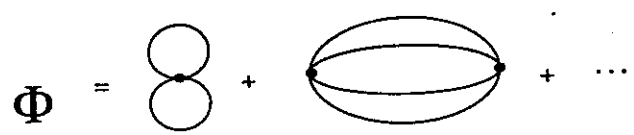

FIG. 4. First two contributions to the Luttinger-Ward functional.

$$\Sigma_{ij}(i\omega_n)=\delta_{ij}\Sigma(i\omega_n). \tag{42}$$

Furthermore, it must be possible to generate the functionals $\phi[G]$ and $\Sigma^{\text{skel}}[G]$ from a purely local theory. A simple inspection of Feynman rules shows that the effective action S_{eff} in Eq. (6) precisely achieves this goal. From this point of view, the Weiss function $\mathcal{G}_0$ just plays the role of a dummy variable which never enters the final forms of ϕ, Σ^{skel}. Once these functionals are known, the actual *value* of Σ is found by writing that the local lattice Green's function is given by $\Sigma_{\mathbf{k}}G(\mathbf{k},i\omega_n)$, namely:

$$G(i\omega_n)=\int_{-\infty}^{+\infty} d\epsilon\,\frac{D(\epsilon)}{i\omega_n-\epsilon-\Sigma^{\text{skel}}[G(i\omega_n)]}. \tag{43}$$

This should be viewed as a functional equation for $G(i\omega_n)$, which is of course equivalent to the self-consistency condition (7). This point of view is formally useful to prove reduction to a single-site problem, but is not practical because of the difficulty in handling skeleton functionals. In fact, it has been so far impossible to obtain exact or even approximate expressions of Σ^{skel} for the Hubbard model, which would give reasonable results when inserted in (43), except for very small U. A remarkable case for which $\Sigma^{\text{skel}}[G]$ can be obtained in closed form is the Falicov-Kimball model (Sec. VIII.B), which is exactly solvable as $d\to\infty$ (Brandt and Mielsch, 1989–1991). For most models, it is much more useful in practice to think of all quantities as *functionals* of $\mathcal{G}_0$ and to promote the latter to the rank of a fundamental quantity which has a clear physical interpretation as a "Weiss function" (Georges and Kotliar, 1992).

This formalism is also useful for establishing the relation between the lattice and the impurity model free-energies, Ω and Ω_{imp} (Brandt and Mielsch, 1991). Indeed, Ω is related to the Luttinger-Ward functional Φ by (see, e.g., Abrikosov *et al.*, 1965):

$$\Omega=\Phi+T\sum_{n,\mathbf{k},\sigma}[\ln G_\sigma(\mathbf{k},i\omega_n)-\Sigma_\sigma(i\omega_n)G_\sigma(\mathbf{k},i\omega_n)], \tag{44}$$

while, for the impurity model (6),

$$\Omega_{\text{imp}}=\phi[G]+T\sum_{n\sigma}[\ln G_\sigma(i\omega_n)-\Sigma_\sigma(i\omega_n)G_\sigma(i\omega_n)]. \tag{45}$$

Eliminating the functional Φ between these two equations [using Eq. (41)], and taking into account translation invariance, one obtains the following expression for the free-energy:

$$\frac{\Omega}{N}=\Omega_{\text{imp}}-T\sum_{n\sigma}\left(\int_{-\infty}^{+\infty}d\epsilon\,D(\epsilon)\right.$$
$$\left.\times\ln[i\omega_n+\mu-\Sigma_\sigma(i\omega_n)-\epsilon]+\ln G_\sigma(i\omega_n)\right), \tag{46}$$

Note also that the internal energy can be expressed terms of local quantities only (see, e.g., Fetter and W lecka, 1971):

$$\frac{E}{N}=T\sum_{n,\sigma}\int_{-\infty}^{+\infty}d\epsilon\,\frac{\epsilon D(\epsilon)}{i\omega_n+\mu-\Sigma_\sigma(i\omega_n)-\epsilon}$$
$$+\frac{1}{2}T\sum_{n,\sigma}\Sigma_\sigma(i\omega_n)G_\sigma(i\omega_n). \quad (47)$$

C. Derivation based on an expansion around the atomic limit

In this section we derive the LISA equations on the basis of an expansion around the atomic limit. This is more than an academic exercise since a successful resummation of the atomic expansion has long been sought, starting with the pioneering work of Hubbard (1964). It is reassuring to see that a systematic analysis of this expansion leads one back to the LISA equations.

This section builds upon early work of Metzner (1991; see also, Hülsenbeck and Stephan, 1994). For any spatial dimension, one can write a general expansion of the free energy and the correlation functions in terms of hopping matrix elements t_{ij} and bare cumulants c_r^0 which are local in space but nonlocal in time. The bare cumulants are defined by

$$c_r^0(\tau_1\cdots\tau_r\ \tau_1'\cdots\tau_r')=\frac{\delta\ln Z_{\rm at}}{\delta\bar\eta(\tau_1)\cdots\delta\bar\eta(\tau_r)\delta\eta(\tau_1')\cdots\delta\eta(\tau_r')},$$

in which $Z_{\rm at}$ is the partition function in the atomic limit,

$$Z_{\rm at}[\eta,\bar\eta]=\int dc^+dc\ e^{-\int_0^\beta\mathcal{L}_{\rm at}+\int_0^\beta\bar\eta c+c^+\eta},$$

where $\mathcal{L}_{\rm at}=\Sigma_\sigma c_\sigma^+(\partial_\tau-\mu)c_\sigma+Un_\uparrow n_\downarrow$ is the Lagrangian in the atomic limit. The rules for the calculation of a Green's function are given by Wortis (1974) and by Metzner (1991). The basic idea is to carry out an expansion of physical quantities in powers of the hopping matrix element, and eliminate all disconnected graphs using linked-cluster type arguments. The diagrammatic rules for the one-particle Green's function $G_{ij,\sigma}(\tau-\tau')$ follow.

(i) Draw all topologically distinct connected diagrams composed of point vertices, directed "internal" lines connecting two vertices (corresponding to hopping matrix elements), and two "external" lines (one entering and one leaving a vertex) such that at each vertex (bare cumulant) the number of entering lines equals the number of exiting lines.

(ii) Label each line with a time and a spin variable. The entering external line is labeled by τ',σ, the exiting one by τ,σ. Label each vertex with a lattice site index; the vertex with the entering external line is labeled by j', the one with the exiting line by j (the external vertices may coincide: in this case $j=j'$).

(iii) Each line running from a vertex j to a vertex i yields a factor t_{ij}; each vertex j with m entering lines (labeled by $s_1',\ldots,s_m'$) and m exiting lines (labeled by $s_1,\ldots,s_m$) yields a factor $c_m^0(s_1,\ldots,s_m|s_1',\ldots,s_m')$.

(iv) Determine the sign of each diagram (plus/minus for an even/odd number of loops).

(v) Determine the symmetry factor $g(D)$ for each diagram D, i.e., the number of distinct permutations of (labeled) vertices and lines which do not alter the topological structure of the diagram.

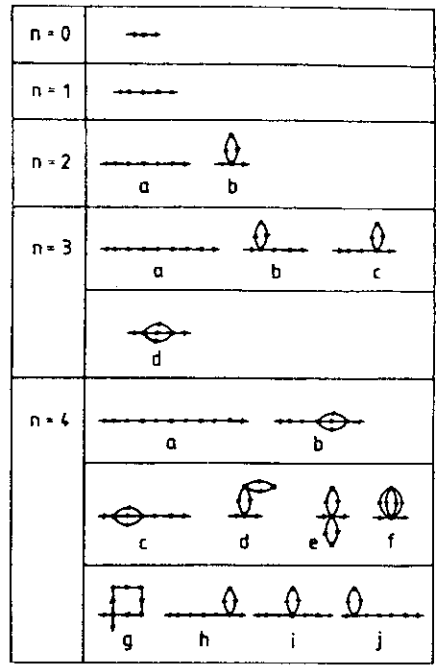

FIG. 5. First few diagrams for the expansion around the atomic limit for the Hubbard model [from Metzner (1991)]. The dots represent bare cumulants.

(vi) For each diagram D, multiply the associated hopping matrix elements and cumulants, integrate each time variable from 0 to β, sum each spin variable and lattice vector *on internal lines* over the whole lattice, and multiply by the sign; the labels of external lines and vertices are kept fixed.

Collecting all these factors, one obtains the weight $w(D)$ of a given diagram D. The one-particle Green's function is finally given by the sum of the weights $w(D)$ of all connected diagrams. The lowest-order diagrams are shown in Fig. 5 from Metzner (1991).

The expansion around the atomic limit is quite complex, and different truncations lead to the Hubbard I and Hubbard III (Hubbard, 1964) approximations (Metzner, 1991). It is natural to define the notion of irreducibility with respect to one line (representing t_{ij}). This leads to the definition of an irreducible cumulant M_1 as the sum of all graphs with two external legs, which cannot be divided into two parts by cutting a single line. Fourier transforming the spatial dependence, one obtains the exact relation between the one-particle irreducible cumulant and the one-particle Green's function,

$$G(\mathbf{k},i\omega_n)=\frac{1}{[M_1^{-1}(\mathbf{k},i\omega_n)-\epsilon_{\mathbf{k}}]} \quad (48)$$

in which $\epsilon_{\mathbf{k}}$ is the Fourier transform of the hopping matrix element. An exact relation between the irreducible one-particle cumulant and the self-energy is thus obtained:

$$M_1^{-1}(\mathbf{k},i\omega_n)=i\omega_n+\mu-\Sigma(\mathbf{k},i\omega_n). \quad (49)$$

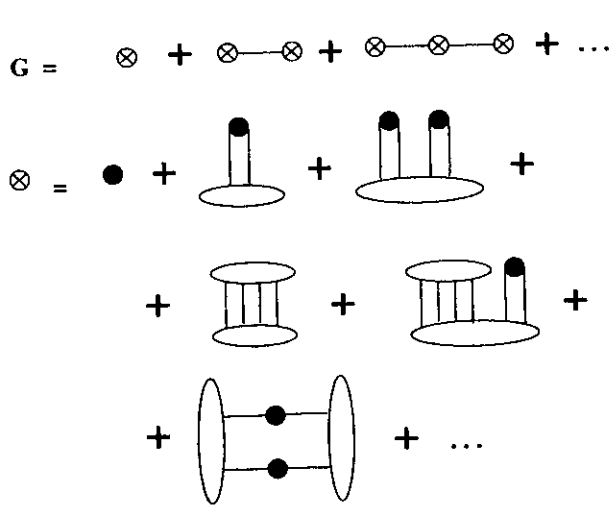

FIG. 6. Diagrammatic representation of the Dyson equation defining the irreducible cumulant M_1 (crossed circle), and its expansion in terms of bare cumulants.

Equation (48) is represented graphically in Fig. 6, in which the first terms in the expansion of M_1 in terms of bare t_{ij} lines and bare cumulants (c^0's) are also depicted.

The expansion described so far is completely general and valid in arbitrary dimensions. The summation over sites are totally unrestricted except for the external vertices which are taken at the same site, say o. In infinite dimensions several important simplifications occur, which are easily explained by means of an example. Consider the diagram in Fig. 7. One shows, just as in the discussion of the weak-coupling expansion in the previous section, that all the bare cumulants connected by more than two lines give a nonzero contribution in $d=\infty$ only when evaluated at the same site. In Fig. 7, i and l have to be equal to o. The contribution from sites $i, l \neq 0$ are of higher order in $1/d$. Notice that the index j in that figure is free. Hence, the irreducible cumulant $M_1(\mathbf{k}, i\omega_n)$ becomes *local* ($\mathbf{k}$ independent) in $d=\infty$, and so does the self-energy.

With this observation, we can identify all the graphs that survive in the $d\to\infty$ limit as originating from the expansion of an Anderson impurity model (AIM) in powers of the hybridization. For the model

$$Z_{\mathrm{AIM}}=\int dc^{+}dc\; e^{-\int \Sigma_\sigma c_\sigma^{+}(\tau)[\partial_\tau-\epsilon_f-\tilde{\Delta}(\tau-\tau')]c_\sigma(\tau')+Un_\uparrow n_\downarrow}. \tag{50}$$

one can derive a diagram expansion in powers of $\tilde{\Delta}$. The elements of a diagram are the bare local cumulants (which we still denote by a dot as in the lattice case), and wavy lines corresponding to $\tilde{\Delta}(\tau-\tau')$. One can introduce the notion of irreducibility with respect to lines, and express the local Green's function in terms of irreducible cumulants. The relation between the impurity orbital Green's function and the renormalized cumulant then becomes

$$G(i\omega)=\frac{1}{[M_1^{-1}(i\omega)-\tilde{\Delta}(i\omega)]}. \tag{51}$$

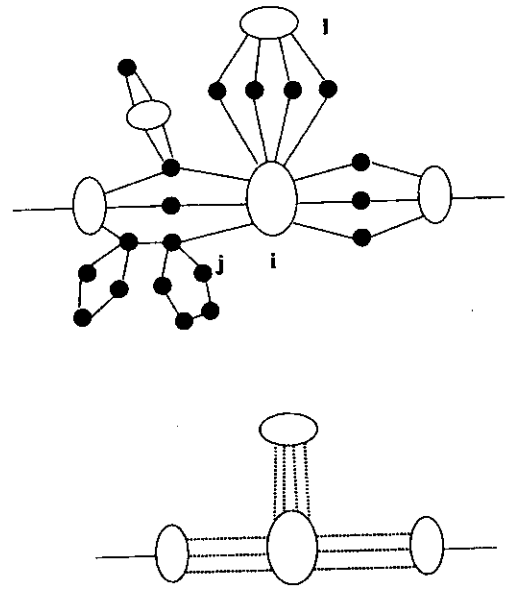

FIG. 7. Examples of the simplifications that take place in the $d=\infty$ limit. The upper plot is a typical graph for M_1. The lower plot is the corresponding Anderson impurity model representation [the dotted lines stand for the hybridization function $\tilde{\Delta}(\tau-\tau')$].

This allows us to identify the renormalized cumulant as

$$M_1^{-1}(i\omega)=i\omega-\epsilon_f-\Sigma(i\omega).$$

Finally, one can express $M_1^{-1}(i\omega)$ in terms of cumulants and $\tilde{\Delta}(\tau-\tau')$. The diagrammatic expansion is identical to that in Fig. 6 for the Hubbard model, provided that one identifies the dotted line representing $\tilde{\Delta}$ with the lines beginning with t_{oi} and ending with t_{jo} as described in Fig. 7. Thus, we conclude that the two expansions coincide provided

$$\tilde{\Delta}(i\omega)=\sum_{(ij)} t_{oi}t_{oj}G_{ij}^{(o)}(i\omega), \tag{52}$$

where $G_{ij}^{(o)}$ denotes, as in Sec. III.A, the Green's function between sites i and j in the absence of site o (and bonds connected to it). This is because the contributions from the site o to the hopping lines that originate from the site labeled j in Fig. 7 vanish in the $d\to\infty$ limit. Other contributions from site o to the diagram described in this figure (such as $l=o$) have been included explicitly in the diagram, thus they should not be included also in the dotted line so as to avoid double counting. The correspondence between the diagrams of the Anderson model and of the $d=\infty$ Hubbard model is illustrated in the case of a specific example in Fig. 7.

Equation (52) is precisely the self-consistency condition (35) derived in the previous sections following different methods. It would be interesting to analyze the effects of the leading order $1/d$ corrections in this framework, in conjunction with a high-temperature expansion.

D. Effective medium interpretation

The dynamical mean-field equations also have simple interpretation as an effective medium (or "cohe

ent potential") approximation (Janis, 1991; Janis and Vollhardt, 1992a; see also Janis 1986, 1989). (For a review of the coherent potential approximation in the noninteracting case, see, e.g., Elliott, Krumhansl, and Leath, 1974). In this approach, one envisions replacing the interacting lattice model by a *noninteracting medium* with a propagator specified by a local self-energy $\Sigma(i\omega_n)$ to be determined self-consistently. The action of this effective medium thus reads

$$\mathcal{S}_{\rm med}=-\int d\tau\int d\tau'\sum_{\mathbf{k}\sigma} c^{+}_{\mathbf{k}\sigma}(\tau)G^{-1}_{\rm med}(\mathbf{k},\tau-\tau')c_{\mathbf{k}\sigma}(\tau'), \tag{53}$$

$$G_{\rm med}(\mathbf{k},i\omega_n)^{-1}=i\omega_n+\mu-\epsilon_{\mathbf{k}}-\Sigma(i\omega_n). \tag{54}$$

One then imagines that the local interaction $Un_{o\uparrow}n_{o\downarrow}$ is introduced *at a single site o* of this effective medium, and that the self-energy Σ has simultaneously been removed at this single-site only. The action of this new lattice model with a single-site embedding thus reads

$$\mathcal{S}_{\rm emb}=\mathcal{S}_{\rm med}+U\int d\tau\, n_{o\uparrow}n_{o\downarrow} - \int d\tau\int d\tau'\sum_{\sigma} c^{+}_{o\sigma}(\tau)\Sigma(\tau-\tau')c_{o\sigma}(\tau'). \tag{55}$$

This can be turned into an effective action for site o only, by integrating out all other sites. Note that sites $i\neq o$ enter only quadratically in $\mathcal{S}_{\rm emb}$, and that this integration is thus performed *exactly*. This is to be contrasted with the cavity method which is rather different in spirit. One obtains

$$S_{\rm eff}=-\int d\tau\int d\tau'\sum_{\sigma} c^{+}_{o\sigma}(\tau)\mathcal{G}_0^{-1}(\tau-\tau')c_{o\sigma}(\tau') + U\int d\tau\, n_{o\uparrow}n_{o\downarrow} \tag{56}$$

with

$$\mathcal{G}_0^{-1}(i\omega_n)=\tilde{D}(i\omega_n+\mu-\Sigma)^{-1}+\Sigma(i\omega_n). \tag{57}$$

One then requires that the interacting Green's function obtained from $S_{\rm eff}$ for the embedded site coincides with the on-site (local) Green's function of the medium:

$$G(i\omega_n)\equiv-\langle Tc^{+}(i\omega_n)c(i\omega_n)\rangle_{S_{\rm eff}} =\sum_{\mathbf{k}} G_{\rm med}(\mathbf{k},i\omega_n)\equiv\tilde{D}(i\omega_n+\mu-\Sigma). \tag{58}$$

Hence, Σ is identified with the self-energy of the effective (impurity) model itself, and this set of self-consistent equations is seen to be exactly identical to the dynamical mean-field equations above.

IV. RESPONSE FUNCTIONS AND TRANSPORT

In this section, we show that the response functions for the lattice can be obtained from the knowledge of the self-energy and of two-particle Green's functions of the impurity model only (Brandt and Mielsch, 1989; Zlatić and Horvatić, 1990; Jarrell, 1992; Jarrell and Pruschke, 1993a, 1993b; Pruschke, Cox, and Jarrell, 1993a, 1993b). Note that, in the $d\to\infty$ limit, no precursor effect of the instability of a given phase towards some kind of symmetry breaking can, in general, be observed at the level of *one-particle* properties (Müller-Hartmann, 1989b). Indeed, the self-energy only probes local properties in this limit, and is thus sensitive only to those instabilities arising simultaneously from all wave vectors in the Brillouin zone. One such example is the Mott transition discussed in Sec. VII. Instabilities associated with a specific wave vector (such as a ferromagnetic or antiferromagnetic transition) will not be detectable from the knowledge of $\Sigma(i\omega_n)$ in the high-temperature phase. Hence it is very important to be able to evaluate response functions within the LISA framework. Alternatively, dynamical mean-field equations directly adapted to the study of phases with some symmetry breaking can also be established, as described in Sec. V.

A. General formalism

Consider the response function $\chi(\mathbf{q},i\omega_n)$ associated with some operator $\mathcal{O}(\mathbf{R},\tau)$, namely,

$$\chi(\mathbf{q},i\omega_n)=\int_0^{\beta} d\tau\, e^{i\omega_n\tau}\sum_j e^{i\mathbf{q}\cdot\mathbf{R}_j}\langle T\mathcal{O}(\mathbf{R}_j,\tau)\mathcal{O}(\mathbf{0},0)\rangle. \tag{59}$$

Some examples are the charge susceptibility, with $\mathcal{O}(\mathbf{R}_j)=\Sigma_\sigma c^{+}_{j\sigma}c_{j\sigma}$; spin susceptibilities χ^{ab} $(a,b=x,y,z)$, with $\mathcal{O}^a(\mathbf{R}_j)=1/2\Sigma_{\sigma\sigma'}c^{+}_{j\sigma}\sigma^a_{\sigma\sigma'}c_{j\sigma'}$; and the frequency-dependent conductivity tensor $\sigma^{ab}(\omega)$ related to the real-frequency current-current correlation function by $\sigma^{ab}(\omega)=[\chi^{ab}_{jj}(\omega+i0^+)-\chi^{ab}_{jj}(i0^+)]/i\omega$, with the x-component of the current on the hypercubic lattice given by $j^x(\mathbf{R}_j)=i\Sigma_\sigma c^{+}_{j\sigma}(c_{j+\hat{x},\sigma}-c_{j\sigma})$.

All these expressions can be Fourier transformed to yield

$$\mathcal{O}(\mathbf{q},\tau)=\sum_{\mathbf{k}\sigma} v_{\mathbf{k}\sigma}c^{+}_{\mathbf{k}\sigma}c_{\mathbf{k}+\mathbf{q},\sigma}, \tag{60}$$

where the vertex factor $v_{\mathbf{k}\sigma}$ equals 1, $\mathrm{sgn}(\sigma)$, $2\sin(k_x)$ in the three examples above, respectively.

Let us define the two-particle vertex function $\Gamma^{\sigma\sigma'}_{\mathbf{k}\mathbf{k}'\mathbf{q}}(i\nu,i\nu';i\omega)$ appropriate to each of these cases and irreducible in the particle-hole channel (Fig. 8). $\chi(\mathbf{q},i\omega_n)$ is obtained from the ladder sum depicted in Fig. 8, in which a thick line stands for the *interacting* fermion propagator $G(\mathbf{k},i\omega_n)$. Explicitly,

$$\chi(\mathbf{q},i\omega_n)=-\sum_{\mathbf{k},i\nu,\sigma} v_{\mathbf{k},\sigma}G(\mathbf{k},i\nu)G(\mathbf{k}+\mathbf{q},i\nu+i\omega)v_{\mathbf{k}+\mathbf{q},\sigma} +\sum_{\mathbf{k},i\nu,\sigma}\sum_{\mathbf{k}',i\nu',\sigma'} v_{\mathbf{k},\sigma}G(\mathbf{k},i\nu)G(\mathbf{k}+\mathbf{q},i\nu+i\omega) \times\Gamma^{\sigma\sigma'}_{\mathbf{k}\mathbf{k}'\mathbf{q}}(i\nu,i\nu';i\omega)G(\mathbf{k}',i\nu') \times G(\mathbf{k}'+\mathbf{q},i\nu'+i\omega)v_{\mathbf{k}'+\mathbf{q},\sigma'}+\cdots. \tag{61}$$

A crucial simplification arises in the $d\to\infty$ limit: Γ can be replaced in this equation by a purely local quantity

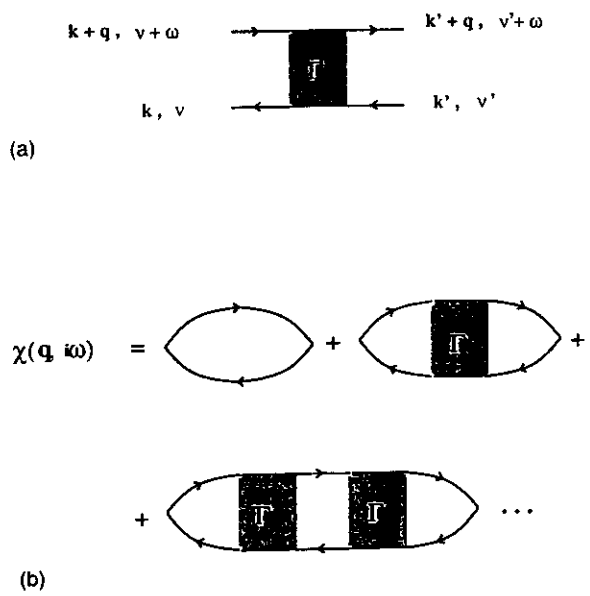

FIG. 8. (a) Two-particle irreducible vertex function. (b) Ladder decomposition of the response function $\chi(\mathbf{q},i\omega_n)$; the *momentum* dependence of Γ can be ignored inside the ladder sum in $d=\infty$.

$\Gamma^{\sigma\sigma'}(i\nu,i\nu';i\omega)$ depending on frequencies only (Zlatić and Horvatić, 1990). This results from the power-counting rules stated in Sec. III.B, since any two sites belonging to Γ in the real-space representation of the ladder series are certainly connected by more than two independent paths. If it were not so, the diagram could be disconnected by cutting two internal propagators in contradiction with the assumption that Γ is irreducible. Note that this assumes that all vertices in Γ can be considered internal (i.e., summed over) and thus Γ can be collapsed to a fully local form *only when inserted in the ladder sum above*. (When considered by itself, Γ does have some momentum dependence, but only its local component contributes to the ladder sum.) As a result of this simplification, the summation over momenta can be performed in each particle-hole bubble independently, ignoring momentum conservation at the vertex Γ. In contrast, note that frequency conservation must be fully taken into account.

For the sake of simplicity, we shall proceed with the example of the spin susceptibility χ^{zz}. All the other response functions can be obtained in an analogous manner. The special case of the frequency-dependent conductivity will also be dealt with in detail below. Only the spin-antisymmetric component Γ^A contributes to χ^{zz} (the superscript A will be omitted everywhere below). We denote by $\tilde{\chi}_{\mathbf{q}}(i\nu,i\nu';i\omega)$ the result of the above ladder sum in which the summation over the first and last frequencies ν,ν' have been omitted [so that the dynamical susceptibility is obtained by summing over frequencies, $\chi(\mathbf{q},i\omega)=\Sigma_{\nu\nu'}\tilde{\chi}_{\mathbf{q}}(i\nu,i\nu';i\omega)$]. $\tilde{\chi}$ satisfies an integral equation:

$$\tilde{\chi}_{\mathbf{q}}(i\nu,i\nu';i\omega)=\tilde{\chi}^0_{\mathbf{q}}(i\nu;i\omega)\delta_{\nu,\nu'} + \tilde{\chi}^0_{\mathbf{q}}(i\nu;i\omega)\frac{1}{\beta}\sum_{\nu''}\Gamma(i\nu,i\nu'';i\omega) \times\tilde{\chi}_{\mathbf{q}}(i\nu'',i\nu';i\omega) \tag{62}$$

in which $\tilde{\chi}^0_{\mathbf{q}}(i\nu;i\omega)$ is obtained by performing the summation over the internal momentum $\mathbf{k}$ in the elementary particle-hole bubble,

$$\tilde{\chi}^0_{\mathbf{q}}(i\nu;i\omega)=-\sum_{\mathbf{k}} G(\mathbf{k},i\nu)G(\mathbf{k}+\mathbf{q},i\nu+i\omega). \tag{63}$$

It is clear from Eq. (62) that the $\mathbf{q}$ dependence of $\chi(\mathbf{q},i\omega_n)$ stems entirely from that of $\tilde{\chi}^0_{\mathbf{q}}$. We shall now characterize more precisely this momentum dependence, concentrating on the case where one really studies a $d=\infty$ lattice model (we choose for simplicity the hypercubic lattice). Later in this section, we shall describe how dynamical mean-field approximations for $\mathbf{q}$-dependent response functions of a finite-dimensional model can be generated in the general spirit of the LISA approach.

For the $d=\infty$ hypercubic lattice, the momentum dependence of the response functions simplifies drastically: as shown in Appendix A, $\tilde{\chi}^0_{\mathbf{q}}$ depends on $\mathbf{q}$ (for the hypercubic lattice) only through the following quantity (Brandt and Mielsch, 1989; Müller-Hartmann, 1989a):

$$X(\mathbf{q})=\frac{1}{d}\sum_{i=1}^{d}\cos q_i \tag{64}$$

Let us discuss in more detail the quite peculiar $\mathbf{q}$ dependence of this quantity [and hence of $\chi(\mathbf{q},i\omega_n)$ in the $d\to\infty$ limit]. For a "generic" $\mathbf{q}$ vector (i.e., for all $\mathbf{q}$'s except a set of measure zero), the summation in Eq. (64) is over arguments that are random in sign, and hence is of order $\sqrt{d}$, so that, as $d\to\infty$,

$$X(\mathbf{q})=0 \quad (\text{"generic" } \mathbf{q}). \tag{65}$$

This implies that, for any generic $\mathbf{q}$, $\chi(\mathbf{q},i\omega_n)$ coincides with its *local* (on-site) component:

$$\chi(\mathbf{q},i\omega_n)=\sum_{\mathbf{q}}\chi(\mathbf{q},i\omega_n)\equiv\chi_{\text{loc}}(i\omega_n) \quad (\text{"generic" } \mathbf{q}). \tag{66}$$

$X(\mathbf{q})$ may take arbitrary values $-1\leq X\leq 1$ for specific values of $\mathbf{q}$, however. Important examples are the uniform wave vector $\mathbf{q}=\mathbf{0}$ (appropriate for ferromagnetic ordering) and the zone-corner wave vectors $\mathbf{q}=(\pm\pi,\ldots,\pm\pi)$ (appropriate for two-sublattice commensurate antiferromagnetic ordering):

$$X(\mathbf{0})=+1, \quad X(\pm\pi,\ldots,\pm\pi)=-1. \tag{67}$$

Intermediate values $-1<X<1$ correspond to *incommensurate orderings*. It is important to realize that even though these types of ordering are not very easy to visualize in real space in the $d\to\infty$ limit, they can be studied through the $X(\mathbf{q})$ dependence of χ and indeed are

known to occur in several models including the $d=\infty$ Falicov-Kimball model (Freericks, 1993a, 1993b, 1993c cf. Sec. VIII.B), Hubbard model (Freericks and Jarrell, 1995a, cf. Sec. VII.H), and Holstein model (Ciuchi *et al.*, 1993, cf. Sec. VIII.E), away from half-filling.

Because of this specific $\mathbf{q}$ dependence, the calculation of response functions for a $d=\infty$ model can be reduced to the evaluation of correlation functions of the effective impurity model only. In order to see this, we apply Eq. (62) to a "generic" wave vector $\mathbf{q}$. This allows us to express the irreducible vertex function in terms of local quantities:

$$\Gamma=[\tilde{\chi}^0_{\rm loc}]^{-1}-[\tilde{\chi}_{\rm loc}]^{-1} \tag{68}$$

in which the $\tilde{\chi}$'s are viewed as matrices in the two indices ν,ν' and $[\tilde{\chi}]^{-1}$ denotes matrix inversion. This equation can be used to reexpress Γ in Eq. (62), leading to the important expression (Zlatić and Horvatić, 1990; Jarrell, 1992)

$$\tilde{\chi}^{-1}_{\mathbf{q}}=[\tilde{\chi}_{\rm loc}]^{-1}+[\tilde{\chi}^0_{\mathbf{q}}]^{-1}-[\tilde{\chi}^0_{\rm loc}]^{-1}. \tag{69}$$

The right-hand side of this equation involves impurity model quantities *only*, since $\tilde{\chi}^0_{\mathbf{q}}$ requires only the knowledge of the self-energy $\Sigma(i\omega_n)$, and the local quantities $\chi_{\rm loc}(i\omega_n)$ and $\tilde{\chi}_{\rm loc}(i\nu,i\nu';i\omega)$ are response functions of the impurity model effective action $S_{\rm eff}$. For the example of the spin susceptibility χ^{zz}, we have explicitly

$$\begin{aligned}\tilde{\chi}_{\rm loc}(i\nu,i\nu';i\omega)=\frac{1}{4}\int_0^\beta d\tau_1\int_0^\beta d\tau_2\int_0^\beta d\tau_3\int_0^\beta d\tau_4 \\ \times e^{i\nu(\tau_1-\tau_2)}e^{i\nu'(\tau_4-\tau_3)} \\ \times e^{i\omega(\tau_4-\tau_2)}\Sigma_{\sigma\sigma'}(-1)^{\sigma}(-1)^{\sigma'} \\ \times\langle Tc^+_\sigma(\tau_1)c_\sigma(\tau_2)c^+_{\sigma'}(\tau_3)c_{\sigma'}(\tau_4)\rangle_{S_{\rm eff}}.\end{aligned} \tag{70}$$

The numerical methods reviewed in Sec. VI for the calculation of the impurity model Green's function can be used to evaluate such a local correlation function (cf. Sec. VI.A.5).

The other ingredients entering Eq. (69) are the uncorrected response functions $\tilde{\chi}^0_{\mathbf{q}}$. These are obtained from the knowledge of the one-particle Green's function by evaluating the momentum sum in Eq. (63). On the $d=\infty$ hypercubic lattice, this sum can be evaluated further in order to show that $\tilde{\chi}^0_{\mathbf{q}}$ only depends on $\mathbf{q}$ through $X(\mathbf{q})$. The relevant expressions for an arbitrary $X(\mathbf{q})$ are given in Appendix A. Here, we shall simply note the important expressions for a generic $\mathbf{q}$ and for $\mathbf{q}=0$, valid for an arbitrary density of states:

$$\tilde{\chi}^0_{\mathbf{q}}=\tilde{\chi}^0_{\rm loc}=-\tilde{D}(\zeta_\nu)\tilde{D}(\zeta_{\nu+\omega})\quad(\text{"generic" }\mathbf{q}), \tag{71}$$

$$\tilde{\chi}^0_{\mathbf{q}=\mathbf{0}}=-\frac{\tilde{D}(\zeta_\nu)-\tilde{D}(\zeta_{\nu+\omega})}{\zeta_{\nu+\omega}-\zeta_\nu} \tag{72}$$

with $\zeta_\nu\equiv i\nu+\mu-\Sigma(i\nu)$, as usual.

Hence, Eq. (69) is crucial in that it allows the determination of any $\mathbf{q}$ dependent response function for a $d=\infty$ lattice model from the knowledge of the effective impurity model self-energy and correlation functions. It is instructive to have a closer look at this equation for the case of a uniform and static response $\mathbf{q}=0$, $\omega=0$. Using the above expressions of $\tilde{\chi}^0$ and Eq. (69), we obtain, in that case,

$$\tilde{\chi}^{-1}_{\mathbf{q}=0}(\omega=0)=\tilde{\chi}^{-1}_{\rm loc}(\omega=0)+\delta_{\nu,\nu'}\left(\frac{1}{\tilde{D}(\zeta_\nu)^2}+\frac{1}{\tilde{D}'(\zeta_\nu)}\right) \tag{73}$$

with $\tilde{D}'=\partial\tilde{D}/\partial\zeta$. This expression simplifies in two special cases. For a Lorentzian density of states, $\tilde{D}(\zeta)^{-1}=\zeta+it$ so that the second term in the right-hand side of Eq. (73) vanishes and one obtains that uniform and local response functions coincide for this model: $\tilde{\chi}_{\mathbf{q}=0}=\tilde{\chi}_{\rm loc}$. This parallels the observation made in Sec. II.C that the self-consistency condition becomes trivial for this model, which is really just an impurity model without the interesting feedback effects from the lattice. For all other cases however, the additional term on the right-hand side of Eq. (73) reflects how a static field applied to the lattice induces a spin dependence of the Weiss function $\mathcal{G}_{0\sigma}(i\omega_n)$ (see Sec. V). For the $z=\infty$ Bethe lattice (with our standard normalization), this term simplifies to yield

$$\tilde{\chi}^{-1}_{\mathbf{q}=0}(\omega=0)=\tilde{\chi}^{-1}_{\rm loc}(\omega=0)+t^2\delta_{\nu,\nu'}. \tag{74}$$

This formula has a simple physical interpretation. Even when the local susceptibility diverges, e.g., near the Mott transition $\tilde{\chi}^{-1}_{\rm loc}\to 0$ the uniform susceptibility may remain finite due to the t^2 term. This term cuts off the divergence in the frequency summation $\chi(\mathbf{q}=0,\omega=0)=\Sigma_{\nu\nu'}\tilde{\chi}_{\mathbf{q}=0}(\omega=0)=\Sigma_{\nu\nu'}[\tilde{\chi}^{-1}_{\rm loc}+t^2\delta_{\nu,\nu'}]^{-1}$, and generates the finite spin-exchange scale $J\simeq t^2/U$.

Finally, we conclude this section by mentioning how approximations of $\mathbf{q}$ dependent response functions for a *finite-dimensional* lattice can be obtained in the LISA framework, in the spirit of a dynamical mean-field approximation. The idea is to neglect the momentum-dependence of the irreducible vertex function Γ, and to use again Eq. (62) in order to relate Γ to local quantities. However, it is no longer strictly true that $\chi_{\mathbf{q}}$ coincides with $\chi_{\rm loc}$ for a "generic" value of $\mathbf{q}$, so that using Eq. (68) to calculate Γ is in fact a supplementary approximation. Other choices could be made to define Γ, but Eq. (68) is certainly a natural possibility. Thus, one can follow the strategy of computing the self-energy and the *local* response function $\tilde{\chi}_{\rm loc}$ from the self-consistent impurity model, and to compute $\mathbf{q}$-dependent response functions from Eq. (69). For an arbitrary lattice, the quantities $\tilde{\chi}^0_{\mathbf{q}}$ are obtained from their definition (63) and the knowledge of the self-energy as

$$\begin{aligned}\tilde{\chi}^0_{\mathbf{q}}(i\nu;i\omega)=-\int_{-\infty}^{+\infty}d\epsilon_1 D(\epsilon_1)\int_{-\infty}^{+\infty}d\epsilon_2 D(\epsilon_2) \\ \times\frac{\Delta_{\mathbf{q}}(\epsilon_1,\epsilon_2)}{(\zeta_\nu-\epsilon_1)(\zeta_{\nu+\omega}-\epsilon_2)},\end{aligned} \tag{75}$$

where $\zeta_\nu \equiv i\nu+\mu-\Sigma(i\nu)$, and $\Delta_{\mathbf{q}}$ is the lattice-dependent function:

$$\Delta_{\mathbf{q}}(\epsilon_1,\epsilon_2)=\sum_{\mathbf{k}} \delta(\epsilon_{\mathbf{k}}-\epsilon_1)\delta(\epsilon_{\mathbf{k}+\mathbf{q}}-\epsilon_2). \tag{76}$$

For a $d=\infty$ lattice, $\Delta_{\mathbf{q}}$ only depends on $\mathbf{q}$ through $X(\mathbf{q})$, as mentioned above, and the distribution $\Sigma_{\mathbf{q}}\delta(X-X(\mathbf{q}))$ is a delta function $\delta(X)$, so that the above approximation becomes exact.

B. Frequency-dependent conductivity, thermopower and Hall effect

We now deal in detail with the case of the frequency dependent conductivity $\sigma(\omega,\mathbf{q}=0)$. In this case, we have seen that the current vertex $v_{\mathbf{k}}$ is *odd* under parity $\mathbf{k}\to-\mathbf{k}$. Since all $\mathbf{k}$ dependence of Γ can be ignored and $\epsilon_{\mathbf{k}}$ is even under parity, this implies that *all* vertex corrections drop out of the current-current correlation function at $\mathbf{q}=0$ in the $d\to\infty$ limit. This observation was first made by Khurana (1990). A more detailed proof follows from the Ward identity

$$\Omega\Gamma^0(\mathbf{k}+\mathbf{q},\mathbf{k})+\sum_{i=1,d}\Delta(\mathbf{q})^i\Gamma^i(\mathbf{k}+\mathbf{q},\mathbf{k}) = G^{-1}(\mathbf{k}+\mathbf{q},\omega+\Omega)-G^{-1}(\mathbf{k},\omega), \tag{77}$$

where Γ^0 and Γ^i denote the density and current vertex respectively and $\Delta(q)^i=2\sin[(q_i)/2]$ on the hypercubic lattice. Since in large dimensions the self-energy is independent of momentum, and the density vertex is even in $\mathbf{q}$ while the current vertex is odd in $\mathbf{q}$, expanding Eq. (77) to lowest order in $\Delta(\mathbf{q})$ proves that the current vertex is unrenormalized. Notice that this conclusion is false as soon as $\mathbf{q}$ is finite, because there are nontrivial cancellations between the density and the current vertex at finite $\mathbf{q}$ so as to obey Eq. (77).

Hence, only the elementary particle-hole bubble survives in Eq. (62) for the current-current correlator at $\mathbf{q}=0$, and one obtains, for the paramagnetic contribution to the optical conductivity (the diamagnetic term cancels the $1/\omega$ divergence of the real part of the retarded current-current correlator),

$$\sigma(i\omega)=\frac{1}{\omega}\frac{1}{\beta}\sum_{\mathbf{k}\nu_n\sigma}\frac{1}{d}\sum_{l=1}^{d}4\sin^2(k_l)G(\mathbf{k},i\nu_n) \times G(\mathbf{k},i\nu_n+i\omega). \tag{78}$$

One could make use of this expression (inserting the self-energy calculated from the impurity model) to generate approximations of the optical conductivity of a finite-dimensional lattice, in the general spirit of the LISA method. For a $d=\infty$ model however, the sum over momenta can be further simplified by expressing it as an energy integration, and noting that $\Sigma_{\mathbf{k}}\Sigma_l\sin^2(k_l)\delta(\epsilon-\epsilon_{\mathbf{k}})\simeq dD(\epsilon)/2$ for $d\to\infty$. This leads to the final form (Schweitzer and Czycholl, 1991b; Moeller, Ruckenstein, and Schmidt-Rink, 1992; Pruschke, Cox, and Jarrell, 1993a, 1993b):

$$\sigma(i\omega)=\frac{1}{\omega}\frac{1}{\beta}\sum_{\nu_n}\int_{-\infty}^{+\infty}d\epsilon\, D(\epsilon)G(\epsilon,i\nu_n)G(\epsilon,i\nu_n+i\omega). \tag{79}$$

Using the spectral representation of the Green's functions, this is also conveniently expressed in terms of the one-particle spectral density $\rho(\epsilon,\nu)=-(1/\pi)\,\mathrm{Im}G(\epsilon,\nu+i0^+)$:

$$\sigma(i\omega)=\frac{1}{\omega}\int_{-\infty}^{+\infty}d\epsilon\int_{-\infty}^{+\infty}d\nu\int_{-\infty}^{+\infty}d\nu' \times D(\epsilon)\rho(\epsilon,\nu)\rho(\epsilon,\nu')\frac{f(\nu)-f(\nu')}{\nu-\nu'+i\omega}, \tag{80}$$

where f is the Fermi function. Performing the analytic continuation yields (reintroducing dimensional prefactors):

$$\mathrm{Re}\,\sigma(\omega+i0^+)=\pi\frac{e^2}{\hbar ad}\int_{-\infty}^{+\infty}d\epsilon\int_{-\infty}^{+\infty}d\nu\, D(\epsilon)\rho(\epsilon,\nu) \times\rho(\epsilon,\nu'+\omega)\frac{f(\nu)-f(\nu+\omega)}{\omega}. \tag{81}$$

Finally, we conclude by noting that the absence of vertex corrections to the current-current correlation function for $d=\infty$ models is not restricted to that correlation function, but actually applies to the $\mathbf{q}=0$ correlation function of any operator such that the vertex factor $v_{\mathbf{k}}$ satisfies

$$\sum_{\mathbf{k}} v_{\mathbf{k}}=0. \tag{82}$$

One additional example is the thermopower Q, associated with the heat current $(\epsilon_k-\mu)\nabla_k\epsilon_k$. The following $d=\infty$ expression can be established (Schweitzer and Czycholl, 1991b; Pruschke, Jarrell, and Freericks, 1996):

$$Q=\frac{\int d\omega\int d\epsilon(\omega-\mu)\frac{\partial f}{\partial\omega}\rho(\epsilon,\omega)^2}{eT\int d\omega\int d\epsilon\frac{\partial f}{\partial\omega}\rho(\epsilon,\omega)^2}. \tag{83}$$

Notice, however, that this expression neglects the contribution to the thermal current due to the transport of doubly occupied sites, which has not been analyzed in detail yet.

Vertex corrections can also be shown to drop out from the Hall coefficient. The proof in this case is more involved, since one needs to consider three-point correlations at finite $\mathbf{q}$, and the limit of small wave vector is taken only at the end of the calculation. Following the careful analysis of Kohno and Yamada (1988), it may be shown that the diagrams neglected in their treatment on the basis of being higher in the small damping constant are in fact higher order in an expansion in $1/d$ relative to the leading terms. This leads to the following expression at finite temperature:

$$\sigma_{xy} \propto B \int d\omega \frac{\partial f}{\partial \omega} \sum_k \rho(k,\omega)^3 \left(\frac{\partial \epsilon_k}{\partial k_x}\right)^2 \times \left[\frac{\partial^2 \epsilon_k}{\partial k_y^2} - \left(\frac{\partial \epsilon_k}{\partial k_y}\right)^2 \frac{\partial^2 \epsilon_k}{\partial k_x \partial k_y}\right] \quad (84)$$

Taking the zero-temperature limit of this expression, one observes that the *noninteracting* result is recovered, leading to the Hall number:

$$R_H = -\frac{a^3}{e} \frac{\frac{1}{N}\Sigma_{k,\sigma}\delta(\epsilon_k-\mu_0)\left(v_x^2 \frac{\partial v_y}{\partial k_y} - v_y^2 \frac{\partial v_y}{\partial k_x}\right)}{\left(\frac{1}{N}\Sigma_{k,\sigma}\delta(\epsilon_k-\mu_0)v_x^2\right)^2}, \quad (85)$$

where $v_k \equiv \nabla_k \epsilon_k$. It is quite remarkable that the Hall coefficient is given by the bare band structure at $T=0$ even when the correlations are strong. This has been applied to the case of $La_{1-x}Sr_xTiO_3$ near the Mott transition by Kajueter, Kotliar, and Moeller (1995).

These expressions can all be simplified further if one considers the special case of the $d=\infty$ hypercubic lattice Eq. (19), in which case summations over $\mathbf{k}$ can be replaced by averages weighted by the bare density of states $D(\epsilon)$, leading to (Pruschke, Jarrell, and Freericks, 1995; Kajueter, Kotliar, and Moeller, 1995; Majumdar and Krishnamurthy, 1995b):

$$\sigma_{xy} \propto -B \int d\epsilon\, D(\epsilon)\epsilon \int d\omega\, \rho(\epsilon,\omega)^3 \frac{\partial f}{d\omega}, \quad (86)$$

$$R_H(T=0) = \frac{a^3}{t^2 e} \frac{\mu_0}{D(\mu_0)}. \quad (87)$$

V. PHASES WITH LONG-RANGE ORDER

For simplicity, the dynamical mean-field equations have been derived in Secs. II and III under the assumption that no long-range order is present. In the previous section, it was shown how response functions signalling some symmetry breaking can be computed. In this section, it will be shown that the dynamical mean-field equations can be generalized to phases with broken symmetry, and a description of the mapping onto an impurity model for these cases will be given (see, e.g., Brandt and Mielsch, 1990, 1991; Georges, Kotliar, and Si, 1992).

A. Ferromagnetic long-range order

In the presence of a magnetic field h coupled to S_z, or if there is a spontaneous uniform magnetization, the Green's functions for up and down electrons are not equivalent. Then one has to retain the spin dependence of the local Green's functions and of the Weiss function in the derivations of Sec. III. The local effective action associated with the Hubbard model in a ferromagnetic phase or in the presence of a uniform field reads

$$S_{\rm eff} = -\int_0^\beta d\tau \int_0^\beta d\tau' \sum_\sigma c_\sigma^+(\tau)\mathcal{G}_{0,\sigma}^{-1}(\tau-\tau')c_\sigma(\tau') + U\int_0^\beta d\tau\, n_\uparrow(\tau)n_\downarrow(\tau). \quad (88)$$

The self-consistent equations for the two functions $G_\uparrow$, $G_\downarrow$ and their corresponding Weiss functions are straightforward generalizations of Eq. (7) to this spin-dependent case. They read

$$G_\sigma(i\omega_n) = \int_{-\infty}^{+\infty} d\epsilon \frac{D(\epsilon)}{i\omega_n + \mu + h\sigma - \Sigma_\sigma(i\omega_n) - \epsilon}, \quad (89)$$

where

$$G_\sigma(i\omega_n) \equiv \langle c_\sigma^+(i\omega_n)c_\sigma(i\omega_n)\rangle_{S_{\rm eff}},$$
$$\Sigma_\sigma(i\omega_n) = \mathcal{G}_{0,\sigma}^{-1} - G_\sigma^{-1}. \quad (90)$$

Note that the dependence of $\mathcal{G}_0^{-1}$ on the external field h is, in general, more complicated than just a linear term $h\sigma$: a uniform field coupling linearly to the lattice model induces a nonlinear, frequency dependent term in the impurity effective action.

From the solution of Eqs. (88) and (89), one can reconstruct the lattice Green's functions:

$$G_\sigma(\mathbf{k},i\omega_n) = \frac{1}{i\omega_n + \mu + h\sigma - \epsilon_{\mathbf{k}} - \Sigma_\sigma(i\omega_n)}. \quad (91)$$

The magnetization as a function of the external field is given by

$$m = \frac{1}{\beta}\sum_n e^{i\omega_n 0^+}[G_\uparrow(i\omega_n) - G_\downarrow(i\omega_n)]. \quad (92)$$

A ferromagnetic phase is signalled by a non-zero spontaneous magnetization $\lim_{h\to 0} m(h) \neq 0$. It is a straightforward but lengthy exercise to check that Eq. (73) for the uniform magnetic susceptibility can be recovered by expanding Eqs. (88) and (89) for small h.

B. Antiferromagnetic long-range order

Similar considerations can be used to study commensurate antiferromagnetic long-range order in the Hubbard model. Note that the $1/\sqrt{d}$ scaling of the hopping amplitude is such that the exchange coupling obtained at large U for a *given* pair of sites, $J_{ij} \simeq t_{ij}^2/U$, scales as $1/d$, which is just the scaling to be performed on a spin model to preserve a Néel transition at a finite temperature $T_N = O(1)$. For simplicity we shall again concentrate on the Hubbard model and we shall add to the Hamiltonian in Eq. (5) a staggered magnetic field:

$$h_s \sum_{i\sigma} e^{i\mathbf{Q}\cdot R_i} c_{\sigma i}^+ c_{\sigma i} \quad (93)$$

with $\mathbf{Q} = (\pi,\ldots,\pi)$.

Let us first derive the mean-field equations in the ordered phase using the cavity method on the $z=\infty$ Bethe lattice. There are two inequivalent sublattices, A and B and a simple relation in the Néel phase between the

local Green's functions on each sublattice: $G_{ii,\sigma}=G_{A,\sigma},G_{B,\sigma}$ for $i\in A,B$ with

$$G_{A\sigma}(i\omega_n)=G_{B,-\sigma}(i\omega_n). \tag{94}$$

Let us focus on a site belonging to sublattice A, and eliminate all other degrees of freedom. The resulting effective action is identical to Eq. (88), but in the present case the Weiss functions read $\mathcal{G}_{0,\sigma}^{-1}=i\omega_n+\mu-h_s\sigma-t^2G_{B\sigma}$. Using Eq. (94), we see that a single-site description still holds, with (on the Bethe lattice)

$$\mathcal{G}_{0,\sigma}^{-1}=i\omega_n+\mu-t^2G_{-\sigma}-\sigma h_s. \tag{95}$$

This is easily generalized to an arbitrary lattice. The $d\to\infty$ skeleton functional Φ now depends on the two local Green's functions: $\Phi=\Phi[G_{A\sigma},G_{B\sigma}]$. The self-energy is purely local and can take two values with $\Sigma_{A\sigma}(i\omega_n)=\Sigma_{B,-\sigma}(i\omega_n)$. It is convenient to write the Hamiltonian in terms of two sublattice operators in the reduced Brillouin zone (RBZ):

$$H_0=\sum_{\sigma\mathbf{k}\in\mathrm{RBZ}}\epsilon_{\mathbf{k}}(c_{A\mathbf{k}\sigma}^{+}c_{B\mathbf{k}\sigma}+c_{B\mathbf{k}\sigma}^{+}c_{A\mathbf{k}\sigma})$$
$$+\sum_{\sigma\mathbf{k}\in\mathrm{RBZ}}\sigma h_s(c_{A\mathbf{k}\sigma}^{+}c_{A\mathbf{k}\sigma}-c_{B\mathbf{k}\sigma}^{+}c_{B\mathbf{k}\sigma}). \tag{96}$$

The Green's functions are obtained by inverting the matrix:

$$\begin{pmatrix}\zeta_{A\sigma} & -\epsilon_{\mathbf{k}}\\ -\epsilon_{\mathbf{k}} & \zeta_{B\sigma}\end{pmatrix}$$

with $\zeta_{A\sigma}=i\omega_n+\mu-\sigma h_s-\Sigma_{A\sigma}$ and $\zeta_{B\sigma}=i\omega_n+\mu+\sigma h_s-\Sigma_{B\sigma}$. The impurity model to be considered is still Eq. (88), but the self-consistency conditions now read (Brandt and Mielsch, 1990, 1991):

$$G_{\alpha\sigma}=\zeta_{\bar{\alpha}\sigma}\int_{-\infty}^{\infty}d\epsilon\,\frac{D(\epsilon)}{\zeta_{A\sigma}\zeta_{B\sigma}-\epsilon^2} \tag{97}$$

with $\alpha=A,B$ and $\bar{\alpha}=B,A$. When a semicircular density of states is inserted in this equation, Eq. (95) is recovered. The staggered magnetization and the free energy of the antiferromagnetic phase are given by similar equations as above.

It is instructive to notice that the simplest approximation to the self-energies, $\Sigma_{A\sigma}=(U/2)(n_{A\sigma}-n_{B\sigma})$, reproduces the usual Hartree-Fock approximation for the staggered magnetization. Also, as soon as Néel order is established and $\Sigma_{A\sigma}\neq\Sigma_{B\sigma}$, it is possible to open a gap in the single particle spectrum, i.e., $\mathrm{Im}G(\omega+i0^+)=0$ if $|\omega+\mu+(\Sigma_B-\Sigma_A)/2|\leq(\Sigma_A+\Sigma_B)/2$. This will always be the case, particularly at half-filling for a nested, bipartite lattice. Note that the effective conduction electron bath entering the impurity model is then also gapped. These are peculiarities of the $d\to\infty$ limit, in which long-wavelength spin-wave excitations are absent. Nevertheless, the LISA method has proven useful for studying the quantum transition between a strongly correlated paramagnetic metal and a metal with spin-density wave order, and some of the results are expected to hold in finite dimensions as well (Sachdev and Georges, 1995; see also Sec. VII.D.3).

In order to study the phase transitions between different magnetic phases we have to compare the free energies of all possible magnetic states, using straightforward generalizations of Eqs. (46) and (47). Alternatively, one can calculate directly the relevant divergent susceptibility, along the lines of Sec. IV (keeping in mind, however, the possibility of first-order transitions). For *incommensurate* magnetic orderings, no simple set of mean-field equations can be written inside the ordered phase in the general case, and one must resort to the study of susceptibilities.

C. Superconductivity and pairing

The LISA mean-field equations are easily extended to take into account superconducting long-range order (Georges, Kotliar, and Krauth, 1993). We illustrate this on the one-band Hubbard model, but the equations are easily generalized to other models, such as the multiband Hubbard model described in Sec. VIII.C. One introduces anomalous Green's functions:

$$F(\mathbf{k},\tau)\equiv-\langle Tc_{\mathbf{k}\uparrow}(\tau)c_{-\mathbf{k}\downarrow}(0)\rangle. \tag{98}$$

In the following, we shall consider only pure singlet pairing, for which $F(-\mathbf{k},-\tau)=F(\mathbf{k},\tau)$ and pure triplet pairing with $S_z=0$ for which $F(-\mathbf{k},-\tau)=-F(\mathbf{k},\tau)$. Within the present $d=\infty$ formalism, the $\mathbf{k}$ dependence of F will be only through $\epsilon_{\mathbf{k}}$, so that only pairing states having the symmetry of the *original* lattice are possible in the limit of $d=\infty$. This can be shown using the absence of vertex corrections to the pair susceptibility (Sec. IV) for pairing states with a different symmetry (Jarrell and Pruschke, 1993a). Pairing with a different symmetry, such as d wave, requires an extension of the LISA formalism to self-consistent clusters, see Sec. IX). However, the *time dependence* of F can be highly nontrivial, which is in fact expected to be crucial for models with repulsive interactions. The underlying physical idea is that on-site *equal-time* pairing is likely to be strongly suppressed in the presence of a strong on-site repulsion, but that pairing involving a time-lag between the members of a pair may occur. This idea dates back to Berezinskii's proposal (Berezinskii, 1974) for triplet pairing in ^{3}He, a generalization of which has been recently considered for cuprate superconductors by Balatsky and Abrahams (1992).

In the presence of a nonzero F, it is convenient to work with Nambu spinors $\Psi_i^{+}\equiv(c_{i\uparrow}^{+},c_{i\downarrow})$—or, in Fourier space, $\Psi_{\mathbf{k}}^{+}\equiv(c_{\mathbf{k}\uparrow}^{+},c_{-\mathbf{k}\downarrow})$—and with the matrix formulation of one-particle Green's functions:

$$\hat{G}(\mathbf{k},\tau)\equiv-\langle T\Psi_{\mathbf{k}}(\tau)\Psi_{\mathbf{k}}^{+}(0)\rangle$$
$$=\begin{pmatrix}G(\mathbf{k},\tau) & F(\mathbf{k},\tau)\\ F(\mathbf{k},\tau)^* & -G(-\mathbf{k},-\tau)\end{pmatrix}. \tag{99}$$

With these notations, the kinetic term of the Hubbard Hamiltonian reads $-\Sigma_{\langle ij\rangle}t_{ij}\Psi_i^{+}\sigma_3\Psi_j$, where σ_3 denotes the Pauli matrix. We shall first illustrate the derivation of the mean-field equations on the $z=\infty$ Bethe lattice. Following the cavity method, we integrate out fermionic

variables on all sites except a single one. The impurity action obtained in this way now reads

$$S_{\rm eff}=U\int_0^\beta d\tau\, n_\uparrow(\tau)n_\downarrow(\tau) - \int_0^\beta d\tau\int_0^\beta d\tau' \Psi^+(\tau)\mathcal{G}_0^{-1}(\tau-\tau')\Psi(\tau'), \quad (100)$$

where the self-consistency equation relating $\mathcal{G}_0$ to the interacting (matrix) Green's function of $S_{\rm eff}$ reads

$$\mathcal{G}_0^{-1}(i\omega_n)=i\omega_n+\mu\sigma_3-t^2\sigma_3\hat{G}(i\omega_n)\sigma_3. \quad (101)$$

We can account for an externally applied dynamic pairing field on all sites in the original lattice problem by adding a forcing term $\Delta(i\omega_n)$ to the off-diagonal components of the right-hand side of Eq. (101).

For an arbitrary lattice, the impurity action keeps the same form, and we introduce a matrix self-energy:

$$\mathcal{G}_0^{-1}-\hat{G}^{-1}=\begin{pmatrix}\Sigma(i\omega_n) & S(i\omega_n)\\ S(i\omega_n) & -\Sigma(i\omega_n)^*\end{pmatrix}. \quad (102)$$

$S(i\omega_n)$ contains information on the time dependence of the pairing. Here and in the following, we have assumed that the symmetry of the pairing is such that the off-diagonal self-energy obeys: $S(i\omega_n)=S(-i\omega_n)^*$. The lattice Green's function reads, in matrix form,

$$\hat{G}^{-1}(\mathbf{k},i\omega_n) =\begin{pmatrix} i\omega_n+\mu-\epsilon_{\mathbf{k}}-\Sigma(i\omega_n) & -S(i\omega_n)\\ -S(i\omega_n) & i\omega_n-\mu+\epsilon_{\mathbf{k}}+\Sigma(i\omega_n)^*\end{pmatrix}. \quad (103)$$

The self-consistency equation is obtained by requiring that the impurity Green's function coincides with the on-site Green's function of the lattice. This yields the relations

$$G(i\omega_n)=\int_{-\infty}^{+\infty} d\epsilon\, D(\epsilon)\,\frac{\zeta^*-\epsilon}{|\zeta-\epsilon|^2+S^2},$$

$$F(i\omega_n)=-S(i\omega_n)\int_{-\infty}^{+\infty} d\epsilon\, D(\epsilon)\,\frac{1}{|\zeta-\epsilon|^2+S^2} \quad (104)$$

with $\zeta\equiv i\omega_n+\mu-\Sigma(i\omega_n)$ as above.

The impurity action (100) describes an Anderson impurity in a superconducting medium. This model is thus the effective local model associated with the superconducting state of a strongly correlated system. Since this problem is known to be highly nontrivial, even with static pairing, we may expect that the self-consistent solution of Eqs. (104) will allow for very intricate densities of states.

The existence of superconducting phases in concrete models is only beginning to be explored. Odd and even frequency pairing is absent in the single-band Hubbard model (Jarrell and Pruschke, 1993a). Some hints that the *two-band* Hubbard model may have a stable superconducting phase were reported by Georges, Kotliar, and Krauth (1993) and Caffarel and Krauth (1994).

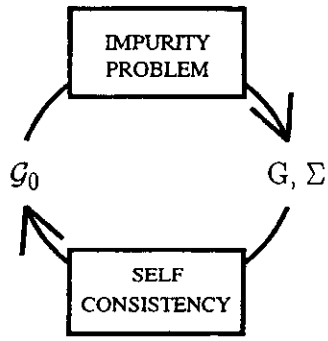

FIG. 9. All methods of solution of the coupled LISA equations involve going through the iteration schematically depicted here. Given $\mathcal{G}_0$, a local interacting Green's function G is obtained by solving the impurity model. This function is used in the self-consistency condition to produce a new bath Green's function $\mathcal{G}_0$. This loop is iterated until a converged set $(G, \mathcal{G}_0)$ is reached.

VI. METHODS OF SOLUTION

As explained in the previous sections, lattice models of correlated fermions can be mapped, in the limit of infinite coordination number, onto a single-impurity model which has to satisfy a self-consistency condition. This condition specifies, for a given lattice, the relation between the Weiss function $\mathcal{G}_0$ (entering the impurity model effective action) and the local Green's function G. On the other hand, G itself is obtained by solving the effective impurity model. Hence, we have a coupled problem to solve for both G and $\mathcal{G}_0$. In practice, all methods deal with this coupled problem in an *iterative* manner: the local Green's function is obtained by solving the impurity effective action given a $\mathcal{G}_0$ (in the first step a guess for $\mathcal{G}_0$ is used). Then, the calculated G (and the self-energy Σ) is used as an input into the self-consistency condition to produce a new Weiss function $\mathcal{G}_0$. The process is iterated until a converged solution $(G,\mathcal{G}_0)$ is reached (Fig. 9). Knowing this converged solution, all $\mathbf{k}$-dependent response functions can be constructed from the impurity model response functions, along the lines of Sec. IV.

To be definite, we concentrate in this section on the case in which the impurity model effective action has the form given by Eq. (6):

$$S_{\rm eff}=-\int_0^\beta d\tau\int_0^\beta d\tau'\sum_\sigma c_\sigma^+(\tau)\mathcal{G}_0^{-1}(\tau-\tau')c_\sigma(\tau') + U\int_0^\beta d\tau\, n_\uparrow(\tau)n_\downarrow(\tau) \quad (105)$$

that corresponds to the local site of the single-impurity Anderson model. In the LISA framework, the $\{c,c^+\}$ operators are associated with a local fermionic variable of the lattice problem.

The most difficult step in the iterative procedure is the repeated solution of the impurity model, for an essentially arbitrary $\mathcal{G}_0$ (i.e., an arbitrary conduction electron effective bath). Even though spatial degrees of freedom

have been eliminated, the impurity model remains a true many-body problem. It is crucial to use *reliable* methods to handle it. Fortunately, quantum impurity models have been studied for over thirty years, and several techniques are available. In this section we review some of these techniques along with some recently developed ones. In particular, we describe in detail a general numerical method which is based on the exact diagonalization of small clusters. We then describe a projective technique, inspired by the renormalization-group method for impurity models, which can be applied to problems with a separation of energy scales.

In contrast to the solution of the single-impurity problem, the implementation of the self-consistency condition in the numerical methods is relatively straightforward. Even though no rigorous proof exists concerning the convergence of the iterative process, practice has shown that it is usually not difficult to reach a self-consistent solution of the LISA equations. Convergence is usually attained after a few iterations. Close to transition points one encounters critical slowing down of the convergence (in the broken symmetry phase) which can however be easily overcome by standard accelerated convergence methods.

This section is organized as follows: we first describe in Sec. VI.A two numerical techniques. These methods are based on a quantum Monte Carlo method and an exact diagonalization solution of the effective impurity problem, and are discussed in full detail. Section VI.A.4 is devoted to the discussion of the problem of the analytic continuation of data from the imaginary to the real axis, which is relevant for some numerical techniques, most notably, the quantum Monte Carlo method. In Sec. VI.A.5, we discuss the calculation of susceptibilities and vertex functions. In Sec. VI.B we review various analytical approximate methods. Among these we devote special attention to the iterated perturbation theory method (Georges and Kotliar, 1992) that is based on the perturbation theory for impurity problems of Yosida and Yamada (1970, 1975). In Sec. VI.C we describe a projective method which allows the detailed solution of problems with separation of energy scales.

The reader is not assumed to have any previous knowledge of the algorithms, which will be thoroughly described in this section. Moreover, we provide with this article a FORTRAN library of programs. The directions to obtain these programs via the internet are explained in Appendix D.

A. Numerical solutions

In this section we review two techniques, the quantum Monte Carlo (QMC) and the exact diagonalization. Both are fully numerical in the sense that the only approximation that is used is a discretization of the mean-field equations. Both methods, when extrapolated to the limit of vanishing discretization, give the exact answer to the problem.

The numerical schemes applied to the LISA equations involve a *discrete* parametrization of the Green's function, and the Weiss field $\mathcal{G}_0$, through a finite number N_P of parameters. This reduces the system of functional equations to a system of N_P nonlinear equations in N_P unknowns. The hope is that as N_P increases, physical quantities converge relatively quickly to their physical values so that the $N_P \to \infty$ value can be inferred by extrapolating results obtained from a finite (and usually small) number of parameters N_P.

We quickly characterize the two numerical techniques and then turn to a detailed description:

(i) The quantum Monte Carlo (QMC) method, and more specifically, the Hirsch-Fye (1986) algorithm considers the single-impurity problem in *discretized imaginary time*. The effective bath only enters through $\mathcal{G}_0$, and there is no need to discretize the conduction band. The first numerical solutions of the LISA equations using this QMC method were obtained independently by Jarrell (1992), Rozenberg, Zhang, and Kotliar (1992), and Georges and Krauth (1992; see also Jarrell, Akhlaghpour, and Pruschke, 1993b).

(ii) The exact diagonalization method (Caffarel and Krauth, 1994; Rozenberg, Moeller, and Kotliar, 1994; Si *et al.*, 1994). In this method, the single-impurity problem is solved exactly with an effective bath that is approximated by a few orbitals only. This introduces a *parametrization* of the effective bath. The parameters correspond to the site energies and hopping amplitudes of the fictitious electrons and to an appropriate choice of the geometry of their connections. Obviously, many different geometries of the electronic bath are possible (cf. Fig. 10). It is the physical insight on a particular problem that indicates the most appropriate choice, which allows one to determine an appropriate parametrization. The number of orbitals that one can effectively treat is severely limited by the size of an exponentially growing Hilbert space. In spite of this limitation, it turns out that the freedom associated with the parametrization more than makes up for the limitations. This freedom concerns the geometry of the electronic bath, and the physical parameters of the orbitals—the site energies and hopping amplitudes. As a consequence, the exact diagonalization algorithm has proven to be very powerful, and in our opinion, clearly superior to the Monte Carlo method.

1. Quantum Monte Carlo method

a. Introduction: A heuristic derivation

The most successful Quantum Monte Carlo method for solving a general impurity problem is due to Hirsch and Fye (1986). Before embarking on a rigorous and self-contained derivation of their method, we describe in this section the algorithm taking a rather different, though less rigorous, approach for the sake of an intuitive understanding of the key ingredients of this method. The method is concerned with the calculation of the local Green's function at finite temperature, which was first introduced in Eq. (8).

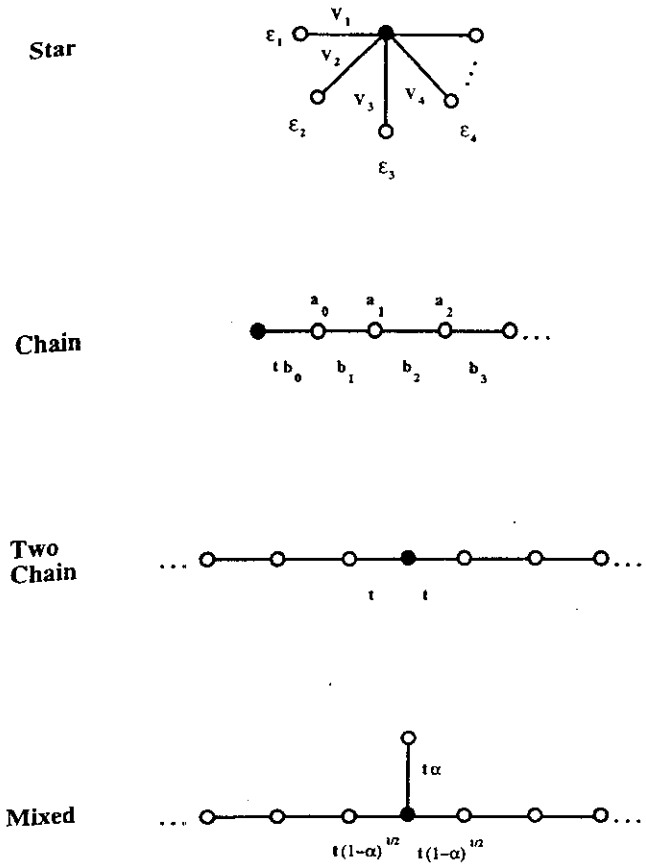

FIG. 10. Various possible geometries used to represent the effective conduction bath in the exact diagonalization algorithm.

(i) The basic principle of the method can be understood as a discretization of the impurity model effective action, Eq. (105):

$$S_{\rm eff} \rightarrow \sum_{\tau\tau'\sigma} c_\sigma^+(\tau)\mathcal{G}_0^{-1}(\tau,\tau')c_\sigma(\tau') + U\sum_\tau n_\uparrow(\tau)n_\downarrow(\tau), \tag{106}$$

where the imaginary time is discretized in L "slices" $\tau=1,2,\ldots,L$ of size $\Delta\tau$, and the timestep $\Delta\tau$ is defined by $\beta=L\Delta\tau$.

(ii) The remaining quartic term can be decoupled using a discrete Hubbard-Stratonovich transformation (Hirsch, 1983):

$$e^{-\Delta\tau U n_\uparrow n_\downarrow + (\Delta\tau U/2)(n_\uparrow + n_\downarrow)} = \frac{1}{2}\sum_{s=\pm 1} e^{\lambda s(n_\uparrow - n_\downarrow)}, \tag{107}$$

where $\lambda=\text{arccosh}\,(e^{\Delta\tau U/2})$ and the discrete field s is an Ising-like variable taking the values ± 1. Performing this transformation at every time slice, we are led to a quadratic action, and the partition function becomes

$$Z = \sum_{s_\tau=\pm 1} \int D[c,c^+]\exp\left\{-\sum_{\tau\tau'} c_\sigma^+(\tau)\mathcal{G}_0^{-1}(\tau,\tau')c_\sigma(\tau') + \lambda\sum_\tau s_\tau[n_\uparrow(\tau)-n_\downarrow(\tau)]\right\} \tag{108}$$

with

$$G_\sigma^{-1}(\tau_l,\tau_{l'}) \equiv \mathcal{G}_{0\sigma}^{-1}(\tau_l,\tau_{l'}) + \sigma\lambda s_l \delta_{l,l'+1} \tag{109}$$

the inverse propagator for a particular realization of the Ising spins $(s_1,\ldots,s_L)$. The antiperiodic delta function is defined by $\delta_{l,l'+1}=1$ if $l=l'+1, l=2,\ldots,L-1$, $\delta_{l,l'+1} = -1$ if $l=1, l'=L$, and is zero otherwise. Its origin is in the proper time ordering of the creation and destruction operators (Blankenbecler, Scalapino, and Sugar, 1981). In the actual implementation of the algorithm, Eq. (109) is replaced by

$$G^{-1}_{\sigma,(s_1,\ldots,s_L)}(\tau,\tau') \equiv \mathcal{G}_{0\sigma}^{-1}(\tau,\tau')e^V + e^V - 1, \tag{110}$$

where e^V is the diagonal matrix with elements $e^V(\tau,\tau) = e^{\sigma\lambda s_\tau}$. This choice of discretization results from the rigorous derivation in Sec. VI.A.1.b following the original Hamiltonian formulation of Hirsch and Fye (1986).

(iii) The replacement of a quartic term for an extra summation on the auxiliary Ising variables $(s_1,\ldots,s_L)$ renders the action quadratic and allows us to apply Wick's theorem at each time slice. We can now perform the Gaussian integration of the Grassmann variables, to obtain

$$Z = \sum_{\{s_1,\ldots,s_L\}} \det[G_\uparrow^{-1}(s_1,\ldots,s_L)]\det[G_\downarrow^{-1}(s_1,\ldots,s_L)]. \tag{111}$$

In principle, the trace over the auxiliary field gives the full interacting Green's function:

$$G_\sigma = \frac{1}{Z}\sum_{\{s_1,\ldots,s_L\}} \det[G_\uparrow^{-1}(s_1,\ldots,s_L)] \times \det[G_\downarrow^{-1}(s_1,\ldots,s_L)]G_\sigma(s_1,\ldots,s_L); \tag{112}$$

this requires the sum over 2^L configurations. Each term in the sum (112) involves the inversion of an $L\times L$ matrix as is clear from Eq. (110). In practice, the full trace can only be performed for small values of L.

(iv) Usually, the interacting Green's function is therefore calculated by stochastic Monte Carlo sampling: the term $\det[G_\uparrow^{-1}(s_1,\ldots,s_L)]\det[G_\downarrow^{-1}(s_1,\ldots,s_L)]$ in Eq. (112) is interpreted as a stochastic weight, and configurations $(s_1,\ldots,s_L)$ are generated by a Markov process with a probability corresponding to their statistical weight.

(v) The Markov process visits configurations of Ising variables $(s_1,\ldots,s_L)$ with a single spin-flip dynamic, in which a possible movement consists in $(s_1,s_2,\ldots,s_k,\ldots,s_L)\rightarrow(s_1,s_2,\ldots,-s_k,\ldots,s_L)$. The formulas given in Sec. VI.A.1.b will allow a rapid calculation of the change in statistical weight, and of the new Green's function for a single spin-flip change.

b. The Hirsch-Fye algorithm: Rigorous derivation

The above derivation leaves us with the impression that there are two discretizations involved: the one of the bath Green's function, and the subsequent discretization of the functional integral. Using a Hamiltonian description of the general Anderson impurity model one

can show (Hirsch and Fye, 1986) that only a single well-defined discretization of the partition function needs to be performed (given by the Trotter breakup). Green's functions corresponding to this discretized partition function can be defined naturally (with the help of the transfer operators). Then, the decoupling using the binary Ising field is performed, and Equation (110) appears as an (exact) Dyson equation relating different discretized Green's functions.

This section is intended mainly for the reader interested in a detailed understanding of the algorithm [this reader should also realize that, in accordance with the *entire* QMC literature, we define in this section temporal Green's functions *without* the minus sign in Eq. (8)]. In order to make it self-contained, the section is accompanied by Appendix B which contains mest derivations.

We temporarily introduce the Hamiltonian description of the local impurity problem, which permits a local-in-time description of the partition function. In order to preserve the standard notations for this model, the impurity orbital (that is associated with a local degree of freedom of the original lattice) will be taken as a d orbital in this section. The conduction bath orbitals are numbered from $p=2,\ldots,n_s$, and the impurity orbital is equivalently denoted by $a_{1\sigma}\equiv d_\sigma$, i.e., corresponds to $p=1$. The Hamiltonian of a general Anderson impurity model reads

$$\mathscr{H}=\sum_{p\geq 2,\sigma}\tilde{\epsilon}_p a^+_{p\sigma}a_{p\sigma}+\sum_{p\geq 2,\sigma}V_p(a^+_{p\sigma}d_\sigma+d^+_\sigma a_{p\sigma}) +\epsilon_d\sum_\sigma d^+_\sigma d_\sigma+Un_{d\uparrow}n_{d\downarrow}. \tag{113}$$

It is written as a sum of terms $\mathscr{H}=\mathscr{H}^0+\mathscr{H}^i$, where $\mathscr{H}^0$ is quadratic in the fermion operators:

$$\mathscr{H}^0\equiv\sum_{p\geq 2,\sigma}\tilde{\epsilon}_p a^+_{p\sigma}a_{p\sigma}+\sum_{p\geq 2,\sigma}V_p(a^+_{p\sigma}d_\sigma+d^+_\sigma a_{p\sigma}) +(\epsilon_d+U/2)\sum_\sigma n_{d\sigma}, \tag{114}$$

whereas $\mathscr{H}^i$ is the interaction term:

$$\mathscr{H}^i=U[n_{d\uparrow}n_{d\downarrow}-\tfrac{1}{2}(n_{d\uparrow}+n_{d\downarrow})]. \tag{115}$$

As in Sec. VI.A.1.a, the imaginary time interval $[0,\beta]$ is now discretized into L time slices, but on the level of the original Hamiltonian $\mathscr{H}$. With $\tau_l=l\Delta\tau$, with $l=1,\ldots,L$ and $\Delta\tau\equiv\beta/L$, the partition function is written as

$$Z=\mathrm{Tr}\,e^{-\beta\mathscr{H}}=\mathrm{Tr}\prod_{l=1}^{L}e^{-\Delta\tau[\mathscr{H}^0+\mathscr{H}^i]} \tag{116}$$

Using the Trotter breakup: $\exp[-\Delta\tau(\mathscr{H}^0+\mathscr{H}^i)]\simeq\exp(-\Delta\tau\mathscr{H}^0)\exp(-\Delta\tau\mathscr{H}^i)$, Z can be approximated by the discretized partition function:

$$Z\simeq Z^{\Delta\tau}\equiv\mathrm{Tr}\prod_{l=1}^{L}e^{-\Delta\tau\mathscr{H}^0}e^{-\Delta\tau\mathscr{H}^i}. \tag{117}$$

Green's functions corresponding to $Z^{\Delta\tau}$ can be defined analogously, by using $U_{\Delta\tau}\equiv\exp(-\Delta\tau\mathscr{H}^0)\exp(-\Delta\tau\mathscr{H}^i)$ as an evolution operator between time slices:

$$g^{\Delta\tau}_{p_1,p_2}(\tau_{l_1},\tau_{l_2})\equiv\langle a_{p_1}(\tau_{l_1})a^+_{p_2}(\tau_{l_2})\rangle =\frac{\mathrm{Tr}U^{L-l_1}_{\Delta\tau}a_{p_1}(\tau_{l_1})U^{l_1-l_2}_{\Delta\tau}a^+_{p_2}(\tau_{l_2})U^{l_2}_{\Delta\tau}}{\mathrm{Tr}\,U^L_{\Delta\tau}} \quad (\text{for } l_1>l_2) \tag{118}$$

(and similarly for $l_1<l_2$). It is important to understand that the object $g^{\Delta\tau}$ will be obtained essentially exactly: The only systematic error of the QMC method will consist in the replacement of $\exp(-\Delta\tau\mathscr{H})$ by $U_{\Delta\tau}$ as an evolution operator between time slices. We are then ultimately interested in the d-site Green's function, which we denote by a capital letter $G^{\Delta\tau}(\tau_{l_1},\tau_{l_2})\equiv g^{\Delta\tau}_{1,1}(\tau_{l_1},\tau_{l_2})$.

After the decoupling of $\mathscr{H}^i$ by the transformation Eq. (102)

$$\exp[-\Delta\tau\mathscr{H}^i]=\frac{1}{2}\sum_{s=\pm1}\exp[\lambda s(n_{d\uparrow}-n_{d\downarrow})], \qquad \cosh(\lambda)\equiv\exp(\Delta\tau U/2) \tag{119}$$

and after inserting Eq. (119) into Eq. (117), the partition function $Z^{\Delta\tau}$ is reduced to

$$Z^{\Delta\tau}=\frac{1^\sigma}{2^L}\sum_{s_1,\ldots,s_L=\pm1}Z^{\Delta\tau}_{s_1,\ldots,s_L} \tag{120}$$

with

$$Z^{\Delta\tau}_{s_1,\ldots,s_L}=\prod_{\sigma=\pm1(=\uparrow,\downarrow)}\mathrm{Tr}e^{-\Delta\tau\mathscr{H}^0}e^{V^\sigma(s_1)} \times e^{-\Delta\tau\mathscr{H}^0}e^{V^\sigma(s_2)}\cdots e^{-\Delta\tau\mathscr{H}^0}e^{V^\sigma(s_L)}. \tag{121}$$

In Eq. (121), the $n_s\times n_s$ matrix $V^\sigma(s)$ is diagonal with

$$e^{V^\sigma(s)}=\begin{pmatrix} e^{\lambda\sigma s} & \cdots & \cdots & 0\\ \cdots & 1 & \cdots & \cdots\\ \cdots & \cdots & 1 & \cdots\\ 0 & \cdots & \cdots & 1\end{pmatrix}. \tag{122}$$

An important observation is that $Z^{\Delta\tau}_{s_1,\ldots,s_L}$ can be written as $Z^{\Delta\tau}_{s_1,\ldots,s_L}=\det\mathscr{O}_{s_1,\ldots,s_L}$ (cf. Appendix B), with the $n_sL\times n_sL$ matrix

$$\mathscr{O}_{s_1,\ldots,s_L}=\begin{pmatrix} 1 & 0 & \cdots & 0 & B(s_L)\\ -B(s_1) & 1 & \cdots & \cdots & 0\\ 0 & -B(s_2) & 1 & \cdots & \cdots\\ \cdots & \cdots & \cdots & 1 & 0\\ \cdots & \cdots & \cdots & -B(s_{L-1}) & 1\end{pmatrix}, \tag{123}$$

where $B(\sigma s)\equiv\exp[-\Delta\tau\mathscr{H}^0]\exp[V^\sigma(s)]$, and $\mathscr{O}$ has been written as an $L\times L$ matrix of $n_s\times n_s$ matrices [$\mathscr{O}$

$\equiv \mathscr{C}_{\{i_l,i_s\},\{i_l',i_s'\}}$ with $i_l=1,\ldots,L$ and $i_s=1,\ldots,n_s$]. $\mathscr{C}$ is related to the discretized Ising-spin dependent Green's function by the identity (cf. Appendix B)

$$g^{\Delta\tau}_{s_1,\ldots,s_L}=\mathscr{C}^{-1}_{s_1,\ldots,s_L}. \tag{124}$$

The matrix $\mathscr{C}_{s_1,\ldots,s_L}$ is large (of size $n_sL\times n_sL$), but it need not be manipulated explicitly, as will be shown below.

The crucial fact noted by Hirsch and Fye is that the Green's functions for two different Ising spin configurations, $(s_1,\ldots,s_L)$ and $(s_1',\ldots,s_L')$, are related to each other by a Dyson equation (also derived in Appendix B). Abbreviating $g\equiv g^{\Delta\tau}_{s_1,\ldots,s_L}$ and $g'\equiv g^{\Delta\tau}_{s_1',\ldots,s_L'}$, etc, this Dyson equation reads

$$g'=g+(g-1)(e^{V'-V}-1)g'. \tag{125}$$

This equation brings us back to the description of the impurity problem given in paragraph (a). In fact, Eq. (125) relates two Green's functions g and g' via a projection operator on the d site, namely $[\exp(V'-V)-1]$

$$[\exp(V'-V)-1]_{\{i_l,i_s\},\{i_l',i_s'\}}\propto\delta_{i_l,i_l'}\delta_{i_s,1}\delta_{i_s',1}. \tag{126}$$

The presence of this projection operator comes from the possibility of integrating out the conduction band. As a consequence, the Dyson equation Eq. (125) directly relates the Green's functions on the d site one to another, and this equation remains equally valid in the subspace $i_s=1,i_s'=1$. Hence, the d site Green's functions $G^{\Delta\tau}_{s_1,\ldots,s_L}$ also satisfy

$$G'=G+(G-1)(e^{V'-V}-1)G', \tag{127}$$

viewed as an $L\times L$ matrix equation. As a first application of this Dyson equation, we use it to derive Eq. (110), which follows by putting $G'\equiv G_{s_1,\ldots,s_L}$, $G\equiv\mathscr{G}_0$. Notice that the Dyson equation allows arbitrary values for the auxiliary spins s_i.

Rearranging Eq. (125), it is straightforward to see that $G_{s_1',\ldots,s_L'}$ for an Ising configuration $(s_1',\ldots,s_L')$ can be obtained from $G_{s_1,\ldots,s_L}$ by inversion of an $L\times L$ matrix $\mathscr{A}$, defined in the following equation

$$\mathscr{A}G'=G,\quad \mathscr{A}\equiv 1+(1-G)[e^{V'-V}-1]$$

(any two configurations). (128)

In the special case in which $(s_1',\ldots,s_L')$ differs from $(s_1,\ldots,s_L)$ by the value of a single spin, say s_l, $\mathscr{A}$ takes on a special form

$$\mathscr{A}=\begin{pmatrix} 1 & 0 & \mathscr{A}_{1l} & 0 & \cdots \\ 0 & 1 & \mathscr{A}_{2l} & \cdots & \cdots \\ \cdots & 0 & \mathscr{A}_{ll} & \cdots & \cdots \\ \cdots & \cdots & \cdots & 1 & 0 \\ \cdots & \cdots & \mathscr{A}_{Ll} & 0 & 1 \end{pmatrix}. \tag{129}$$

In that case, $\det\mathscr{A}=\mathscr{A}_{ll}=1+(1-G_{ll})[\exp(V_l'-V_l)-1]$. Expanding $\mathscr{A}^{-1}$ in minors, it can easily be seen that $(\mathscr{A}^{-1})_{lk}=0$ for $k\neq l$. In that case Eq. (128) simplifies to

$$G'_{l_1l_2}=G_{l_1l_2}+(G-1)_{l_1l}e^{V'-V}(\mathscr{A}_{ll})^{-1}G_{ll_2}$$

(single flip), (130)

which is a special case of a Sherman-Morrison formula (cf. Press *et al.*, 1991). Equation (125) can also be used to show that

$$\frac{\det\mathscr{C}'}{\det\mathscr{C}}=\frac{\det G}{\det G'}$$

$$=\det\mathscr{A}=1+(1-G_{ll})[\exp(V_l'-V_l)-1] \tag{131}$$

It is remarkable that all the Eq. (127)–(131) express *exact* relations between discretized Green's functions $G^{\Delta\tau}$. The only error committed is related to the Trotter breakup [cf. Eq. (121)]. Further comments on this discretization error can be found in Appendix B.

c. Implementation of the Hirsch-Fye algorithm

We can now assemble the essential ingredients of the Hirsch-Fye algorithm:

(1) The calculation starts from the Green's function $G^{\Delta\tau}_{s_1,\ldots,s_L}(\tau_i,\tau_j)$, with all Ising spins formally set to $s_1=\cdots=s_L=0$. In the LISA context, $G^{\Delta\tau}_{s_1=0,\ldots,s_L=0}(\tau_i-\tau_j)$ is a discretized version $\mathscr{G}_0^{\Delta\tau}$ of the Weiss function $\mathscr{G}_0$, which generally has been determined in the previous iteration by the self-consistency condition (whose implementation will be discussed shortly). At the first step of the iteration, an initial guess is made for $\mathscr{G}_0^{\Delta\tau}$.

(2) The Green's function $G^{\Delta\tau}_{s_1,\ldots,s_L}(\tau_l,\tau_{l'})$ for an arbitrary initial configuration with $s_1=\pm1\cdots s_L=\pm1$ is calculated by explicit inversion of the matrix $\mathscr{A}$ in Eq. (128).

(3) From then on, configurations are visited using single spin flips. In that case, Green's functions can be updated using Eq. (130) (every so often, one checks that the precision has not degraded by doing a complete update as indicated above).

(4) Physical Green's functions $G^{\Delta\tau}(\tau_l-\tau_{l'})$ are determined as averages of the configuration-dependent functions $G^{\Delta\tau}_{s_1,\ldots,s_L}(\tau_l,\tau_{l'})$ with the Ising spin configurations weighted according to Eq. (131).

The last point may benefit from some additional remarks. From Eqs. (118) and (120), it is easily seen that the physical Green's function is given by

$$G^{\Delta\tau,\uparrow\downarrow}(\tau_l,\tau_{l'})$$

$$=\frac{\Sigma_{s_1,\ldots,s_L}\Pi_{\sigma=\pm1}\det\mathscr{O}(\sigma)_{s_1,\ldots,s_L}\mathscr{C}^{-1}(\uparrow\downarrow)_{s_1,\ldots,s_L}(\tau_l,\tau_{l'})}{\Sigma_{s_1,\ldots,s_L}\Pi_{\sigma=\pm1}\det\mathscr{O}(\sigma)_{s_1,\ldots,s_L}} \tag{132}$$

[in order to be explicit, we have reintroduced the dependence on physical spin in Eq. (132)]. If a complete enumeration of Ising spin configurations is possible, the Green's function can be readily evaluated using this formula. It is advisable in this case (Georges and Krauth, 1993) to perform this enumeration using the so-called Gray code, which allows enumerating all the configurations of the Ising spins via single spin flips (cf. Appendix

B). The Gray code enumeration of Eq. (132) produces *numerically exact* results for $G^{\Delta\tau}$.

In a Monte Carlo simulation, Ising spin configurations are generated with a probability proportional to $\det\mathcal{O}^{\dagger}\det\mathcal{O}$, and the physical Green's function $G^{\Delta\tau}$ is then given from Eq. (132) as an average of $G^{\Delta\tau}_{s_1,\ldots,s_L}$ with this measure. As usual, there is some freedom in the choice of the Monte Carlo dynamics, which must, however, satisfy the detailed balance property:

$$\frac{P(s\to s')}{P(s'\to s)}=\frac{\Pi_\sigma \det\mathcal{O}(\sigma)_{s'}}{\Pi_\sigma \det\mathcal{O}(\sigma)_s}. \tag{133}$$

Both the heat-bath and the Metropolis dynamics satisfy this condition:

$$P(s\to s')=\frac{\Pi_\sigma \det\mathcal{O}(\sigma)_{s'}}{[\Pi_\sigma \det\mathcal{O}(\sigma)_{s'}+\Pi_\sigma \det\mathcal{O}(\sigma)_s]} \quad \text{(Heat bath)}, \tag{134}$$

$$P(s\to s')=\begin{cases} 1 & \text{if } \Pi_\sigma \det\mathcal{O}(\sigma)_{s'}>\Pi_\sigma \det\mathcal{O}(\sigma)_s \\ \dfrac{\Pi_\sigma \det\mathcal{O}(\sigma)_{s'}}{\Pi_\sigma \det\mathcal{O}(\sigma)_s} & \text{otherwise} \end{cases} \quad \text{(Metropolis)}. \tag{135}$$

In both cases, the transition probability is a function of the ratio of determinants, which can be computed easily [cf. Eq. (131)] with a computational effort of $O(1)$. If the move $s\to s'$ is accepted, $G^{\Delta\tau}_{s_1,\ldots,s_L}$ is updated with a computational burden of $O(L^2)$, using Eq. (130). The computational effort is thus large for each *accepted* move only. This fact renders the simulation rather insensitive to the problem of small acceptance probabilities. Notice also that the physical Green's function $G^{\Delta\tau}$ is translation invariant in time $G^{\Delta\tau}(\tau_i,\tau_j)=G^{\Delta\tau}(\tau_i-\tau_j)$, a property which the Ising spin dependent quantities $G^{\Delta\tau}_{s_1\cdots s_L}$ lack. This property can be used to reduce statistical noise. We also note that the fermionic sign problem plays no role in any of the calculations. The determinants in Eq. (133) generally have the same sign, and their ratio can be interpreted as a ratio of probabilities.

d. The LISA-QMC algorithm and a practical example

The Hirsch-Fye algorithm is remarkably stable, and a full-size program (such as the program LISAQMC.F provided with this article) can be written relatively easily. The only problem consists in reducing the statistical uncertainties as much as possible, since $G^{\Delta\tau}(\tau_l-\tau_{l'})$ is needed as an input for the self-consistency condition at the next iteration step.

The numerical implementation of this condition—the second building block of the full QMC-LISA algorithm—is contained in the program LISASELF.F also provided with this article. The self-consistency condition is expressed in terms of the Fourier-transformed Green's functions $G(i\omega_n)$ and $\mathcal{G}_0(i\omega_n)$. The direct Fourier transform (FT)—say, calculated by a standard fast Fourier transform (FFT) algorithm—is not applicable here, since the periodicity of $G^{\Delta\tau}(\tau_l)$ would imply that its FFT is a *periodic* function of $i\omega_n$, rather than show the correct asymptotic behavior $G(i\omega_n)\sim 1/i\omega_n$ for large arguments. As detailed in Appendix B, it is more convenient to calculate $G(i\omega_n)$ as the Fourier transform of a (linear or spline) interpolation of $G^{\Delta\tau}(\tau_i)$, with due care paid to the discontinuity of the Green's function at $\tau=0$. Finally, we also need to perform inverse Fourier transforms (IFT), from the Matsubara frequency to imaginary time. Again, we do not use the FFT for this purpose, since L, the number of τ values, is usually very much smaller than the number $n_{\max}$ of frequencies (typical values are $L\sim 64,128$ and $n_{\max}\sim 2^{13}$).

We have now described all the ingredients required to set up the full QMC algorithm for the iterative solution of the LISA equations. One loop of this iteration consists in two steps. In the first step, the self-energy $\Sigma(i\omega_n)$ is computed by performing the following operations:

$$\mathcal{G}_0(\tau)\to\left\{\begin{array}{ll} \xrightarrow{\text{Hirsch-Fye}} G(\tau) & \xrightarrow{\text{FT}} G(i\omega_n) \\ \xrightarrow{\text{FT}} & \mathcal{G}_0(i\omega_n) \end{array}\right\}\to\Sigma(i\omega_n)$$
$$\equiv \mathcal{G}_0(i\omega_n)^{-1}-G(i\omega_n)^{-1}. \tag{136}$$

The self-energy determined in Eq. (136) is then used for the computation of a "new" Green's function by evaluating the Hilbert transform:

$$G^{\text{new}}(i\omega_n)=\int_{-\infty}^{+\infty} d\epsilon\,\frac{D(\epsilon)}{i\omega_n+\mu-\Sigma(i\omega_n)-\epsilon}. \tag{137}$$

From $G^{\text{new}}(i\omega_n)$, the self-consistency loop is then closed as follows:

$$G^{\text{new}}(i\omega_n)\xrightarrow{\mathcal{G}_0^{-1,\text{new}}=G^{-1}+\Sigma}\mathcal{G}_0^{\text{new}}(i\omega_n)\xrightarrow{\text{IFT}}\mathcal{G}_0^{\text{new}}(\tau). \tag{138}$$

The reader may find additional technical comments in the programs LISAQMC.F and LISASELF.F implementing these various steps. Directions to obtain the FORTRAN codes may be found in Appendix D.

The self-consistency loop in Eqs. (136) and (138) is iterated until a converged solution $(G,\mathcal{G}_0)$ is reached. It is remarkable that the process actually converges in almost all cases that have been considered so far. Occasionally, simple cycles appear. To avoid the cycles it is generally sufficient to use $[\mathcal{G}_0(\tau)+\mathcal{G}_0^{\text{new}}(\tau)]/2$ instead of $\mathcal{G}_0^{\text{new}}(\tau)$ in Eq. (138). A direct implementation of the self-consistency loop does however not *always* converge. A counter example is the Hubbard model in a magnetic field close to the Mott transition. The solution to the convergence problem in this case is described in Laloux *et al.* (1994).

As a practical illustration of the LISA-QMC algorithm, we invite the reader to perform the computation of Green's functions for the half-filled Hubbard model with a semicircular density of states for $U=3(D/\sqrt{2})$ and $\beta D/\sqrt{2}=6,8,\ldots,16$. As will be discussed in Sec. VII, for this choice of parameters solutions with and without long range magnetic order may be obtained. To select the paramagnetic solution it suffices to enforce the sym-

metry of spin by averaging the spin up and down Green's functions entering the self-consistency condition. On the other hand, to obtain solution with magnetic order one must include a small difference in the initial guess for $\mathcal{G}_{0\sigma}$.

Using the programs LISAQMC.F and LISASELF.F provided with this paper, it is a simple matter to reproduce the results given in Fig. 11. Another simple calculation consists in reproducing the results of Fig. 14, which will be compared to the exact diagonalization results for the same values of the parameters in Sec. VI.A.3.

e. Relationship with other QMC algorithms

Historically, the first applications of Quantum Monte Carlo methods to impurity models did not use the Hirsch-Fye algorithm, but the original method for performing QMC calculations for lattice fermions, which is due to Blankenbecler, Scalapino, and Sugar (1981). The two methods are very closely related: The Blankenbecler, Scalapino, and Sugar algorithm simply computes the determinant of $\mathcal{O}_{s_1,\ldots,s_L}$, as follows:

$$Z^{\Delta\tau}_{s_1,\ldots,s_L} = \prod_{\sigma=\pm 1} \det[1+B(\sigma s_1)B(\sigma s_2)\ldots B(\sigma s_{L-1})B(\sigma s_L)] \equiv \prod_{\sigma=\pm 1} \det W_{s_1,\ldots,s_L}(\sigma), \tag{139}$$

which is further commented on in Appendix B. Similarly, discretized Green's functions can also be expressed in terms of the matrices B_i:

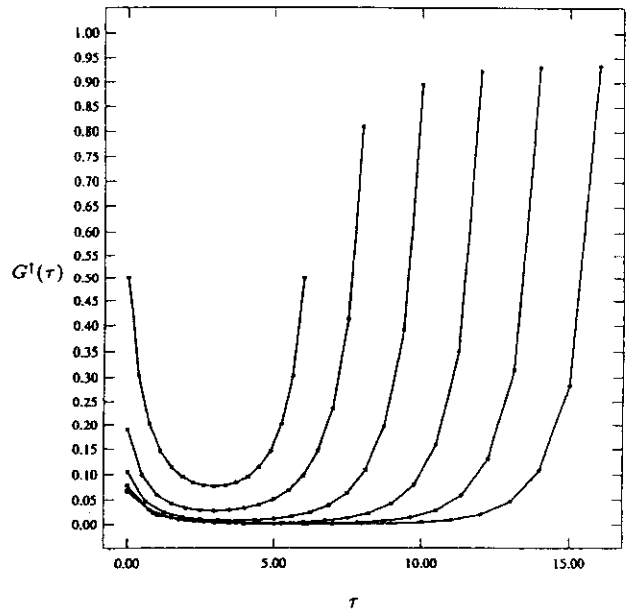

FIG. 11. Self-consistent solution $G^{\uparrow}(\tau)$ of the LISA equations for the half-filled Hubbard model (with a semicircular density of states of half-width D) at $U=3D/\sqrt{2}$ and $\beta D/\sqrt{2}$ =16,14,12,10,8,6 (bottom to top) obtained by the QMC method with $L=16$. The self-consistency condition used in this calculation allows for antiferromagnetic order, which does appear for $\beta \geq 8$ [$G^{\downarrow}(\tau)=G^{\uparrow}(\beta-\tau)$ has not been shown]. The paramagnetic solution can also be continued to larger values of β, by imposing $G^{\downarrow}=G^{\uparrow}$ and using the paramagnetic self-consistency condition (the corresponding result at $\beta D/\sqrt{2}=32$ is displayed in Fig. 14).

$$G^{\Delta\tau}_{s_1,\ldots,s_L}(\tau_l,\tau_{l'}) = \left[B(s_l)B(s_{l-1})\ldots B(s_{l'+1}) \frac{1}{1+B(s'_l)\ldots B(s_1)B(s_L)\ldots B(s_{l'+1})} \right]_{1,1} \quad (l \geq l') \tag{140}$$

[cf. Blankenbecler, Scalapino, and Sugar, (1981) for $l<l'$]. The matrices in Eqs. (139) and (140) are of size $n_s \times n_s$, independently of the number of time slices, and the determinant of $W_{s_1,\ldots,s_L}$ can be computed explicitly. Notice that in this formulation $W_{s_1,\ldots,s_L}$ is a $n_s \times n_s$ matrix, and the number of time slices is reflected solely by the number of matrices appearing in the products of Eqs. (139) and (140). Unfortunately, the product of matrices $B(s_1)B(s_2)\cdots B(s_{L-1})B(s_L)$ is usually very badly conditioned. This generates numerical instabilities that render the calculation of $\det(W_{s_1,\ldots,s_L})$ difficult in practice. As a result of the severe numerical instabilities, the early attempts to treat the single impurity problem with QMC methods (Gubernatis *et al.* 1986), which used the Blankenbecler, Scalapino, and Sugar algorithm, have met with little success. Note, however, that the more recent "balancing schemes" for the Blankenbecler, Scalapino, and Sugar algorithm (Sugiyama and Koonin, 1986; White *et al.*, 1989) have to our knowledge not been applied to impurity models, and could lead to an important improvement.

In order to avoid misunderstandings, we clarify the following: usual (finite-dimensional) QMC calculations, which apply the Blankenbecler, Scalapino, and Sugar algorithm, are haunted by two completely unrelated problems: the bad conditioning of the product of matrices $B(\sigma s_1)\cdots B(\sigma s_L)$, and the fermionic sign problem [$\det(W_{s_1,\ldots,s_L})$ may not always have the same sign]. In impurity problems, one usually encounters neither of these problems, since one is able to use a stable algorithm (Hirsch-Fye), and since the fermionic sign problem is empirically found to play no role. There are techniques—"balancing schemes"—which attempt to solve the problem of the numerical instability.

Rather than expand further on the relationship between the Hirsch-Fye and the Blankenbecler, Scalapino, and Sugar algorithm, we illustrate the above considerations on a toy example in which the Green's function $G^{\Delta\tau}_{s_1,\ldots,s_L}$ is calculated using different approaches. To this aim, a purely pedagogical test program QMCEXAMPLE.F is provided with this paper (cf. Appendices B and D). In this program, the case of an impurity coupled to a small number of conduction electron orbitals (with given values of $\tilde{\epsilon}_p, V_p$) is solved by three possible routes (with identical results):

(1) The original Blankenbecler, Scalapino, and Sugar algorithm: In that case, the two different matrices $B_i(\sigma)$ are calculated for $\sigma=\pm 1$ and the Green's function is obtained by direct matrix multiplication [cf. Eq. (140)]. The eigenvalue spectrum of the large product of matrices appearing in Eq. (139) is computed, and the numerical instabilities can be tracked explicitly.

(2) The explicit calculation of the matrix $\mathscr{O}$. Here $\det\mathscr{O}$ and $\mathscr{O}^{-1}$ are computed by standard matrix inversion. What looks like a very awkward method in this case, in which the conduction orbitals are retained, has in fact been used for calculations in lattice models because of its larger inherent stability (cf. Hirsch, 1988; White *et al.*, 1988 for an application to the two-dimensional Hubbard model).

(3) The use of the Dyson equation, following Hirsch and Fye.

Besides contributing to the reader's understanding of the auxiliary-field QMC method, and helping in the actual implementation of the Hirsch-Fye algorithm, the test can also be used in order to illustrate the numerical instabilities encountered in the Blankenbecler, Scalapino, and Sugar algorithm, which the Hirsch-Fye algorithm overcomes.

Compared to the Blankenbecler, Scalapino, and Sugar algorithm, the method of Hirsch and Fye thus not only yields a very natural numerical implementation of the impurity problem that integrates out the conduction band electrons from the beginning (i.e., allows a general Weiss field $\mathscr{G}_0$). It also presents the enormous advantage of being numerically stable at low temperature, and allows the reaching of temperatures significantly lower than the bandwidth. The remaining limitations of the Hirsch-Fye algorithm can be described as follows:

(i) Only imaginary-time (or Matsubara frequency) quantities can be obtained directly. Real-frequency calculations require analytic continuation algorithms (cf. Sec. VI.A.4).

(ii) The lowest temperatures that can be reached are limited by the number of time slices that one can handle, because the matrices to be multiplied become prohibitively large. On a present-day workstation, the computations with, let us say, 256 time slices already present a considerable investment in computer time. If the problem at hand is not altogether trivial, we may expect (and notice in fact) that the finite $\Delta\tau$ behavior is intricate, which means that we have to choose $\Delta\tau$ sensibly smaller than 1 (cf. the discussion in Appendix B). Thus, even if U is not too big, the range of accessible temperatures is limited to temperatures of the order of $\beta\simeq 30$ or smaller (in the units of the half-bandwidth D). We shall see in the next section that very accurate descriptions of the relevant impurity models, which are much more economical in the number of parameters used (256 in the present example), are possible. The condition for this is that one uses an *adaptive* discretization, which may change with the problem at hand, instead of a fixed grid, as is done in the QMC procedure, in which $\tau_i = i\cdot\Delta\tau$.

2. Exact diagonalization method

In this section we review the implementation of methods that are based on the exact diagonalization of the effective Anderson impurity Hamiltonian Eq. (113). In this method, a rational approximation for $\mathscr{G}_0$ is found. This corresponds to approximating the Anderson impurity Hamiltonian in Eq. (113) by a Hamiltonian made up of a finite number of orbitals n_s (in practice $n_s\sim 5$–12). This Hamiltonian can then be diagonalized exactly using standard algorithms. In order to avoid misunderstandings, we emphasize from the beginning that the exact diagonalization method reviewed here does not deal with a finite-size lattice for the original lattice model: the discretization concerns only the effective conduction bath in the impurity-model formulation. As in all methods of solution of the LISA equations detailed in this article, the infinite-size limit for the actual spatial lattice is implemented from the start. For studies of $d=\infty$ models through a truncation of the physical lattice into subclusters, see the work of Gros *et al.* (1994). We note that analytical approximations involving a continuous fractional expansion of the Green's function, somewhat close in spirit to the Lanczos method detailed below, have recently been considered by Hong and Kee (1995a, 1995b) and Kee and Hong (1995).

All the exact diagonalization algorithms reviewed here to solve the LISA equations adopt the following three basic steps:

(i) The Weiss function

$$\mathscr{G}_0(i\omega_n)^{-1} = i\omega_n + \mu - \int_{-\infty}^{+\infty} d\omega' \, \frac{\Delta(\omega')}{i\omega_n - \omega'} \tag{141}$$

is approximated by a discretized version, for instance:

$$\mathscr{G}_0^{n_s}(i\omega_n)^{-1} = i\omega_n + \mu - \sum_{p=2}^{n_s} \frac{V_p^2}{i\omega_n - \tilde{\epsilon}_p} \tag{142}$$

corresponding to the Anderson impurity Hamiltonian (113). It is also useful to think of this replacement as a *projection* onto a restricted functional subspace (Fig. 12) containing all functions of the form (142) (for a given fixed n_s). The different algorithms that have been used differ only in the choice of the projection operator. From the mathematical point of view one is dealing with the problem of rational approximation of functions. There are many different algorithms (Pade approximation, Continuous fractions, minimization with respect to a given norm) for carrying out the task, and for a small number of approximants the quality of the results may depend on the method used.

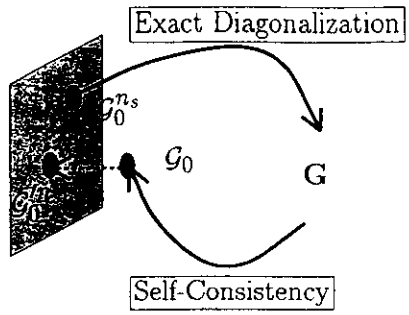

FIG. 12. The exact diagonalization method involves a projection of the bath Green's function $\mathcal{G}_0$ onto the space of functions $\{\mathcal{G}_0^{n_s}\}$ built out of n_s orbitals. At self-consistency $\mathcal{G}_0^{n_s} = \mathcal{G}_0^{n_s}$. The quality of the approximation can be inferred from the distance that separates $\mathcal{G}_0^{\text{new}}$ and $\mathcal{G}_0^{n_s}$. This distance is usually very small, and decreases approximately by a constant factor as n_s is incremented by one.

(ii) The n_s-orbital Hamiltonian (113) corresponding to Eq. (142) is then diagonalized *exactly*, and the Green's function $G(i\omega_n)$ is computed.

(iii) The self-consistency condition Eq. (137) then leads to a new function $\mathcal{G}_0$, which in turn is approximated by a function $\mathcal{G}_0^{n_s}$ with a *new* set $V_p, \tilde{\epsilon}_p$. The process is iterated until a converged set of parameters is reached. Notice that the bath Green's function $\mathcal{G}_0$ obtained at the previous step of the iteration has no reason to belong to this subspace in general, but that it can be *projected* onto this subspace.

Let us discuss in more detail the various steps of this algorithm, starting with the diagonalization of $\mathcal{H}$. In contrast to the Monte Carlo method, the exact diagonalization algorithm provides a numerically *exact* relationship between $\mathcal{G}_0^{n_s}$ and G, since G is the true Green's function of $\mathcal{H}$. (Note also that the QMC does not in fact determine the Green's function of a specific Hamiltonian, but a related object $G^{\Delta\tau}$, which approaches a Green's function in the limit $\Delta\tau \to 0$). The states of the finite-dimensional Hilbert space of $\mathcal{H}$ are given by

$$|n_1^\uparrow, n_2^\uparrow, \ldots, n_{n_s}^\uparrow\rangle |n_1^\downarrow, n_2^\downarrow, \ldots, n_{n_s}^\downarrow\rangle \tag{143}$$

with $n_p^\sigma = 0,1$ and $\Sigma_p n_p^\sigma \equiv n^\sigma$. $\mathcal{H}$ does not mix the different sectors $(n^\uparrow, n^\downarrow)$. In consequence, all sectors can be diagonalized independently. The full diagonalization is feasible for values of n_s of the order of $n_s = 6$ [which leads to the diagonalization of a 400×400 matrix in the sector $(n^\uparrow = 3, n^\downarrow = 3)$] or $n_s = 7$ (1225×1225). At finite temperature, the Green's function is calculated from the full set of states $|i\rangle$ (with eigenvalues E_i) according to

$$G(i\omega_n) = \frac{1}{Z} \sum_{i,j} \frac{(\langle i|d^+|j\rangle)^2}{E_i - E_j - i\omega_n} \times [\exp(-\beta E_i) + \exp(-\beta E_j)]. \tag{144}$$

Using the Lanczos algorithm (cf. Golub and Van Loan, 1983; Gagliano *et al.*, 1986; Lin and Gubernatis, 1993), the *zero-temperature* Green's function of much larger matrices can be computed ($n_s \lesssim 12$). The algorithm is used in a two-step procedure. In the first step, the ground-state wave function $|\Psi_0\rangle^{n^\uparrow, n^\downarrow}$ is determined in each of the sectors $(n^\uparrow, n^\downarrow)$. This is done in the usual way by picking an arbitrary vector $|p_0\rangle$ [within the sector $(n^\uparrow, n^\downarrow)$], and diagonalizing $\mathcal{H}$ in the linear hull of $|p_0\rangle, \mathcal{H}|p_0\rangle, \ldots, \mathcal{H}^n|p_0\rangle$. In a subsequent application of the Lanczos procedure, the initial vector is taken to be $|p_0\rangle = d^+|\text{g.s.}\rangle$ where $|\text{g.s.}\rangle$ is the *overall* ground state of the Hamiltonian. This second Lanczos procedure allows the computation of the ground-state Green's function, which is written in two continued-fraction expansions that describe the "particle" ($\omega > 0$) and "hole" ($\omega < 0$) excitations:

$$G(\omega) = G^>(\omega) + G^<(\omega) \tag{145}$$

with

$$G^>(\omega) = \cfrac{\langle \text{g.s.}|dd^\dagger|\text{g.s.}\rangle}{\omega - a_0^> - \cfrac{b_1^{>2}}{\omega - a_1^> - \cfrac{b_2^{>2}}{\omega - a_2^> - \cdots}}},$$

$$G^<(\omega) = \cfrac{\langle \text{g.s.}|d^\dagger d|\text{g.s.}\rangle}{\omega - a_0^< - \cfrac{b_1^{<2}}{\omega - a_1^< - \cfrac{b_2^{<2}}{\omega - a_2^< - \cdots}}}. \tag{146}$$

It is the parameters entering this parametrization that are determined by the second Lanczos procedure, in a way further detailed in Appendix C.

The most subtle aspect of these methods is in the implementation of the projection of $\mathcal{G}_0$ onto $\mathcal{G}_0^{n_s}$. The following methods for carrying out this projection have been proposed.

(i) A distance d between $\mathcal{G}_0$ and the finite-orbital function $\mathcal{G}_0^{n_s}$ is chosen (Caffarel and Krauth, 1994), e.g.:

$$d = \frac{1}{n_{\max}+1} \sum_{n=0}^{n_{\max}} |\mathcal{G}_0(i\omega_n)^{-1} - \mathcal{G}_0^{n_s}(i\omega_n)^{-1}|^2 \tag{147}$$

(where $n_{\max}$ is a very large upper cutoff). For the runs at finite temperatures, the ω_n are of course taken to be the Matsubara frequencies. Even at zero temperature, they are taken to be the Matsubara frequencies associated with a "fictitious" temperature, which serves as a low-energy cutoff. The precise functional form plays a minor role in this formula, but the crucial aspect of the definition is that the Green's functions are compared with each other at *imaginary* frequencies, and *not* on the real axis. This is illustrated pictorially on Fig. 13. As a practical matter, the "projection" is performed using a *minimization* algorithm. A modern conjugate gradient algorithm has of course no trouble in locating the minimum of the $(2n_s)$-dimensional function in Eq. (147) for $n_s \lesssim 12$. Using repeated projection operations, converged solutions $\mathcal{G}_0^{n_s}$ within the subspace (142) can be found. The quality of the solution can be assessed from the "distance" between $\mathcal{G}_0$ and the corresponding $\mathcal{G}_0^{n_s}$, and from the behavior of this distance as a function of n_s.

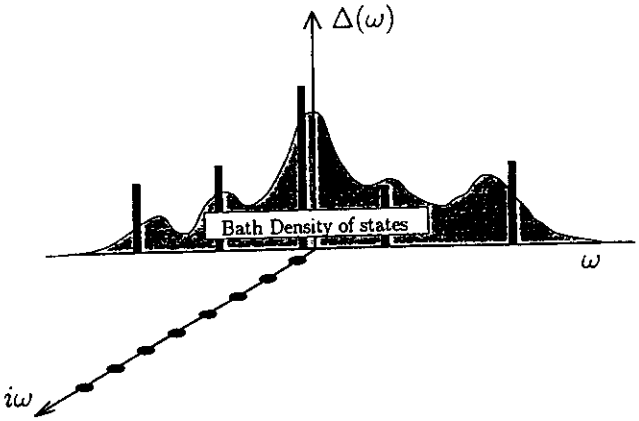

FIG. 13. Schematic representation of the fitting procedure used by Caffarel and Krauth (1994). The spectral density associated with $\mathcal{G}_0^{-1}$ is represented by a finite set of poles ($\tilde{\epsilon}_p$) and weights (V_p^2) on the real frequency axis, but the fitting procedure involves a minimization of the distance between $\mathcal{G}_0(i\omega_n)$ and $\mathcal{G}_0^{fs}(i\omega_n)$ on the *imaginary frequency* axis.

This distance is an estimate of the distance between the *actual* solution of the LISA equations (which is generically *not* part of the restricted subspace for a finite n_s) and the converged discretized $\mathcal{G}_0^{fs}$ that has been found within the restricted subspace. This state of affairs is no different in principle from the QMC method (in which a converged solution is found for a given discretization $\Delta\tau$). An illustration of this comparison will be given in Appendix C.

A key to the success of this approximation lies in that *both* the positions of the orbitals $\tilde{\epsilon}_p$ and the hybridizations V_p are free to adjust themselves. The exact diagonalization method is thus formulated on an adaptive "grid" in ω, and shows the excellent convergence and economy common to variable-grid methods. The power of such methods is lost when $d=\infty$ models are studied by exact diagonalization of subclusters of the original lattice itself (cf. Gros *et al.*, 1994).

A second reason behind the fast convergence of this algorithm is related to the fact that the poles of the function $\mathcal{G}_0$ all lie on the real axis, i.e., far away from the region in which we search to fit the functions. Nevertheless, we will show in Sec. VI.A.4 that the real-frequency properties are very well represented.

(ii) An alternative projection method (Si *et al.*, 1994), which avoids the need for a minimization procedure in several variables, is based on the continued-fraction representation of a rational function (cf. Haydock, 1985). The basic idea is to write the hybridization function of the Anderson model as a sum of two continuous fraction expansions (describing the positive and negative parts of the spectral function) $\Delta^>$ and $\Delta^<$ and define the projection as the truncation of the continued fraction down to a given level. Because of the well-known connection between the moments and the coefficients of the continued fraction expansion this can be thought of as a "moment by moment" systematic fitting on the *real axis* of the one-particle spectral density:

$$\Delta^>(\omega)=\cfrac{b_0^{>2}}{\omega-a_0^>-\cfrac{b_1^{>2}}{\omega-a_1^>-\cfrac{b_2^{>2}}{\omega-a_2^>-\cdots}}},$$

$$\Delta^<(\omega)=\cfrac{b_0^{<2}}{\omega-a_0^<-\cfrac{b_1^{<2}}{\omega-a_1^<-\cfrac{b_2^{<2}}{\omega-a_2^<-\cdots}}}. \tag{148}$$

The Hamiltonian that needs to be diagonalized now has a natural representation in the form of two one-dimensional chains, with parameters as shown in Fig. 10 (the $b_i^{>/<}$ are hopping elements between sites of the chains, and the $a_i^{>/<}$ are atomic energies of the sites). It is easy to see that the two chains generate the Weiss field *precisely* in the truncated continued-fraction form (with n_c the length of the chain, $2n_c+1=n_s$):

$$\mathcal{H}=\sum_\sigma \sum_{\rho=>,<}\left(\sum_{\alpha=0}^{n_c-1} a_\alpha^\rho c_{\alpha\sigma}^{\rho+}c_{\alpha\sigma}^\rho + b_0^\rho(c_{0\sigma}^{\rho+}d_\sigma+\text{H.c.})\right.$$
$$\left.+\sum_{\alpha=1}^{n_c-2}(b_\alpha^\rho c_{\alpha\sigma}^{\rho+}c_{\alpha+1\sigma}^\rho+\text{H.c.})\right)$$
$$+U(n_{d\uparrow}-\tfrac{1}{2})(n_{d\downarrow}-\tfrac{1}{2}). \tag{149}$$

This algorithm can be most easily programmed in the case of the $z=\infty$ Bethe lattice at zero temperature, because in this case the self-consistency condition reads $\Delta^>=t^2G^>$ and $\Delta^<=t^2G^<$. Since the Green's function is obtained in a continued-fraction representation [cf. Eq. (146)] the variables a and b are obtained without further work. The self-consistency is thus translated into the self-consistent determination of the parameters of a continued fraction representation of $\mathcal{G}_0^{-1}$, or equivalently, G.

In this case, the approximation consists in the truncation of the length of the continued fractions due to the finite size of the effective electron bath that can be dealt with. This approximation relies on the fact that the continued-fraction representation captures exactly the moments of the Hamiltonian, up to the order retained in the continued fraction.

This method avoids the multidimensional fit of the Green function but has the disadvantage of giving a high weight to the high-frequency features. This is because the low-energy features of the spectral function have a very small contribution to the moments. For this reason, this method is best adapted to the calculation of the total energy (for which it gives very accurate results), and particularly well suited for the study of insulating phases.

(iii) A third implementation of the projection in the LISA exact diagonalization procedure (which is a mixture of the two previous ones) was introduced to describe a strongly correlated metal (Rozenberg, Moeller, and Kotliar, 1994). An extra site at the Fermi energy is added to the scheme (ii) in order to better represent the

low-frequency region. The hopping amplitude to this extra site $t\delta^{1/2}$ is calculated by a (single-parameter) minimization of the expression:

$$\chi^2(\delta)=\sum_{n;\omega_L<\omega_n<\omega_H}|G_A(i\omega_n,\delta)-G(i\omega_n)|^2, \quad (150)$$

where now G is the full Green's function and $G_A(i\omega_n,\delta)=(\delta/i\omega_n)+(1-\delta)G_n(i\omega_n)$. G_n is the truncated Green's function to length $n=n_s/2-1$ and ω_L and ω_H are low and high energy cutoffs that can be defined, for instance, as the lowest poles of G and G_n, respectively. δ decreases as n_s is increased and scales as $1/n_s$ as $n_s\to\infty$. This is the behavior expected from all the residues in the spectral representation of the hybridization function. For the half-filled Hubbard model with a semicircular density of states of half-width D, the quasiparticle residue as a function of U obtained with this procedure vanishes at a value $U_c/D\simeq 3$, which is very close to the more precise value obtained from the projective self-consistent method.

The projection via the moments captures most easily the high-energy features, and is quite insensitive to the low-energy features. Conversely, the χ^2 fit is most sensitive to the low-energy behavior of the spectral features but seems to capture the high-energy features reasonably well when n_s is not too small. Combination of the two approaches optimized for a specific problem are worth exploring.

Working codes for the solution of the LISA equations by exact diagonalization are provided with this article (cf. Appendix D). Two versions of the code are available:

(1) The program LISADIAG.F performs an explicit (sector-by-sector) diagonalization of the Hamiltonian, and constructs the Green's function from the eigenvalues and eigenvectors according to Eq. (144). This is the code that is used for calculations at finite temperature. We will apply it in the next section for a detailed comparison with the QMC calculations. For $n_s=6$, a single loop of the program will take of the order of one minute to run on a modern workstation (HP 735, or IBM RS6000).

(2) The program LISALANC.F uses the Lanczos algorithm in a two-step procedure.

Naturally, the two completely independent programs agree essentially to machine precision at zero temperature for the values of n_s which can be handled by the full diagonalization. There is also very good agreement between the different ways of choosing the projection operator to compute $\mathcal{G}_0^{n_s}$, given a $\mathcal{G}_0$.

Both codes can more easily be written than explained, and we refer for details to the well-documented FORTRAN programs. Compared to the Monte Carlo programs, they are much faster, and easier to run, since the difficult convergence problems of the stochastic QMC algorithm are absent.

3. Comparison of exact diagonalization and Monte Carlo methods

In this section we compare in detail the QMC and exact diagonalization algorithms. The section serves two purposes:

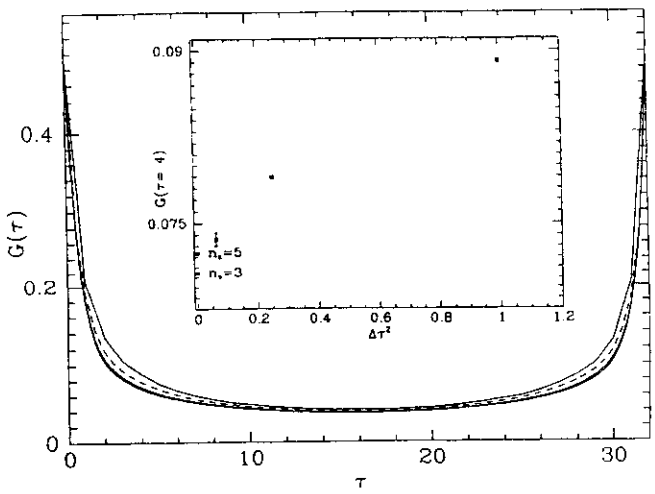

FIG. 14. Comparison between the imaginary-time Green's functions $G(\tau)$ obtained by the QMC and the exact diagonalization methods, for the half-filled Hubbard model with $U=3D/\sqrt{2}$, $\beta D/\sqrt{2}=32$). From top to bottom: $\Delta\tau=1,1/2,1/4$. The bottom curve is the exact diagonalization result for $n_s=5$ (which cannot be resolved from $\Delta\tau=1/4$ on the scale of the figure). The inset shows the scaling of the QMC results for a fixed value of $\tau=4$ as a function of $(\Delta\tau)^2$: the result converges to a value which is readily obtained within exact diagonalization.

(i) First, by actually comparing the methods, we lend credibility to both. Both methods are able to produce well-converged results which can be taken as they stand, since the thermodynamic limit has been built in from the start. This is quite an exceptional situation in current fermionic many-body simulations. In comparing the two methods we will furthermore be able to clearly expose the advantages of the exact diagonalization algorithm.

(ii) Secondly, we also judge it important to address the wider issue of the confidence limits with which various quantities can presently be computed. Given the importance of the numerical results in the field (in discussions such as the Mott transition, for example), a critical discussion of the numerical methods is needed.

We will first consider three quantities in the context of the $d=\infty$ single-band Hubbard model: the calculation of imaginary-time (or Matsubara frequency) Green's functions at finite temperature, the calculation of the quasiparticle residue Z, and the computation of susceptibilities. The more difficult question of real-frequency quantities will be dealt with in Sec. VI.A.4, where a critical discussion of the results that can be obtained from maximum-entropy analytic continuations of very high precision Monte Carlo data will be given. These calculations will be compared to the discrete spectra obtained from exact diagonalization and to results of analytic approximations.

The most instructive comparison between the QMC and exact diagonalization methods is in imaginary time, where the QMC result is guaranteed to converge quadratically to the exact result [with an error $O(\Delta\tau^2)$, cf. Appendix B]. In Fig. 14 we present results (Caffarel and Krauth, 1994) for the Green's function $G(\tau)$ of the half-filled Hubbard model with a semicircular density of

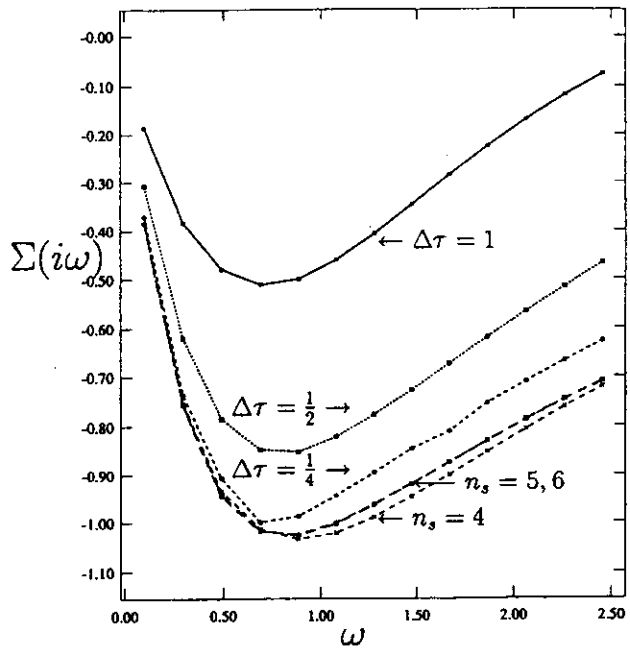

FIG. 15. Finite-temperature self-energy as a function of Matsubara frequency, computed by exact diagonalization (n_s=4,5,6) and QMC $\Delta\tau$=1,1/2,1/4 for the half-filled Hubbard model, with parameters as in Fig. 14.

states of half-width D at $U/D=3/\sqrt{2}$ and $\beta D/\sqrt{2}=32$. The figure shows calculations at $\Delta\tau=(1,1/2,1/4)$ for the Monte Carlo algorithm, and $n_s=(3,4,5)$ for the exact diagonalization (in the paramagnetic phase). The excellent agreement between the numerical results is immediately apparent. To see the differences between the methods, we consider a single τ value, as done for $\tau=4$ in the inset of the figure. The Monte Carlo results are plotted against $(\Delta\tau)^2$. It is evident from the figure that the exact diagonalization results for $n_s=5$ (which the reader can himself reproduce within a few minutes on a regular work station using the program LISADIAG.F) are more precise than the Monte Carlo data at $\Delta\tau=1/4$ ($L=128$), which necessitate a few *days* of computer time.

The comparison for imaginary frequencies gives a very similar picture, of course with the additional ingredient that, for $\omega>1/(\Delta\tau)$, the Monte Carlo data contain no more information. An illustration of this is shown for the self-energy at finite temperature in Fig. 15, which compares again QMC and the exact diagonalization data. The low-frequency behavior of the self-energy is important in order to determine the nature of the physical state (insulating or metallic), and a good quantitative knowledge is crucial in order to be able to calculate the quasiparticle residue Z, a zero-temperature quantity defined from the retarded self-energy as $Z^{-1}=1-\partial\,\mathrm{Re}\Sigma(\omega+i0^+)/\partial\omega|_{\omega=0}$. A plot of this quantity for the half-filled Hubbard model will be displayed in Sec. VII, in connection with our discussion of the Mott transition. The exact diagonalization method and the (much more costly) QMC method converge to the same values of $\Sigma(i\omega_n)$ down to the first Matsubara frequency at a given finite temperature. Therefore, these values are known up to a precision of the order of 0.3%. Notice however that the error on the quasiparticle residue Z may be much larger, since this is a zero-temperature quantity. More precisely, the estimate $\zeta(T)=[1-\mathrm{Im}\Sigma(i\omega_1)/\omega_1]^{-1}$ suffers from additional systematic errors because at *finite temperature* the analytic continuation of $\Sigma(i\omega_n)$ has a branch cut at zero frequency. For the half-filled Hubbard model, these systematic errors are very small for small or intermediate U, but become larger as the Mott transition is reached. Very close to the transition point, more elaborate methods (Sec. VI.C) are needed to access the true low-frequency regime.

In the process of an actual computation, it is very important to track the behavior of the exact diagonalization algorithm. This is done by analyzing the effect of the "projection" in going from $\mathcal{G}_0$ to $\mathcal{G}_0^{n_s}$ at the self-consistent solution (cf. Fig. 12). The behavior of the mismatch between these functions as a function of n_s allows us to evaluate whether we may trust the results (in the QMC algorithm, we would check whether the data scale properly with $1/\Delta\tau$). In general, $\mathcal{G}_0$ and $\mathcal{G}_0^{n_s}$ differ the most at *small* imaginary frequencies, closest to the real axis and very quickly agree to machine precision for larger values of $i\omega$. An actual example for this comparison is displayed and discussed in Appendix C.

From the discussion of this section, the superiority of the exact diagonalization method over the Monte Carlo method is evident. We would, however, like to mention the very costly scaling of the exact diagonalization algorithm with the size n_s, if we think, e.g., of the obvious generalization to the self-consistent embedded clusters, which are the subject of Sec. IX. Even a small cluster, with a few surrounding orbitals per cluster site, could not possibly be treated with the exact diagonalization method. It seems to us that the QMC method still has a lot of untapped potential: It seems very likely that such systems would most easily be treated by a combination of the Hirsch-Fye algorithm and the original BSS method, suitably stabilized (cf. the detailed discussion of Sec. VI.A.1.e).

4. Spectral densities and real frequency quantities: Comparison of various methods

In this section, we provide some guidelines concerning the calculation of *real-frequency* quantities, such as the one-particle spectral function $\rho(\omega)=-(1/\pi)\,\mathrm{Im}G(\omega+i0^+)$ [or the response functions $\chi''(\omega)=-(1/\pi)\,\mathrm{Im}\chi(\omega+i0^+)$]. The determination of such quantities faces some limitations in both numerical methods treated in Secs. VI.A.1 and VI.A.2. The most severe ones are found in the case of the QMC method. There, only imaginary time/frequency data are obtained directly, and one needs to perform an analytic continuation from numerical data. In the exact diagonalization method, $\rho(\omega)$ is obtained directly, but in the form of an approximation by a set of delta functions (since one is using a finite number of orbitals in the effective bath). Analytic approximation schemes are always best

adapted to computing such quantities, but it is crucial to be able to compare the results to the ones obtained numerically. We present such a comparison here in the case of the half-filled Hubbard model.

The standard algorithm for the analytic continuation of QMC data is the maximum entropy method [Gubernatis *et al.*, 1991; see also Jarrell and Gubernatis (1996) for a recent review]. One is trying to retrieve by inverse Laplace transform the spectral function $\rho(\omega)$ from the imaginary-time Green's function $G(\tau)$, such that

$$G(\tau)=\int_{-\infty}^{\infty} d\omega \, \frac{e^{-\tau\omega}}{1+e^{-\beta\omega}} \rho(\omega). \tag{151}$$

The problem is ill-posed and altogether hopeless if the data for $G(\tau)$ are not of extremely good quality, and if the errors and the correlations between errors are not carefully taken into account (Gubernatis *et al.*, 1991). The interplay between statistical errors and systematic ($\Delta\tau$-dependent) errors has also been much discussed in the literature. In addition, the "guess" of the correct density of states $\rho(\omega)$ using Bayesian logic usually brings in an *a priori* choice of a "possible" $\rho(\omega)$, which generally requires an independent approximation method and justification. In the LISA context, all these difficulties are present, and also the additional one associated with the self-consistency condition ($\mathcal{G}_0$ itself is only known up to numerical errors). We will see that a consistent determination of the spectral density is nevertheless possible at sufficiently high temperature. However, in spite of the tremendous effort which has been spent on maximum entropy methods, it is still very difficult, if not impossible, to predict—solely from Monte Carlo calculations—reliable densities of states at low temperature.

The difficulty arises from two different sources: (i) analytic continuation to the real-axis of the *exact* $G(i\omega_n)$ is a numerically "ill-posed" problem, which requires a regularization (see, e.g., the discussion in Press *et al.*, 1991), and (ii) the numerical data for $G(i\omega_n)$ have systematic and/or statistical errors. The first difficulty is alleviated as the temperature decreases because more information becomes available. Unfortunately, the errors in the numerical data (for a given computation efficiency) increase as the temperature decreases.

It is very instructive to deal first with an example in which the interplay between statistical and systematic errors can be disentangled, and for which an exact determination of $\rho(\omega)$ can be achieved, up to discretization errors only. This can be achieved by performing the summation over Ising auxiliary spins using the full Gray-code enumeration mentioned in the QMC section above. In that case we are able to calculate the discretized Green's function $G^{\Delta\tau}(\tau)$ for up to $L=18$ slices exactly, and produce a self-consistent solution to machine precision (the reader can reproduce these calculations with the QMC programs provided). Because of the complete absence of statistical errors we can in this special case perform a Padé transformation (Vidberg and Serene, 1977) in order to compute $\rho(\omega)$, thus avoiding the difficulties of the maximum entropy method. In Fig. 16, we show the results of such a calculation for the

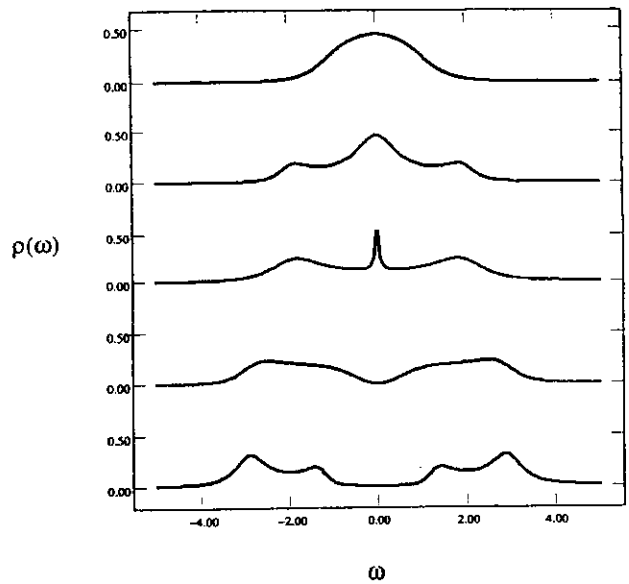

FIG. 16. Finite-temperature spectral densities for the half-filled Hubbard model with a semicircular density of states of half-width D, obtained by the QMC method with $L=16$ time slices at $\beta D/\sqrt{2}=10$ and $U\sqrt{2}/D=1,2,3,4,5$ (top to bottom). An *exact enumeration* of the 2^{16} Ising spin configurations has been used, so that these results correspond to the *exact* analytic continuation of the discretized $G(\tau)$ (for the specific value of $\Delta\tau=10/16$).

half-filled Hubbard model with $\beta=10$ and $L=16$ (i.e., $\Delta\tau=10/16$) as a function of $U=1,2,3,4,5$ (in the units of $D/\sqrt{2}$). Without using any prior knowledge, the results display correctly the buildup of the upper Hubbard band associated with high-energy charge excitations at a scale $\sim\pm U/2$ (cf. Sec. VII). The narrowing of the quasiparticle peak around $\omega=0$ is also apparent. At larger U, a gap opens, indicative of the Mott transition.

It is very interesting to notice that the result of such a simple calculation agrees very well with the results of a full-fledged maximum entropy calculation [along the lines of Gubernatis *et al.* (1991)], as displayed in Fig. 17 at the same values of the physical parameters. Just to indicate the enormous investment needed for the maximum entropy calculation, we indicate that the data were obtained with 100 samples of $G^{\Delta\tau}(\tau)$, which were obtained by performing each time 10^5 sweeps of the Monte Carlo algorithm (with $L=64$). It would be quite inconceivable to redo this calculation at much smaller temperature. In the same figure, we also show the results of the iterated perturbative theory approximation (at finite temperature), which will be discussed in Sec. VI.B.2. It agrees very well with both the maximum entropy and the complete enumeration results. Similar agreement (between maximum entropy and iterated perturbation theory) was obtained for the Hubbard model on a hypercubic lattice (Georges and Krauth, 1993; Jarrell, 1992), again at the rather high temperature accessible to maximum entropy.

Finally, we consider (Caffarel and Krauth, 1994) the spectral densities obtained by the exact diagonalization

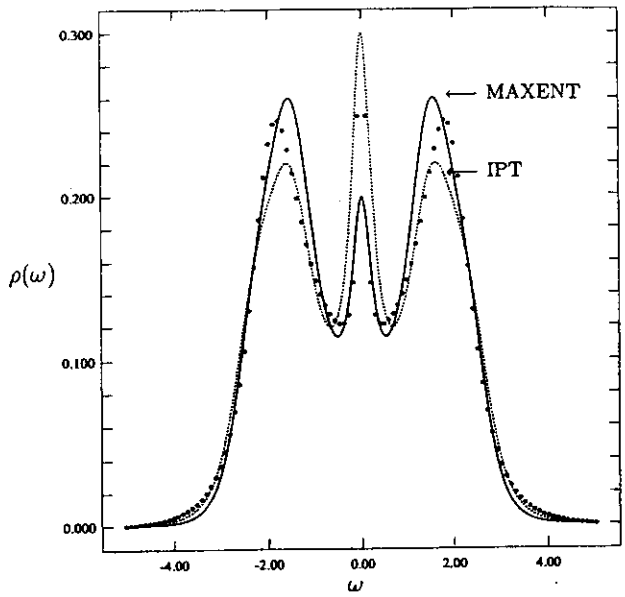

FIG. 17. For the same temperature $\beta D/\sqrt{2}=10$ as in Fig. 16, and $U=3D/\sqrt{2}$, this figure compares spectral densities obtained by the iterated perturbation theory approximation (dotted line), by the QMC method with $L=64$ supplemented by a maximum entropy analytic continuation (full line), and by the Padé interpolation of the exact enumeration data (Fig. 16) with $L=16$ (dots).

method, which consists of a large number of discrete δ functions, directly obtained at $T=0$. The one-particle spectral densities $\rho(\omega)=-\mathrm{Im}G(\omega+i\epsilon)/\pi$ as obtained from the Lanczos calculation ($n_s=10$) are displayed together with the iterated perturbation theory approximation solutions (cf. Sec. VI.B.2) in Fig. 18 for different values of U. In the Fermi-liquid regime the spectrum of the finite-size Anderson model consists of a large number of peaks, while in the insulating phase we systematically observe a simpler structure made of only a few peaks. As U is increased we see that $\rho(\omega)$ develops three well-separated structures: a central quasiparticle feature and two broad high-energy satellite features corresponding to the formation of the upper Hubbard band. At large U, a gap is observed in good agreement with the approximate iterated perturbation theory solution. In the insets of Fig. 18 we also present the integrated single particle density of states corresponding to Lanczos and iterated perturbation theory solutions. The agreement between both curves is seen to be very good, provided we average over a frequency interval of $\omega\sim 0.5$. This indicates that the calculated spectral density contains coarse-grained information about the exact solution, as it should be. Due to the discrete nature of the Anderson model used, the fine details of the spectrum are poorly reproduced, but the agreement of the coarse-grained results with those obtained by the other methods is remarkable.

5. Numerical calculation of susceptibilities and vertex functions

In this short section, we explain how susceptibilities and vertex functions can be computed numerically

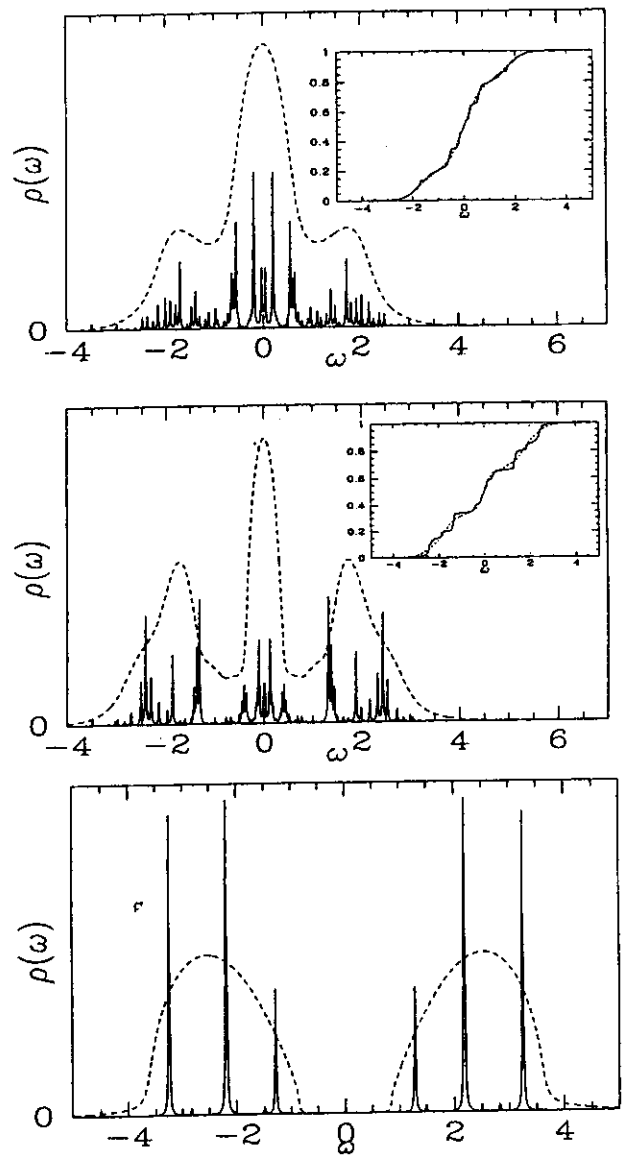

FIG. 18. $T=0$ spectral density for the half-filled Hubbard model at $U\sqrt{2}/D=2,3,4.8$ (top to bottom), as calculated by the exact diagonalization method (Lanczos at $n_s=10$). Also shown are the corresponding results from the iterated perturbation theory approximation (on a different, arbitrary, scale). For a comparison between the two results, the inset contains the integrated density of states $\int_{-\infty}^{\omega}\rho(\omega')d\omega'$ in each case.

within the various methods described above. The theoretical formalism relevant to this section is that of Sec. IV. There, it was shown that **q**-dependent response functions for the lattice model can be related, in the LISA framework, to local response functions of the impurity model through the formula [Eq. (69)]

$$\tilde{\chi}_{\mathbf{q}}^{-1}=\tilde{\chi}_{\mathrm{loc}}^{-1}+\tilde{\chi}_{\mathbf{q}}^{0-1}-\tilde{\chi}_{\mathrm{loc}}^{0-1}, \tag{152}$$

in which $\tilde{\chi}_{\mathrm{loc}}$ is a local response function depending on three frequencies. In the case of the S^z-S^z response function, it reads

$$\tilde{\chi}_{\rm loc}(i\nu,i\nu';i\omega)=\frac{1}{4}\int_0^\beta d\tau_1\int_0^\beta d\tau_2\int_0^\beta d\tau_3\int_0^\beta d\tau_4 e^{i\nu(\tau_1-\tau_2)}$$
$$\times e^{i\nu'(\tau_4-\tau_3)}e^{i\omega(\tau_4-\tau_2)}$$
$$\times\sum_{\sigma\sigma'}(-1)^{\sigma}(-1)^{\sigma'}\langle Tc_\sigma^+(\tau_1)c_\sigma(\tau_2)$$
$$\times c_{\sigma'}^+(\tau_3)c_{\sigma'}(\tau_4)\rangle_{S_{\rm eff}}. \quad (153)$$

A local correlator such as $\langle Tc_\sigma^+(\tau_1)c_\sigma(\tau_2)c_{\sigma'}^+(\tau_3)c_{\sigma'}(\tau_4)\rangle_{S_{\rm eff}}$ can be calculated numerically within both the QMC and exact diagonalization algorithms.

In the QMC method, Wick's theorem applies once the interaction term has been decoupled through the auxiliary Ising variables $s_1\cdots s_L$, so that:

$$\langle Tc_\sigma^+(\tau_1)c_\sigma(\tau_2)c_{\sigma'}^+(\tau_3)c_{\sigma'}(\tau_4)\rangle_{S_{\rm eff}}$$
$$=\overline{g^{\sigma}_{s_1\cdots s_L}(\tau_2,\tau_1)g^{\sigma'}_{s_1\cdots s_L}(\tau_4,\tau_3)}$$
$$-\delta_{\sigma\sigma'}\overline{g^{\sigma}_{s_1\cdots s_L}(\tau_2,\tau_3)g^{\sigma}_{s_1\cdots s_L}(\tau_4,\tau_1)}. \quad (154)$$

The overlines denote an average over the Ising spin configurations, with the measure given above. As in the case of the calculation of Green's functions from the QMC, the physical four-point correlation function has symmetries that the Ising-spin dependent quantities lack. This fact can again be used to reduce the importance of statistical noise.

In the exact diagonalization algorithm, a spectral representation can be derived for such a correlator, by inserting a complete set of eigenstates. Since the full formula is rather lengthy, we simply quote it for the local spin correlator $\chi_{\rm loc}(\tau)=\langle S_z(0)S_z(\tau)\rangle$ [i.e., $\chi_{\rm loc}(i\omega)=\Sigma_{\nu\nu'}\tilde{\chi}_{\rm loc}(i\nu,i\nu';i\omega)$]:

$$\chi_{\rm loc}(i\omega)=\frac{1}{Z}\sum_{i,j}\frac{|\langle i|S_z|j\rangle|^2}{i\omega+E_i-E_j}(e^{-\beta E_j}-e^{-\beta E_i}). \quad (155)$$

In this expression, Z is the partition function $Z\equiv\Sigma_i e^{-\beta E_i}$. At finite temperature in the exact diagonalization algorithm, such an expression can be evaluated explicitly. At $T=0$, the Lanczos procedure for the Green's function can be adapted to the calculation of $\chi_{\rm loc}$, by starting the (second) Lanczos iteration with the vector $S_z|{\rm g.s.}\rangle$ instead of $d^+|{\rm g.s.}\rangle$ (cf. Appendix C).

In Fig. 19, we show a comparison of the QMC and exact diagonalization results for the local correlator $\chi_{\rm loc}(\tau)$ of the half-filled Hubbard model at $U/D=3/\sqrt{2}$. Again we notice the almost complete absence of finite-n_s effects, this time in a response function (at lower temperature, however, these effects are more pronounced for the susceptibility than for the Green's functions).

A word of caution is in order however. In the metallic phase at $T=0$, the ground state of an impurity model with a *finite* number of orbitals is a singlet, and there is a finite gap to excited states, so that Eq. (155) should yield a vanishing result at $T=0$ as long as n_s is finite. The correct method for obtaining the asymptotic $n_s\to\infty$ result is to work at a small but finite temperature $T>T^*(n_s)$, where $T^*(n_s)$ is roughly of the order of the finite-size gap of the Anderson chain. As n_s becomes large, $T^*(n_s)$ does vanish, but the limits $T\to 0$ and $n_s\to\infty$ should not be interchanged.

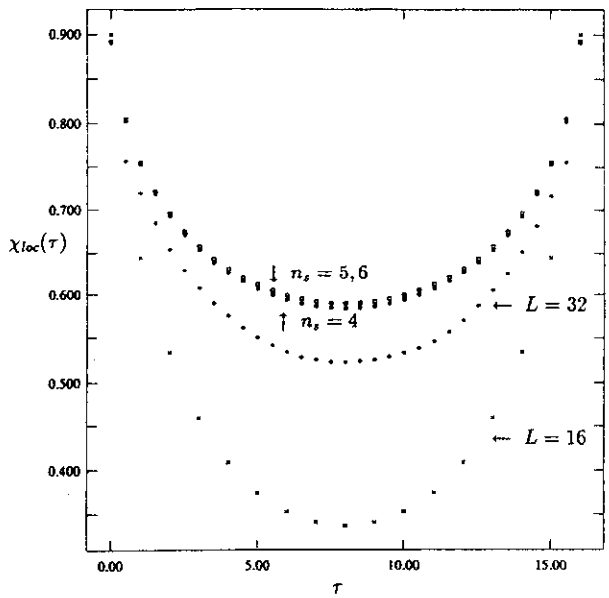

FIG. 19. Local spin correlation function $\chi_{\rm loc}(\tau)=\langle[n_\uparrow(0)-n_\downarrow(0)][n_\uparrow(\tau)-n_\downarrow(\tau)]\rangle$ obtained by the QMC and exact diagonalization methods for the half-filled Hubbard model with $\beta D/\sqrt{2}=16$ and $U=3D/\sqrt{2}$.

Let us finally consider the calculation of the static, uniform susceptibility $\chi=\Sigma_{\mathbf{q}}\chi(\mathbf{q},\omega=0)=\partial m/\partial h|_{h=0}$. This quantity is chosen for illustrative purposes: similar considerations would apply, e.g., to the staggered susceptibility. There are essentially two ways to compute such a quantity numerically:

(i) Compute the *local* response function $\tilde{\chi}_{\rm loc}(i\nu,i\nu';i\omega)$ as described above, and perform the matrix inversion required in (152). The $\tilde{\chi}^0$ can be obtained from the knowledge of the self-energy. A second matrix inversion yields $\tilde{\chi}_{\mathbf{q}=0}(\nu,\nu',\omega=0)$, and finally χ by summing this quantity over ν,ν'. This procedure has been used, e.g., in the work of Jarrell (1992).

(ii) Solve the LISA equations in the presence of a small uniform external field h, and compute the susceptibility as a finite difference $\chi=\Delta m/\Delta h$. The presence of the field enters the self-consistency condition (Sec. V), resulting in a spin-dependent Weiss function $\mathcal{G}_{0\sigma}$ in the impurity effective action.

The second method is probably the simplest if one is interested only in the zero-frequency static susceptibility.

The same method can be used for the static susceptibility at other values of $\mathbf{q}$, such as the staggered susceptibility obtained by including a small staggered field. Note that a similar procedure can be used to obtain the local static susceptibility $\chi_{\rm loc}=\Sigma_{\mathbf{q}}\chi(\mathbf{q})$, instead of the explicit evaluations described above. To do this, one has first to compute the self-consistent solution $G(h=0)$, $\mathcal{G}_0(h=0)$ at zero external field. In a second step, one

then calculates the Green's function $G(h)$ while keeping the Weiss field $\mathcal{G}_0(h=0)$ (this means that the calculation is done for a spin-dependent chemical potential $\mu \rightarrow \mu - h\sigma$). The local susceptibility is then given by

$$\chi_{\rm loc} = \lim_{h=0} [G^{\uparrow}(\tau=0,h)|_{\mathcal{G}_0(h=0)} - G(\tau=0,h=0)]/h, \tag{156}$$

which corresponds to putting a magnetic field solely onto the impurity site.

The finite-field method for calculating both local and uniform susceptibilities is perfectly practical, especially in the exact diagonalization framework, where the complete absence of *statistical* noise allows calculations at arbitrarily small h (such as $h \sim 1.0\times10^{-5}$, i.e., fully in the linear regime). Equation (155) describes a linear-response formula which is valid for any Hamiltonian. It is numerically equivalent to the calculation at very small magnetic field. This is of course only true if no further approximations are introduced, as in the exact diagonalization framework [where the sum over states in Eq. (155) is actually computed]. In the Monte Carlo procedure, an exact linear response formula to an external field (at finite $\Delta\tau$) can be derived by expanding the Dyson equation in a field h with respect to h at $h=0$. The method using four-point functions agrees with the finite-field procedure only in the limit of $\Delta\tau \rightarrow 0$.

In phases with broken symmetry (where there is a finite effective field), it is again evident that the two procedures result in the same determination of the critical temperatures whenever we are able to write a self-consistency condition for the broken-symmetry phase. An illustration of this point is the calculation of the Néel temperature of the Hubbard model for the hypercubic lattice obtained by Jarrell (1992) by following the first method, and reproduced by Georges and Krauth (1993) following the second one, and on the Bethe lattice calculated by Rozenberg, Kotliar, and Zhang (1994) using the first method and by Ulmke, Janis, and Vollhardt (1994) using both methods.

B. Analytic methods

This article is not the place for an exhaustive review of the rather large variety of analytical methods designed to handle quantum impurity models. These methods can rather generally be divided into two broad classes. On one side, we find several analytical tools for the study of *low-energy* universal properties of these models. These are important in the LISA context since they allow for a classification of the various low-energy behaviors that are *a priori* possible, on a qualitative level. In Sec. VI.B.1 we simply give a list of such methods, with appropriate references. A second class of analytical methods is designed for a full quantitative solution of impurity models, including the calculation of dynamical quantities such as the impurity Green's function. This is precisely what is needed for a full quantitative solution of the LISA equations. Unfortunately, these methods are less numerous and are most of the time *approximate methods* (which may become exact in some extreme limit of the model). We briefly describe in the following three of these methods that have proven useful in the LISA context, namely, weak-coupling perturbation theory (leading to the iterated perturbation theory approximation in the LISA context), the non-crossing approximation, and the (high-temperature) equation of motion method. The description of these methods will be short, and the reader is directed to the original references for a detailed exposition. Two useful general sources on quantum impurity models are the review article by Tsvelick and Wiegmann (1983), and the recent book by Hewson (1993).

1. Exact methods at low energy

When faced with the LISA equations for a specific problem, the first thing to attempt is a characterization of the possible low-energy behaviors. In order to achieve this, one starts by assuming a specific low-energy form for the Weiss function $\mathcal{G}_0(i\omega_n)$ [i.e., for the effective conduction bath density of states $\Delta(\omega)$]. Then, one uses some of the various analytical tools listed below in order to access the low-energy behavior of the impurity Green's function $G(i\omega_n)$ [i.e., of the spectral density $\rho(\omega)$]. This is subsequently inserted into the self-consistency condition in order to decide whether the initial assumption made for $\mathcal{G}_0$ and Δ is indeed compatible with the coupled LISA equations. One may also proceed in the reverse order, namely postulate a low-energy behavior of $G(i\omega_n)$, insert it into the self-consistency condition in order to find the corresponding behavior of $\mathcal{G}_0$ and Δ, and then analyze the impurity problem at low-energy in order to decide on the validity of the initial ansatz for G. For a concrete illustration of this procedure, the reader is directed to the qualitative analysis of the LISA equations for the half-filled Hubbard model in Sec. VII.C, and for the doped case in Sec. VII.H.1. Of course, this analysis only results in a classification of the low-energy behavior that is *a priori* possible, and does not allow for a quantitative determination of the regions of parameter space of the original lattice model that lead to a specific, allowed low-energy behavior. In order to achieve this, these low-energy methods must be combined with some information on the high-energy physics. This information must be obtained either from the numerical methods described above, or from some quantitative analytic approximation technique, like the ones described below in Secs. VI.B.2 and VI.B.3.

The method to be employed for the analysis of the low-energy problem depends crucially on the low-energy behavior of the effective conduction bath density of states $\Delta(\omega)$ parametrizing the Weiss function $\mathcal{G}_0$. Different fixed points (in the renormalization group sense) will generally control the low-energy behavior of the impurity model for different low-frequency behaviors of Δ. An important distinction is whether the effective bath has states at low-energy [i.e., $\Delta(\omega)$ is nonzero in some finite range around $\omega=0$], or whether $\Delta(\omega)$ displays a gap.

A. Periodic Anderson model and the Kondo lattice

1. The periodic Anderson model

The periodic Anderson model (PAM) consists of a band of conduction electrons that hybridizes with localized f-electron states at each lattice site. The double occupation of the f sites is disfavored by a repulsive local term that corresponds to the screened Coulomb interaction. With a local hybridization, the Hamiltonian is defined by

$$H=\sum_{\mathbf{k}\sigma}\epsilon_{\mathbf{k}}c^{+}_{\mathbf{k}\sigma}c_{\mathbf{k}\sigma}+V\sum_{i\sigma}(c^{+}_{i\sigma}f_{i\sigma}+f^{+}_{i\sigma}c_{i\sigma})+\epsilon_f\sum_{i\sigma}f^{+}_{i\sigma}f_{i\sigma}+U\sum_i(n_{fi\uparrow}-\tfrac{1}{2})(n_{fi\downarrow}-\tfrac{1}{2}). \tag{276}$$

This model Hamiltonian is widely considered to be relevant for the description of a large class of strongly correlated systems, most notably the heavy fermion compounds and the so-called "Kondo insulators."

Using the fact that in the $d\to\infty$ limit the local interaction gives rise to a local (i.e., $\mathbf{k}$-independent) self-energy, the various components of the Green's functions are obtained in the form:

$$G_c(i\omega_n,\mathbf{k})^{-1}=i\omega_n-\epsilon_{\mathbf{k}}-\frac{V^2}{i\omega_n-\epsilon_f-\Sigma_f(i\omega_n)}, \tag{277}$$

$$G_f(i\omega_n,\mathbf{k})^{-1}=i\omega_n-\epsilon_f-\Sigma_f(i\omega_n)-\frac{V^2}{i\omega_n-\epsilon_{\mathbf{k}}}, \tag{278}$$

$$G_{cf}(i\omega_n,\mathbf{k})^{-1}=\frac{1}{V}\{[i\omega_n-\epsilon_{\mathbf{k}})(i\omega_n-\epsilon_f-\Sigma_f(i\omega_n)]-V^2\}. \tag{279}$$

In these expressions, $\Sigma_f(i\omega_n)$ is the self-energy of the f electrons, and the chemical potential μ has been absorbed in the definitions of $\epsilon_{\mathbf{k}}$ and ϵ_f. Using the methods of Secs. II and III, the reduction to a self-consistent single-site model is easily performed and the effective action reads

$$S_{\text{eff}}=-\int_0^\beta d\tau\int_0^\beta d\tau'\sum_\sigma f^{+}_\sigma(\tau)\mathcal{G}_0^{-1}(\tau-\tau')f_\sigma(\tau')+U\int_0^\beta d\tau[n_{f\uparrow}(\tau)-\tfrac{1}{2}][n_{f\downarrow}(\tau)-\tfrac{1}{2}] \tag{280}$$

with the f self-energy obtained from

$$\Sigma_f=\mathcal{G}_0^{-1}-G_f^{-1},\quad G_f\equiv-\langle Tff^{+}\rangle_{S_{\text{eff}}}. \tag{281}$$

Not surprisingly, the effective action is that of a single-impurity Anderson model. The self-consistency condition requires that the local f Green's function of the lattice model coincides with the Green's function of the impurity problem, namely:

$$\int_{-\infty}^{\infty}\frac{d\epsilon\,D(\epsilon)}{i\omega_n-\epsilon_f-\Sigma_f(i\omega_n)-V^2/(i\omega_n-\epsilon)}=G_f(i\omega_n), \tag{282}$$

where $D(\epsilon)$ refers as usual to the noninteracting density of states of the conduction electrons. It is often useful to rewrite this self-consistency condition in terms of the Hilbert transform $\tilde{D}$ of the density of states [cf. Eq. (11)] as

$$G_f(i\omega_n)=\frac{1}{i\omega_n-\epsilon_f-\Sigma_f}+\frac{V^2}{i\omega_n-\epsilon_f-\Sigma_f}\times\tilde{D}\left(i\omega_n-\frac{V^2}{i\omega_n-\epsilon_f-\Sigma_f}\right). \tag{283}$$

Note that the Hilbert transform appearing in the right-hand side of this equation coincides with the local conduction electron Green's function $G_c(i\omega_n)$.

This description of the Anderson lattice as a self-consistent single impurity Anderson model was originally introduced by Kuramoto and Watanabe (1987). Generalizations of these equations to the description of the ordered phases of this model can be easily constructed following the lines of Sec. V.

In the work of Georges, Kotliar, and Si (1992), these dynamical mean-field equations were combined with general theorems on the single-impurity Anderson model (Langreth, 1966), along similar lines to those reviewed in Sec. VII.H for the Hubbard model. This analysis shows that the metallic phase of the $d=\infty$ PAM (in the absence of long-range order and in zero magnetic field) is a Fermi liquid and has a Fermi surface which accommodates the *total number* n_c+n_f *of conduction and f electrons.*

Most quantitative studies of the $d=\infty$ PAM that have appeared in the literature have focused on the (insulating) half-filled case, which is reviewed in the next section. A notable exception is the early work of Schweitzer and Czycholl (1989, 1990a, 1991b) who make use of second-order perturbation theory in the coupling U. Both the direct weak-coupling expansion (in which the free fermions Green's function enters the second-order self-energy) and the "self-consistent" one (in which the full interacting propagator is used) were considered. One-particle spectral densities, and the temperature dependence of the resistivity $\rho(T)$ and thermopower $Q(T)$, were calculated using these approximations. The results for $\rho(T)$ and $Q(T)$ at various electron densities are reproduced in Figs. 65 and 66. Schweitzer and Czycholl make the interesting observation that $\rho(T)$ has a monotonic behavior (characteristic of a normal metal) at low electron fillings (i.e., when μ is far below the effective f level), while a plateau develops for higher electron densities, which turns into a resistivity maximum at the Kondo scale (followed by a regime with a negative slope $\partial\rho/\partial T$) as one enters the mixed valence regime (i.e., when μ is close to the effective f level). A concomitant change in behavior is observed for $Q(T)$. Both types of behavior are observed experimentally in heavy fermion compounds.

A crucial issue in the field of heavy fermions is the competition between Fermi-liquid coherence (the Kondo effect) and magnetic (Ruderman-Kittel-Kasuya-Yosida, or RKKY, and superexchange) interactions. The

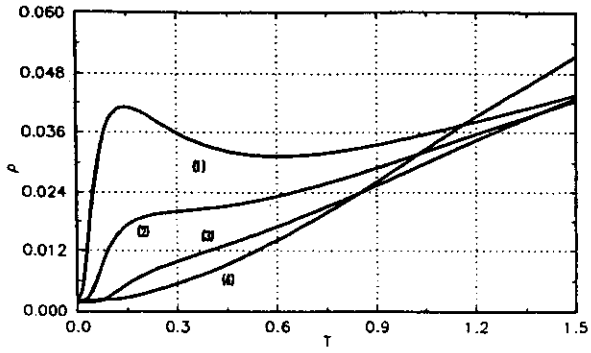

FIG. 65. Temperature dependence of the resistivity for the periodic Anderson model on the hypercubic lattice with U=1 and V=0.4 ($t_{ij} = 1/\sqrt{2d}$), as obtained from "self-consistent" second-order perturbation theory. (1) n_{tot}=0.8, (2) n_{tot}=0.6, (3) n_{tot}=0.4, (4) n_{tot}=0.2 (from Schweitzer and Czycholl, 1991b).

LISA (d=∞) approach does have a bearing on this issue, albeit a partial one (Georges, Kotliar, and Si, 1992; Jarrell, 1995). Namely, both the superexchange and the RKKY couplings are indeed present: the RKKY coupling scales as $1/d$ between nearest-neighbor sites, $1/d^2$ between next nearest neighbors, etc. which is precisely the correct scaling such that a finite contribution to the magnetic energy is obtained. [For a more detailed analysis of the RKKY coupling in large dimensions, see Jarrell (1995).] Therefore, phases with long-range order do appear. This makes the LISA approach more suitable to capture these effects than the large-N methods (in which magnetic effects only appear at order $1/N^2$, cf. Read, Newns, and Doniach, 1984). These magnetic scales also appear in two-particle response functions at a fixed value of **q** above the ordering temperature. However, they do not show up in single-particle properties such as the self-energy, so that no precursor effect of the magnetic transitions exists, e.g., for the effective mass in this approach. Also, collective excitations (e.g., spin waves) are absent. The problem was already discussed in Sec. VII in connection with the Mott transition, and is intrinsic to single-site descriptions. Extensions of the LISA method are required to capture these effects (cf. Sec. IX).

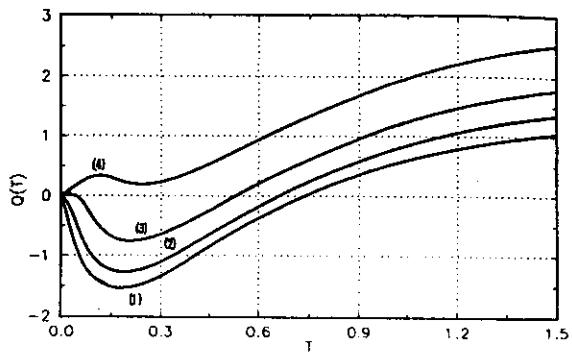

FIG. 66. Temperature dependence of the thermopower $Q(T)$ for the same parameters as in Fig. 65 (from Schweitzer and Czycholl, 1991b).

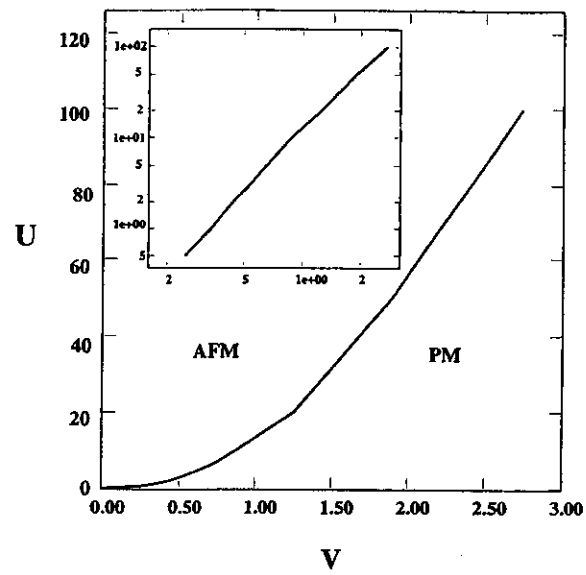

FIG. 67. Phase diagram of the periodic Anderson model on the z=∞ Bethe lattice. The inset shows, in a log-log plot, that the second-order critical line obeys $U_c \approx V_c^2$ as U becomes large. The results are from exact diagonalization with n_s=6.

2. Half-filled case: Kondo insulators

More recently, quantitative studies of the LISA equations for the periodic Anderson model going beyond perturbative approximations have appeared in the literature, focusing particularly on the half-filled case $\langle n_c \rangle + \langle n_f \rangle = 2$ (ϵ_f=0 with the notations above). This case is relevant for the so-called "Kondo insulators" such as CeNiSn, $Ce_3Bi_4Pt_3$, and SmB_6 (and perhaps also FeSi). In the work of Jarrell, Akhlaghpour, and Pruschke (1993a) and Jarrell (1995), the quantum Monte Carlo method is used to solve the associated impurity problem and calculate densities of states and various response functions. It was also found that the half-filled solution has an antiferromagnetic instability for some range of parameters.

The study of solutions with commensurate antiferromagnetic long-range order was considered by Sun, Yang, and Hong (1993) within a slave-boson approximation for the impurity problem, and in more detail by Rozenberg (1995) using the exact diagonalization method. The resulting phase diagram is depicted in Fig. 67. The paramagnetic and antiferromagnetic phases are separated by a second-order critical line that obeys $V^2/UD \approx J_c/D$, with $J_c \approx 0.075D$. Thus the large dimensional solution of the PAM realizes early ideas of Doniach (1977), who found that at the (static) mean field level $J_c/D \sim O(1)$, and argued that dynamical fluctuations should strongly reduce this ratio. It is also interesting to note that the phase diagram is in good agreement with the recent results of Vekić *et al.* (1995) for the *two-dimensional* PAM obtained from quantum Monte Carlo simulations on a finite lattice, and to those of Möller and Wölfle (1993) in the three-dimensional case.

A typical result for the spectral density of the half-filled PAM in the paramagnetic phase is depicted in Fig.

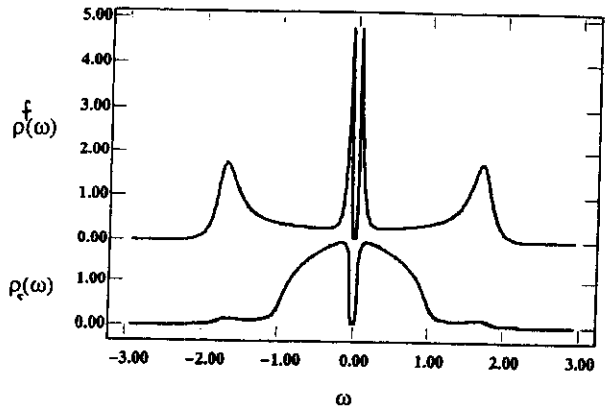

FIG. 68. Density of states for the c and f electrons (bottom and top) in the half-filled periodic Anderson model for $U/D=2.5$ and $V/D=0.4$ at $T/D=0.01$.

68. The result was obtained by the iterated perturbation theory method (Sec. VI.B.2), and compares favorably with the results of exact diagonalizations or quantum Monte Carlo [there are small differences, though, as noted in the work of Jarrell, Akhlaghpour, and Pruschke (1993a)]. It is useful to note that the iterated perturbation theory method, similarly to what happens in the case of the Hubbard model, bases its success on the property of capturing correctly the limit in which either $D\to 0$ or $V\to 0$, and also (by construction) the weak-coupling limit $U\to 0$. The spectral density displays a narrow insulating gap $\Delta_{\rm ind}$, with two sharp peaks on each side. As discussed below, this gap corresponds to an *indirect gap* of the renormalized band structure. Furthermore, satellites at $\pm U/2$ are also found, as expected from the study of the atomic limit. As already observed for the Hubbard model in Sec. VI.B.2, these high-energy satellites are not correctly captured by the "self-consistent" weak-coupling expansions mentioned above; a comparison with Figs. 3(a)–3(c) of Schweitzer and Czycholl (1990a), in which these peaks are absent, illustrates the point. We believe that the sharp peaks on the gap edges are related to the features observed by photoemission on FeSi by Park, Shen, *et al.* (1994).

These results can be understood by performing a low-frequency analysis of the dynamical mean-field equations. Let us make the assumption that the f-electron spectral density displays a gap $\Delta_{\rm ind}$. This implies that the low-frequency behavior of the f-electron Green's functions is $G_f(i\omega_n)\sim i\omega_n$. A convenient parametrization of this linear behavior is

$$V^2 G_f(i\omega_n)=-\left(1+\frac{\langle\epsilon^2\rangle}{V_*^2}\right)i\omega_n+O(\omega_n^3). \tag{284}$$

In this expression, V_* is an effective hybridization renormalized by the interaction (for $U=0$, it is easily checked that $V_*=V$) and $\langle\epsilon^2\rangle$ simply denotes $\int d\epsilon\, D(\epsilon)\epsilon^2$. Inserting this into the self-consistency condition (283), one finds that the density of states of the effective bath entering the impurity model take the form

$$\Delta(\omega)\equiv-\frac{1}{\pi}\,\mathrm{Im}\mathcal{G}_0^{-1}(\omega+i0^+)$$
$$=\frac{V_*^2}{V_*^2+\langle\epsilon^2\rangle}\,\delta(\omega)+\Delta_g(\omega), \tag{285}$$

in which $\Delta_g(\omega)$ denotes a nonsingular density of states also displaying a gap. Hence, the effective bath density of states has a single localized level at zero energy, in the middle of the insulating gap. Solving the Anderson impurity model with this bath shows that (i) the assumption of a gap is a self-consistent one and (ii) a local Kondo effect does take place (despite the insulating character of the lattice problem), involving the f orbital and this localized level. The low-energy expansion of the self-energy reads

$$\mathrm{Re}\,\Sigma_f(\omega+i0^+)=-\left(\frac{V^2}{V_*^2}-1\right)\omega+O(\omega^3) \tag{286}$$

while $\mathrm{Im}\Sigma_f(\omega+i0^+)$ vanishes inside the gap, and is actually zero within a wider interval of energies (or "direct gap"): $-\Delta_{\rm dir}/2<\omega<+\Delta_{\rm dir}/2$, as we will show. The "renormalized" (quasiparticle) bands $E_{\mathbf{k}}$ are obtained by locating the poles of the conduction electron Green's function $G_c(\mathbf{k},\omega)$; i.e., the bands are solutions of

$$[E_{\mathbf{k}}-\epsilon_{\mathbf{k}}][E_{\mathbf{k}}-\Sigma_f(E_{\mathbf{k}})]-V^2=0. \tag{287}$$

An approximation of the band structure and of $\Delta_{\rm ind}$ and $\Delta_{\rm dir}$ can be obtained by substituting the self-energy in this equation by its low-frequency linear behavior (286). This leads to

$$E_{\mathbf{k}}^{\pm}\simeq\frac{1}{2}\left[\epsilon_{\mathbf{k}}\pm\sqrt{\epsilon_{\mathbf{k}}^2+4V_*^2}\right]. \tag{288}$$

This expression is identical to the one for $U=0$, with the replacement $V\to V_*$. The indirect gap corresponds to the distance between renormalized band edges. Denoting by D the half-width of the noninteracting density of states, we obtain

$$\Delta_{\rm ind}\simeq\sqrt{D^2+4V_*^2}-D \tag{289}$$

while the smallest direct gap is for $\epsilon_{\mathbf{k}}=0$ and reads

$$\Delta_{\rm dir}\simeq 2V_*. \tag{290}$$

It is seen that $\Delta_{\rm ind}\simeq 2V_*^2/D\ll\Delta_{\rm dir}$ when $V_*\ll D$.

The indirect gap appearing in the spectral density also sets the low-energy scale appearing in the temperature dependence of the uniform spin and charge susceptibilities. Consistently with the existence of sharp peaks at the gap-edges in the spectral density, the magnetic susceptibility raises sharply as a function of temperature for $T>\Delta_{\rm ind}$, and reaches a maximum at a scale set by the gap $\Delta_{\rm ind}$ itself. This behavior is in good qualitative agreement with the experimental findings of Jaccarino *et al.* (1967) for FeSi. The QMC result of Jarrell, Akhlaghpour, and Pruschke (1993a) for $\chi(T)$ is displayed in Fig. 69. Jarrell (1995) reports a charge and spin gap comparable to each other: $\Delta_c\simeq\Delta_s\simeq 2\Delta_{\rm ind}$, but recent results of Rozenberg, Kotliar, and Kajueter (1995) in the deep

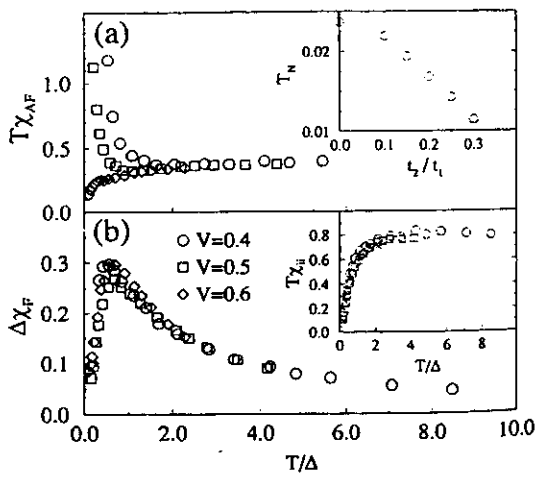

FIG. 69. Staggered (AF) and uniform (F) spin susceptibilities of the symmetric PAM with $U=2$ on the hypercubic lattice $[t_{ij}=1/2\sqrt{d}$, for various values of V (from Jarrell, Akhlaghpour, and Pruschke (1993a, 1993b)]. The inset of (a) shows the Néel temperature T_N when $V=0.4$ as a function of a frustrating hopping t_2/t_1. The inset of (b) shows the local spin susceptibility.

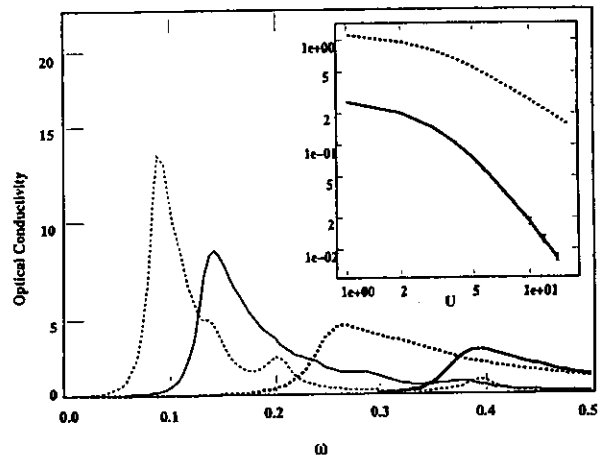

FIG. 70. The optical conductivity spectra of the periodic Anderson model, obtained by iterated perturbative theory for values of the interaction $U=0.5,1,2,3$ (right to left), keeping the hybridization $V=0.25$ fixed. The inset shows the gap from the optical spectra $\Delta_c \approx \Delta_{dir}$ and the indirect gap Δ_{ind} from the local density of states for $V=0.6$. The slopes of these curves indicate that $V^{*2}/D \propto \Delta_{ind}$ and $V^* \propto \Delta_{dir}$ in the strong correlation region. Similar results have been obtained by Jarrell (1995) using the QMC method.

Kondo regime may indicate deviation from this behavior, and we regard this issue as yet unresolved. Note that, in the one-dimensional case, $\Delta_c \gg \Delta_s$ (Nishino and Ueda, 1993), while the Gutzwiller approximation (Rice and Ueda, 1986) leads to $\Delta_c \simeq \Delta_s$. Jarrell (1995) has also studied the behavior of the thermodynamic properties as a function of temperature, and whether a scaling behavior applies to each of them, as a function of T/Δ_{ind}. Recent work by Saso and Itoh (1995) studies the effect of an applied magnetic field on Kondo insulators using the LISA.

We now briefly describe the results for the optical conductivity. This was first investigated by Jarrell (1995) using QMC, and recently by Rozenberg, Kotliar, and Kajueter (1995) using exact diagonalization and the iterated perturbation theory approximation to treat the strong coupling regime. These results can be compared to the recent experimental results of Bucher *et al.* (1994) and Schlesinger *et al.* (1993) on the optical response of $Ce_3Bi_4Pt_3$ and FeSi respectively. A plot of the optical conductivity $\sigma(\omega)$ for different values of U at $T=0$ is shown in Fig. 70. These results show that the optical gap is set by the *direct gap* Δ_{dir} of the renormalized band structure. This is because $\mathrm{Im}\Sigma$ becomes nonzero at this scale. Thus the emerging picture is consistent with the usual interpretation of the hybridization band insulator, with a renormalized hybridization as described above. However, interesting effects are found as a function of temperature. In Fig. 71 we show the optical conductivity for different temperatures and the parameters $U=3$ and $V=0.25$ fixed. The gap is essentially temperature independent. It begins to form at $T^* \approx \Delta_{dir}/5$, and is fully depleted only at temperatures of the order of $T^*/5$, that is, when T becomes comparable to the size of the gap in the density of states. It is actually interesting to compare how the process of filling of the optical gap is correlated with the filling of the gap in the coherent features of the single-particle spectra and with their subsequent disappearance at high temperature. This comparison makes more evident the different energy scales associated with the optical gap and the coherent gap in the density of states. The single-particle spectra for the c and f electrons is displayed in Fig. 72.

The behavior described above is qualitatively similar to the experimental observations in the Kondo insulator systems mentioned above, which are reproduced in Figs. 73 and 74. Note that, while they correspond to different compounds, the two spectra have many common features. A point worth mentioning is that the solution of the model within the iterated perturbation theory

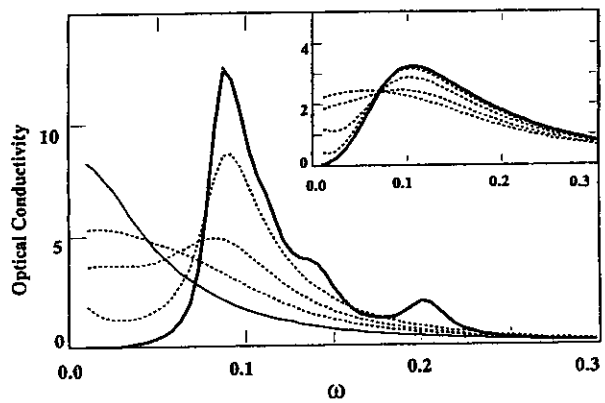

FIG. 71. The optical conductivity for the Anderson model at $T=0.001$ (bold), 0.005, 0.01, 0.02 (dotted), 0.03 (thin). The interaction $U=3$ and $V=0.25$. Inset: The same quantity at $T=0.001$ (bold); 0.005, 0.01, 0.02, 0.03 (dotted); with Lorentzian random site disorder of width $\Gamma=0.005$.

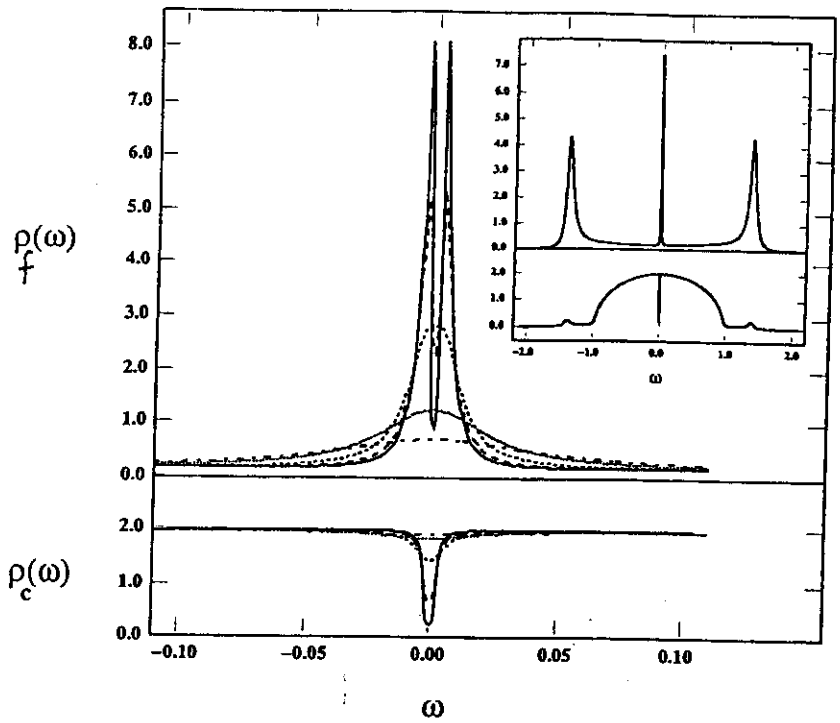

FIG. 72. Low-frequency part of the density of states for the f and c electrons (top and bottom) obtained from iterative perturbation theory at T=0.001 (full), 0.005 (long-dashed), 0.01 (short-dashed), 0.02 (dotted), 0.03 for U=3 and V=0.25. Inset: The density of states in the full frequency range at T=0.001.

method predicts an interesting nonmonotonic behavior of the total integrated optical spectral weight as a function of the temperature. It is observed that the integrated weight initially increases with temperature, up to temperatures of the order of the size of the optical gap. A further increase of T leads to a decrease of the integrated weight as the system turns metallic and correlations become unimportant. The fact that in the low-temperature range the integrated weight increases with T may be relevant for the resolution of the problem of the "missing spectral weight" experimentally observed in the Kondo insulators compounds (Schlesinger *et al.*, 1993; Bucher *et al.*, 1994).

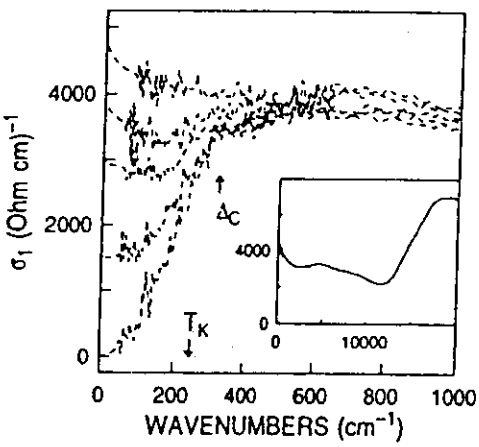

FIG. 73. Optical conductivity $\sigma(\omega)$ of $Ce_3Bi_4Pt_3$ for different temperatures (from below: 25, 50, 75, 100, and 300 K), from Bucher *et al.* (1994). A gap is opening below 100 K; the prominent feature at Δ_c seems to be independent of temperature. The inset presents the optical region of σ.

To end this section, we mention that an alternative model for FeSi has been proposed and studied in the $d\to\infty$ limit by Fu and Doniach (1994). The model is that of a strongly correlated semiconductor consisting of two bands of dominantly iron character. The proposed Hamiltonian reads

$$H=\sum_{\langle ij\rangle\sigma} -t(c^{\dagger}_{i1\sigma}c_{j1\sigma}-c^{\dagger}_{i2\sigma}c_{j2\sigma}+\text{H.c.}) + \sum_{i\sigma} V(c^{\dagger}_{i1\sigma}c_{i2\sigma}+\text{H.c.}) + \sum_{i} U(n_{c_{i1\uparrow}}n_{c_{i1\downarrow}}+n_{c_{i2\uparrow}}n_{c_{i2\downarrow}}). \quad (291)$$

The opposite sign of the two hopping terms provides a direct gap between the valence and conduction band. The self-consistent perturbation theory was used by Fu and Doniach to compute various quantities, among which are the temperature dependence of the susceptibility and the spectral functions. At this moment, we are

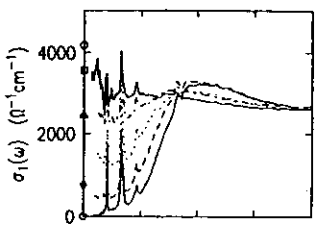

FIG. 74. Optical conductivity $\sigma(\omega)$ of cubic FeSi for different temperatures (from below: 20, 100, 150, 200, and 250 K), from Schlesinger *et al.* (1993). The symbols at ω=0 show the measured values of σ_{dc} for the same temperature sequence.

$$w_1=\left\{1+\exp(\beta(\epsilon_f-\mu)+\sum_n \{\ln[\mathcal{G}_0^{-1}(i\omega_n)] - \ln[\mathcal{G}_0^{-1}(i\omega_n)-U]\}e^{i\omega_n 0^+})\right\}^{-1}, \quad (303)$$

Differentiating the partition function with respect to ϵ_f, we see that w_1 is the f particle number per site. The local conduction electron self-energy is defined as usual through

$$G(i\omega_n)^{-1}=\mathcal{G}_0^{-1}(i\omega_n)-\Sigma(i\omega_n). \quad (304)$$

When combined with the explicit form of the Green's function Eq. (302), this leads to the functional form of the self-energy $\Sigma(i\omega_n)\equiv\Sigma_n$ in terms of the local Green's function $G(i\omega_n)\equiv G_n$:

$$\Sigma_n(G_n)=U/2-1/2G_n\pm\sqrt{(U/2-1/2G_n)^2+w_1U/G_n}, \quad (305)$$

where the sign is to be chosen (depending on frequency) in such a way that Σ has the appropriate analytic properties. Furthermore, the self-consistency equation reads, as usual,

$$G_n=\int_{-\infty}^{\infty}d\epsilon\,\frac{D(\epsilon)}{i\omega_n+\mu-\epsilon-\Sigma_n(G_n)}, \quad (306)$$

where $D(\epsilon)$ is the conduction electron bare density of states. Equations (303), (305), and (306), first derived by Brandt and Mielsch (1989), form a closed set of equations for the *conduction electron* Green's function and self-energy in phases without long-range order. An interpretation of these equations as a mean-field theory, rather different in spirit to the mapping onto an effective impurity problem, has been given by van Dongen and Vollhardt (1990) and van Dongen (1991a, 1992).

Before turning to the description of possible long-range order and of the phase diagram of the model, let us mention some results on the behavior of the Green's function in phases without order (e.g., at high temperature). van Dongen (1991a, 1992) established that the model displays a metal-insulator transition as a function of U at half-filling $n_c+n_f=1$, at $U_c=D$ when $D(\epsilon)$ is semicircular with a half-bandwidth D. Si, Kotliar, and Georges (1992) established that there are two regions, as a function of the total density $n=n_c+n_f$ and U:

(i) For U larger than $U_c(n)$, the number of f electrons per site is either $n_f=0$ or $n_f=1$. In that region, the conduction electrons obviously behave as a free Fermi gas.

(ii) For U smaller than $U_c(n)$, there is a finite occupancy $0<n_f<1$, and the chemical potential *remains pinned* at the effective f-electron level: $\mu=E_f$, with E_f defined by $w_1=\{1+\exp\beta(E_f-\mu)\}^{-1}$. In this regime, the conduction electron self-energy has a *finite imaginary part* at zero frequency, and the Fermi-liquid theory breaks down.

The f electron (ion) Green's functions is more difficult to obtain than the conduction electron one. To this aim, it is useful to realize that the Hamiltonian form of the impurity effective action (301) is the x-ray edge Hamiltonian:

$$H=\sum_{\mathbf{k}}E_{\mathbf{k}}a_{\mathbf{k}}^+a_{\mathbf{k}}+(\epsilon_f-\mu)f^+f+Uf^+f\sum_{\mathbf{k}\mathbf{k}'}a_{\mathbf{k}}^+a_{\mathbf{k}'} \quad (307)$$

with the spectral representation

$$\mathcal{G}_0^{-1}=\left\{\sum_{\mathbf{k}}\frac{1}{i\omega_n-E_{\mathbf{k}}}\right\}^{-1}-\mu. \quad (308)$$

It results from this mapping that, in the pinning region mentioned above, the f-electron spectral function has an x-ray edge singularity at low frequencies (Si, Kotliar, and Georges, 1992). A numerical study of the heavy electron Green's function of this model (Brandt and Urbanek, 1992) is consistent with a thermal smearing of the x-ray singularity. Further analytic work on this problem was carried out by Janiš (1993).

At low temperature, the $d=\infty$ Falicov-Kimball model displays ordered phases in which both the conduction electron and f-electron (ion) charge densities acquire nonzero values, at a given ordering vector $\mathbf{q}$. For the symmetric half-filled case ($\epsilon_f=0$, $n_c=n_f=1/2$), the ordering is towards a commensurate $[\mathbf{q}=(\pi,\ldots,\pi)]$ ordered state, in which the particles order in a checkerboard pattern: the conduction electrons occupy one sublattice, and the ions the other one. (Viewing each electrons species as a given spin species, this state can be called a spin-density wave state, and is the direct analog of the Néel state). This is true in any dimension on a bipartite lattice, and has been established rigorously (Brandt and Schmidt 1986, 1987; Kennedy and Lieb, 1986). For $d=\infty$, Brandt and Mielsch (1989, 1990, 1991) were able to establish equations for the CDW susceptibility $\chi(\mathbf{q})$, and computed the critical temperature at half-filling as a function of U. van Dongen and Vollhardt (1990) showed analytically that $T_c\sim 1/U$ for large U, while $T_c\sim U^2\ln(1/U)$ for small U. The CDW transition is second-order (Ising-like), but can be driven first-order in the presence of a nearest-neighbor repulsion V (van Dongen, 1991a, 1992). For $V>U/2$, a charge-density wave transition is found instead, with doubly occupied sites on one sublattice, and holes on the other (van Dongen, 1991a, 1992).

These results have been extended for arbitrary electron density n_c (keeping $n_f=1/2$) by Freericks (1993a), for the $d=\infty$ hypercubic lattice. He showed that, for a given U, the ordering becomes *incommensurate* for a range of electron concentrations. For still smaller densities, a segregated phase is found (in which ions and electrons cluster in separate regions). As explained in Sec. IV, the ordering wave vector can be characterized by $X(\mathbf{q})=1/d\sum_{i=1}^{d}\cos q_i$. It varies continuously with U and n_c within the incommensurate phase. The phase diagram established by Freericks (1993a) is displayed in Fig. 76. Freericks (1993b) also used the LISA as a dynamical mean-field approximation to the *finite-dimensional* Falicov-Kimball model, and concluded that the approximation is inaccurate at strong coupling in $d=1$, but is a very good description of the model in $d\geq 2$. The optical conductivity of the Falicov-Kimball model on the hypercubic lattice was computed by Moeller, Ruckenstein, and Schmitt-Rink (1992).

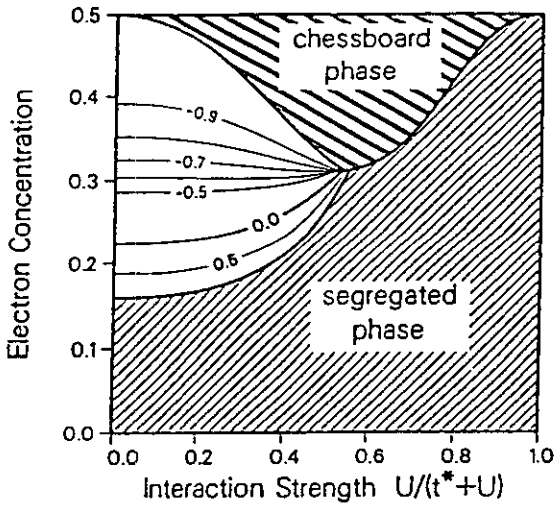

FIG. 76. Phase diagram of the Falicov-Kimball model on the hypercubic lattice for $n_f=1/2$, $\epsilon_f=0$, as a function of U and electron concentration n_c. Contour lines of constant $X(\mathbf{q})$ are indicated. From Freericks (1993a).

Finally, let us mention that the Falicov-Kimball model has been used by several authors to devise *approximations* to the solution of the $d=\infty$ Hubbard model. The general idea behind these approaches is to treat one of the spin species as moving in the background of the other one, considered frozen and static (Janiš and Vollhardt, 1992a; Li and d'Ambrumenil, 1992; Edwards, 1993; Laad, 1994).

C. Multiband models: Combining LISA and LDA

The models considered up to now in this article are idealized models of strongly correlated electron systems containing a single conduction electron band. In actual materials, one is always faced with the issue of orbital degeneracy. Even in relatively simple systems such as the transition-metal monoxides (e.g., NiO, FeO, etc.), a minimal realistic description must take into account a fivefold d band splitted by crystal field effects into, for example, $d_{x^2-y^2}$, $d_{3z^2-r^2}$, d_{xy}, d_{xz}, d_{yz}, and a threefold oxygen band p_x, p_y, p_z. This also allows a classification of transition-metal oxides into Mott insulators (for $U_{dd} \ll \epsilon_p - \epsilon_d$) and charge-transfer insulators (for $U_{dd} \gg \epsilon_p - \epsilon_d$; see Zaanen, Sawatzky, and Allen, 1985). In this section, we describe how the LISA approach can be used as a dynamical mean-field *approximation* to deal with the band degeneracy and lattice structure of actual materials in a more realistic way. Quantitative calculations along these lines are only starting, but we expect it to be a fruitful direction for further research.

The starting point of any such calculation is the band structure of the material, as obtained e.g., by the LDA method (or some other technique). This zeroth-order starting point provides one with a Hamiltonian

$$H_0=\sum_{\nu\sigma\mathbf{k}} \epsilon_\nu(\mathbf{k}) c^+_{\mathbf{k}\sigma\nu} c_{\mathbf{k}\sigma\nu} \tag{309}$$

in which ν denotes a band index. Band calculations are an excellent description of many materials, but are well-known to fail to predict correctly the insulating character of oxides such as CoO or FeO because of the neglect of electron-electron interactions. Various schemes have been proposed to include those in the LDA approach (such as the "LDA+U" method of Anisimov, Zaanen, and Andersen, 1991). These schemes do lead to significant improvement, but obviously do not include all the dynamical effects of the interaction. Capturing these effects is the main motivation of the LISA method.

Starting from H_0, the most straightforward way of implementing the LISA method is to use a *tight-binding projection* of the band structure. This consists in projecting the Bloch waves onto a set of orbitals $d_{i\sigma\alpha}$ localized at the sites $\mathbf{R}_i$ of a lattice appropriate to the material considered:

$$c^+_{\mathbf{k}\sigma\nu}=\sum_{i\alpha} e^{i\mathbf{k}\cdot\mathbf{R}_i} A_{\nu\alpha}(\mathbf{k}) d^+_{i\sigma\alpha}. \tag{310}$$

In this formula, the $A_{\nu\alpha}(\mathbf{k})\equiv\langle\alpha|\nu,\mathbf{k}\rangle$ are the eigenvectors of the single-particle Schrödinger equation and satisfy the closure relations:

$$\sum_{\mathbf{k}\nu} A_{\nu\alpha}(\mathbf{k}) A_{\nu\beta}(\mathbf{k})^* = \delta_{\alpha\beta},$$

$$\sum_{\alpha} A_{\nu\alpha}(\mathbf{k}) A_{\nu'\alpha}(\mathbf{k})^* = \delta_{\nu\nu'}. \tag{311}$$

In terms of the tight-binding orbitals, the free Hamiltonian H_0 takes the form

$$H_0=\sum_{ij,\sigma} t_{ij}^{\alpha\beta} d^+_{i\sigma\alpha} d_{j\sigma\beta}, \tag{312}$$

in which the hopping amplitudes $t_{ij}^{\alpha\beta}$ reads

$$t_{ij}^{\alpha\beta}=\sum_{\mathbf{k}} e^{i\mathbf{k}\cdot(\mathbf{R}_i-\mathbf{R}_j)} \sum_{\nu} A_{\nu\alpha}(\mathbf{k}) A_{\nu\beta}(\mathbf{k})^* \epsilon_\nu(\mathbf{k}), \tag{313}$$

or, in reciprocal space,

$$t_{\mathbf{k}}^{\alpha\beta}=\sum_{\nu} A_{\nu\alpha}(\mathbf{k}) \epsilon_\nu(\mathbf{k}) A_{\nu\beta}(\mathbf{k})^*. \tag{314}$$

Electron-electron interactions must now be added to H_0. A word of caution is in order here, since the LDA eigenstates $\epsilon_\nu(\mathbf{k})$ already contain some of the effects of these interactions. One of the main difficulties in this context is thus to separate the static terms, taken into account by LDA, from the additional terms, to be treated dynamically, without double counting. Without dealing further with this difficulty, we shall assume that interactions can be introduced in the tight-binding representation in the simplified form of Hubbard type local interactions, and we shall consider the Hamiltonian

$$H=H_0+\sum_i \sum_{\alpha\beta} U_{\alpha\beta} d^+_{i\uparrow\alpha} d_{i\uparrow\alpha} d^+_{i\downarrow\beta} d_{i\downarrow\beta}. \tag{315}$$

The Hubbard parameters $U_{\alpha\beta}$ can in principle also be calculated in the framework of the LDA. Of course, a more complete description of the interactions should include nonlocal terms coupling different sites, but the treatment of the dynamical effects of such terms requires an extension of the LISA method (cf. Sec. IX).

The LISA method maps this Hamiltonian onto the solution of a self-consistent single-impurity problem. The effective single-site action associated with H reads (restricting ourselves to the paramagnetic phase)

$$S_{\rm eff}=-\int_0^\beta d\tau\int_0^\beta d\tau'\sum_\sigma d^+_{\sigma\alpha}(\tau)[\mathcal{G}_0^{-1}]_{\alpha\beta}(\tau-\tau')d_{\sigma\beta}(\tau')$$
$$+\sum_{\alpha\beta}U_{\alpha\beta}\int_0^\beta d\tau d^+_{\uparrow\alpha}d_{\uparrow\alpha}d^+_{\downarrow\beta}d_{\downarrow\beta}. \quad (316)$$

In order to obtain the self-consistency equation, we consider the lattice Green's function:

$$G_{\alpha\beta}(\mathbf{k},\tau-\tau')\equiv-\langle Td_{\mathbf{k}\sigma\alpha}(\tau)d^+_{\mathbf{k}\sigma\beta}(\tau')\rangle \quad (317)$$

and postulate a momentum-independent self-energy matrix:

$$G_{\alpha\beta}(\mathbf{k},i\omega_n)^{-1}=(i\omega_n+\mu)\delta_{\alpha\beta}-t^{\alpha\beta}_{\mathbf{k}}-\Sigma_{\alpha\beta}(i\omega_n). \quad (318)$$

The self-consistency condition requires that the local (on-site) Green's function coincides with the impurity model one, with identical self-energies:

$$G_{\alpha\beta}(i\omega_n)_{\rm imp}=\sum_{\mathbf{k}}G_{\alpha\beta}(\mathbf{k},i\omega_n), \quad (319)$$

with

$$G_{\alpha\beta}(\tau-\tau')_{\rm imp}\equiv-\langle Td_{\sigma\alpha}d^+_{\sigma\beta}\rangle_{S_{\rm eff}},$$
$$G_{\alpha\beta}(i\omega_n)^{-1}_{\rm imp}=[\mathcal{G}_0^{-1}]_{\alpha\beta}-\Sigma_{\alpha\beta}. \quad (320)$$

Note that not only the knowledge of the band energies $\epsilon_\nu(\mathbf{k})$ and the associated partial density of states is required to implement this self-consistency condition, but also that of the matrix elements $A_{\nu\alpha}(\mathbf{k})$.

In this general context, the LISA, despite its local character, leads to "renormalized bands" [i.e., quasiparticle poles of $G_{\alpha\beta}(\mathbf{k},i\omega_n)$] that do not have, in general, the same $\mathbf{k}$ dependence as the LDA ones $\epsilon_\nu(\mathbf{k})$, and the self-energy does acquire $\mathbf{k}$ dependence when expressed in the basis of Bloch states:

$$\Sigma_{\nu\nu'}(\mathbf{k},i\omega_n)=\sum_{\alpha\beta}A_{\nu\alpha}(\mathbf{k})^*\Sigma_{\alpha\beta}(i\omega_n)A_{\nu'\beta}(\mathbf{k}). \quad (321)$$

Obviously, the results will depend strongly on the choice of the tight-binding basis onto which the LDA results are projected. As a result, the procedure is expected to apply better to those materials for which a set of well-defined localized orbitals is unambiguously dictated by physical considerations.

In order to illustrate this strategy on a simple concrete example, let us consider the three-band model of the CuO_2 layers in cuprate superconductors (Emery, 1987; Varma, Schmitt-Rink, and Abrahams, 1987). The Hamiltonian involves $d_{x^2-y^2}$ and p_x,p_y orbitals in the hole representation (so that the vacuum corresponds to the Cu^+ configuration). Including correlations only on copper sites as a first step, the Hamiltonian reads

$$H_{3B}=-t_{pd}\sum_{i\sigma}d^+_{i\sigma}(p_{i+x,\sigma}-p_{i-x,\sigma}+p_{i+y,\sigma}-p_{i-y,\sigma})$$
$$+4t_{pp}\sum_{\mathbf{k}\sigma}s_xs_yp^+_{\mathbf{k}x\sigma}p_{\mathbf{k}y\sigma}+\text{H.c.}$$
$$+\epsilon_p\sum_{i,\sigma}(p^+_{ix\sigma}p_{ix\sigma}+p^+_{iy\sigma}p_{iy\sigma})+\epsilon_d\sum_{i\sigma}d^+_{i\sigma}d_{i\sigma}$$
$$+U_d\sum_i n^d_{i\uparrow}n^d_{i\downarrow} \quad (322)$$

with $s_{x,y}\equiv\sin(k_{x,y}/2)$. In the LISA method, this model is mapped onto a single-impurity Anderson model associated with copper sites:

$$S_{\rm eff}=U_d\int_0^\beta d\tau\, n_{d\uparrow}(\tau)n_{d\downarrow}(\tau)$$
$$-\int_0^\beta d\tau\int_0^\beta d\tau'\sum_\sigma d_\sigma(\tau)\mathcal{G}_0^{-1}(\tau-\tau')d^+_\sigma(\tau') \quad (323)$$

and the self-consistency condition requests that the on-site copper Green's function $\Sigma_{\mathbf{k}}G_d(\mathbf{k},i\omega_n)$ coincides with the impurity Green's function. Introducing a momentum-independent copper self-energy $\Sigma_d(i\omega_n)$ and expressing the matrix Green's function in the (d_k,p_{kx},p_{ky}) basis, this condition reads

$$\sum_{\mathbf{k}}\begin{pmatrix}\zeta_d & i2t_{pd}s_x & -i2t_{pd}s_y\\ -i2t_{pd}s_x & \zeta_p & 4t_{pp}s_xs_y\\ i2t_{pd}s_y & 4t_{pp}s_xs_y & \zeta_p\end{pmatrix}^{-1}_{dd}$$
$$=G_d(i\omega_n)\equiv[\mathcal{G}_0^{-1}-\Sigma_d]^{-1}, \quad (324)$$

where $\zeta_p\equiv i\omega_n+\mu-\epsilon_p$ and $\zeta_d=i\omega_n+\mu-\epsilon_d-\Sigma_d(i\omega_n)$. This equation takes a much simpler form in the absence of direct oxygen-oxygen hopping $t_{pp}=0$. In this case, the copper and oxygen Green's functions read

$$G_d(\mathbf{k},i\omega_n)=\frac{\zeta_p}{\zeta_p\zeta_d-\gamma_k^2},$$
$$G_{p_x,p_y}(\mathbf{k},i\omega_n)=\frac{\zeta_d\zeta_p-4t_{pd}^2s_{y,x}}{\zeta_p(\zeta_p\zeta_d-\gamma_k^2)} \quad (325)$$

with $\gamma_k^2\equiv4t_{pd}^2(s_x^2+s_y^2)$. Hence the self-consistency condition reads, in this case,

$$G_d(i\omega_n)=\frac{\zeta_p}{2t_{pd}^2}\tilde{D}\left(\frac{\zeta_p\zeta_d}{2t_{pd}^2}-2\right), \quad (326)$$

where $\tilde{D}$ is the Hilbert transform of the square lattice density of states:

$$\tilde{D}(z)=\int\frac{d^2k}{(2\pi)^2}\frac{1}{z-\cos k_x-\cos k_y}. \quad (327)$$

These equations are easily extended to allow for symmetry breaking (e.g., antiferromagnetic or superconducting), along the lines of Sec. V. They can also be extended to include an oxygen-oxygen repulsion U_{pp}. In this case, one has to solve *two* impurity models, one associated with copper sites and the other with oxygen sites. This is because the copper and oxygen orbitals live on two different sublattices in the above Hamiltonian. For the same reason, the dynamical (excitonic) effects of the nearest-neighbor copper-oxygen repulsion (Varma, Schmitt-Rink and Abrahams, 1987) cannot be captured in the single-site LISA description. These effects, which are considered in more detail in the next section (Sec. VIII.D), can only be addressed in the LISA framework for multiband models in which the various orbitals live *on the same lattice sites*. For models such as (322), only an extension of the LISA framework to self-consistent *clusters* (Sec. IX) would be able to capture these effects.

Finally, let us mention that it is possible to construct a model very similar to Eq. (322) which has a well-defined (and nontrivial) $d=\infty$ limit such that the LISA equations become exact (Georges, Kotliar, and Krauth, 1993). The precise geometry of the CuO_2 layer is not suitable for this purpose; moreover, the CuO_d lattice with one oxygen halfway between each copper site reduces to an atomic problem as $d\to\infty$ [cf. Valenti and Gros, 1993; see, however, the recent suggestion of Schmalian *et al.* (1995) for a different scaling of the hopping in this model]. Alternatively, one may consider a simplified model, which is not quite realistic for the cuprates, but has the advantage of having a nontrivial $d=\infty$ limit. The model is simply a two-band CuO lattice involving a correlated "copper" orbital d_σ living on the A sublattice of a bipartite lattice, and an "oxygen" orbital living on the B sublattice. The copper-copper hopping is scaled as $t_{pd}/\sqrt{z}$, and the direct hopping is scaled as t_{pp}/z. In the limit $z\to\infty$, this model can be solved by considering a single-impurity Anderson model on copper sites (when only U_d is included), and the self-consistency condition reads (on the Bethe lattice)

$$\mathcal{G}_0^{-1}(i\omega_n)=i\omega_n+\mu-\epsilon_d-t_{pd}^2 G_p(i\omega_n),$$
$$G_p(i\omega_n)^{-1}=i\omega_n+\mu-\epsilon_p-t_{pd}^2 G_d(i\omega_n)-t_{pp}^2 G_p(i\omega_n). \tag{328}$$

Some aspects of this model have been studied by Georges, Kotliar, and Krauth (1993) and Caffarel and Krauth (1994). It displays a metal to charge-transfer insulator transition as a function of $(\epsilon_p-\epsilon_d)/t_{pd}$ for large U_d at half-filling, and a Mott insulator to metal transition as a function of U_d/t_{pd} for large $(\epsilon_p-\epsilon_d)/t_{pd}$. The crossover diagram is very similar to the analysis of Zaanen, Sawatzky, and Allen (1985). Finally, a superconducting instability has been suggested to exist in this model for some range of parameters.

D. The extended Hubbard model and excitonic effects

In this section, we shall review some insights provided by the LISA approach into the physics of excitonic effects, that is, the dynamical effects due to the interband Coulomb interaction. There has recently been a renewed theoretical interest in these effects, with the following motivations.

(i) There is new experimental evidence in favor of Bose condensation of excitons (Lin and Wolfe, 1993; Fortin, Fafard, and Mysyrowicz, 1993) and new experimental tools for studying these effects in strongly illuminated semiconductors. There is a strong need for an approach that can describe simultaneously collective and single particle excitations, and the coherent and incoherent parts of the excitation spectra going beyond the Hartree-Fock approximation (Compte and Nozieres, 1982).

(ii) Interband Coulomb interactions may lead to important physical effects in the context of the LISA description of real materials using multiband models reviewed in the previous section (Sec. VIII.C). For cuprate superconductors for example, the copper-oxygen repulsion has been proposed as playing a crucial role by Varma, Schmitt-Rink, and Abrahams (1987; see also Varma and Giamarchi, 1994, for a review). In the limit of large connectivity z, intersite Coulomb interactions must be scaled as $1/z$, and thus produce only Hartree renormalizations of the band. Hence, excitonic effects must be studied in models where the various orbitals live on the *same* sublattice sites, as done in the present section.

(iii) It has been shown by Si and Kotliar (1993) that the Anderson impurity model, in the weak coupling limit can lead to different type of phases when the position of the impurity level is tuned to the Fermi level. In the lattice (Si, Kotliar, and Georges 1992), this tuning of the impurity level to the Fermi level occurs in a *finite range* of densities when the hybridization renormalizes to zero as in the Falicov-Kimball model (Sec. VIII.B). From this perspective, the interband interaction is a parameter that allows us to vary independently the relevant variables of the local impurity model.

Si and Kotliar (1993) considered a model in which localized ("copper") orbitals d_σ and itinerant ("oxygen") orbitals p_σ live on the *same* lattice sites. The motivation is to retain the dynamical effects of the copper-oxygen repulsion and a nontrivial off-diagonal self-energy Σ_{pd}. The Hamiltonian of the model is in the same general class as Eq. (315) and reads

$$\begin{aligned}H=&\sum_{\mathbf{k}}\sum_{\sigma=1}^{N}(\epsilon_{\mathbf{k}}-\mu)p_{\mathbf{k}\sigma}^{+}p_{\mathbf{k}\sigma}+\sum_{i}\sum_{\sigma=1}^{N}(\epsilon_d^0-\mu)d_{i\sigma}^{+}d_{i\sigma}\\&+\frac{U}{2}\sum_{i}\sum_{\sigma\neq\sigma'}^{N}d_{i\sigma}^{+}d_{i\sigma}d_{i\sigma'}^{+}d_{i\sigma'}\\&+\sum_{i}\sum_{\sigma=1}^{N}t(d_{i\sigma}^{+}p_{i\sigma}+\text{H.c.})\\&+\frac{V_1}{N}\sum_{i}\sum_{\sigma,\sigma'=1}^{N}p_{i\sigma}^{+}p_{i\sigma}d_{i\sigma'}^{+}d_{i\sigma'}\\&+\frac{V_2}{N}\sum_{i}\sum_{\sigma,\sigma'=1}^{N}p_{i\sigma}^{+}p_{i\sigma'}d_{i\sigma'}^{+}d_{i\sigma}.\end{aligned} \tag{329}$$

model. Accordingly, a detailed study of the $d=\infty$ limit does not provide only a mean-field description of the problem, but also determines the form of the leading corrections resulting from fluctuations. Corrections to physical quantities at the one-loop level have, however, not been calculated to date. The transverse fluctuations in these theories are the soft modes identified by Finkhelstein (1987) in his pioneering work on the interplay of localization and interactions. A detailed study of the effects of fluctuations still remains to be carried out. The methods of Sec. VI.C may prove to be very useful for the evaluation of the coefficients of the effective Lagrangian.

In the derivation presented in this section, the randomness on the hopping matrix elements greatly facilitated the formulation of a path-integral approach. Nevertheless it seems to us that it only played the role of a technical trick, and in fact one should be able to formulate a similar loop expansion for the nonrandom models. This is clearly an important problem for further research.

X. CONCLUSION

This rather long article can only end with a brief conclusion. The main message that we have tried to convey is that the local impurity self-consistent approximation (LISA) provides a powerful framework for the quantitative description of strongly correlated fermion systems. This approximation becomes exact in the limit of infinite dimensions/infinite lattice coordination, but can be viewed more generally as a *dynamical mean-field theory* for these systems. As reviewed in this article, this approach has led to significant progress on several problems in the physics of strongly correlated fermions. Some favorable comparisons of the LISA results to experimental findings on various materials have already been made.

In the hope of stimulating further work in this area, we have tried to emphasize in this article the physical content of the LISA method, and to review in detail the derivation of the dynamical mean-field equations, and the various analytical techniques and numerical algorithms available to solve them. It seems to us that there are at least three general directions in which further research is needed and progress is possible:

(i) Improvements in the efficiency and flexibility of the algorithms for the solution of the LISA dynamical mean-field equations would be technically very helpful (cf. Sec. VI).

(ii) In an attempt to push further the comparison with experiments (particularly on transition metal oxides), an effort could be made to include more realistic features of the actual materials (such as band structure aspects and orbital degeneracy) within the LISA method. It may even be possible to incorporate ideas from the LISA method into electronic structure calculations of real materials (cf. Sec. VIII.C).

(iii) The LISA method is a mean-field approximation in the sense that it freezes *spatial* fluctuations. It is clearly an outstanding theoretical problem in the field to go beyond the LISA, and treat these fluctuations in a consistent manner (both from the point of view of short-range correlations and of long wavelength collective modes, cf. Sec. IX).

In our view, the field of strongly correlated electron systems is ripe for new progress, and we expect the LISA method to play a major role in the quantitative description of these fascinating materials.

ACKNOWLEDGMENTS

We are deeply indebted to our collaborators in the field, M. Caffarel, V. Dobrosavljević, D. S. Fisher, H. Kajueter, L. Laloux, G. Moeller, S. Sachdev, D. D. Sarma, A. Sengupta, Q. Si, G. Thomas, X. Y. Zhang, and have benefitted from very useful discussions with C. Castellani, P. van Dongen, D. Feinberg, J. Freericks, T. Giamarchi, C. Gros, M. Imada, K. Ingersent, I. Inoue, V. Janiš, M. Jarrell, Y. Kuramoto, A. Millis, E. Müller-Hartmann, W. Metzner, P. Nozières, A. Ruckenstein, A. Schofield, Z. X. Shen, and D. Vollhardt. We acknowledge expert help with computers from T. Besancon. We would like to thank G. Toulouse and D. Pines for their encouragement in writing this article. During the course of this work, we have benefitted from the hospitality of the International Center for Theoretical Physics (Trieste), the Institute for Scientific Interchange (Torino), and the Aspen Center for Physics. Laboratoire de Physique Théorique de l'Ecole Normale Supérieure is Unité propre du CNRS (UP 701) associée à l'ENS et à l'Université Paris-Sud. Laboratoire de Physique Statistique de l'Ecole Normale Supérieure is Laboratoire associé au CNRS (URA 1306) et aux Universités Paris VI et Paris VII. G.K. was supported by the NSF under Grant DMR-92-2400. We acknowledge support from a joint CNRS-NSF grant (NSF-INT-93-14273COOP) which has been instrumental for carrying out this work.

APPENDIX A: FERMIOLOGY IN $d=\infty$

In this appendix, we collect various useful results on the fermiology of tight-binding electrons on infinite-dimensional lattices. A large part of this section follows the paper of Müller-Hartmann (1989a).

1. Density of states of some $d=\infty$ lattices

We start with the simplest case of free electrons on a d-dimensional cubic lattice with nearest-neighbor hopping. The lattice spacing a is set to $a=1$. The hopping is normalized to

$$t_{ij}=\frac{t}{\sqrt{2d}} \tag{A1}$$

so that the Fourier transform of the kinetic energy per spin reads

$$\epsilon_{\mathbf{k}}=-\frac{2t}{\sqrt{2d}}\sum_{i=1}^{d}\cos k_i . \tag{A2}$$

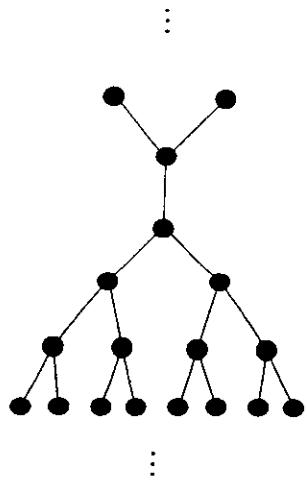

FIG. 86. Bethe lattice (depicted here with connectivity $z=3$).

with nearest-neighbor hopping $t_{ij}=t/\sqrt{z}$, for arbitrary connectivity z. We concentrate on site o and perform the Gaussian integration over all other sites (Fig. 86). Setting $\zeta \equiv i\omega_n+\mu$, this yields

$$G_{oo}^{-1}(\zeta)=\zeta-\frac{t^2}{z}\sum_{\langle i,o\rangle} G_{ii}^{(o)}=\zeta-t^2 G_{ii}^{(o)}. \tag{A39}$$

In this equation i denotes a neighbor of o and $G_{ii}^{(o)}$ is the Green's function of site i *once o has been removed.* Translation invariance has been used, all sites i being identical. For finite connectivity however, $G_{ii}^{(o)}$ does not coincide with G_{oo} even in the limit of an infinite lattice. This is because the local topology has been changed when removing site o: each neighbor i now has only $z-1$ nearest neighbors. For large connectivity, this is of course a $1/z$ effect, and $G_{ii}^{(o)}$ can be identified to G_{oo} in the equation above, yielding a closed formula. Even for finite connectivity however, the elimination process can be taken one step further, performing the Gaussian integration over the $z-1$ neighbors of each site i. This yields

$$[G_{ii}^{(o)}]^{-1}=\zeta-(z-1)\frac{t^2}{z}G_{jj}^{(o,i)}. \tag{A40}$$

In this equation, $G_{jj}^{(o,i)}$ denotes the Green's function of a neighbor j of i, in the truncated tree where both sites o and i have been removed. For an infinite lattice, j is entirely similar to i, so that $G_{ii}^{(o)}=G_{jj}^{(o,i)}$. This yields a closed equation for this quantity:

$$\frac{z-1}{z}t^2[G_{ii}^{(o)}]^2-\zeta G_{ii}^{(o)}+1=0, \tag{A41}$$

from which the local Green's function $G\equiv G_{oo}$ [which is also the Hilbert transform $\tilde{D}(\zeta)$ of the density of states] is finally obtained as [for $\mathrm{Im}(\zeta)>0$]

$$G\equiv\tilde{D}(\zeta)=\frac{(z-2)\zeta-z\sqrt{\zeta^2-4(z-1)t^2/z}}{2(zt^2-\zeta^2)}. \tag{A42}$$

The density of states $D(\epsilon)=-\mathrm{Im}G(\epsilon+i0^+)/\pi$ thus reads

$$D(\epsilon)=\frac{\sqrt{\epsilon^2-4(z-1)t^2/z}}{2\pi(t^2-\epsilon^2/z)}. \tag{A43}$$

(One can check that the familiar $d=1$ expression can be recovered for $z=2$.) Taking the $z\to\infty$ limit yields the expressions often used in this article:

$$G\equiv\tilde{D}(\zeta)=\frac{\zeta-\sqrt{\zeta^2-4t^2}}{2t^2},\quad D(\epsilon)=\frac{\sqrt{\epsilon^2-4t^2}}{2\pi t^2}. \tag{A44}$$

It may also be useful to quote the expression of the reciprocal function $R(G)$ of the Hilbert transform $\tilde{D}(\zeta)$, i.e., such that $R(\tilde{D}(\zeta))=\zeta$. For arbitrary connectivity, it is the solution of the quadratic equation:

$$(z-1)R^2+\frac{(z-1)(z-2)}{G}R-(z-1)^2\left(\frac{z}{z-1}t^2+\frac{1}{G^2}\right)=0. \tag{A45}$$

For $z\to\infty$, one recovers (Sec. II)

$$R(G)=t^2G+\frac{1}{G}. \tag{A46}$$

APPENDIX B: DETAILS OF THE MONTE CARLO ALGORITHM

In this Appendix, we first sketch the derivation of some of the formulas in Sec. VI.A.1, and show the equivalence of the Hirsch-Fye approach with the Blanckenbeckler, Scalapino, and Sugar algorithm. We also provide some guidance for the QMC programs provided with this article. Finally, details are given on the numerical implementation of the self-consistency condition.

1. Some derivations

Equation (139) for the discretized partition function can be established by making use of the following identity:

$$Tr_{c_i^+,c_i}\{e^{-\Sigma_{ij}c_i^+A_{ij}c_j}e^{-\Sigma_{ij}c_i^+B_{ij}c_j}e^{-\Sigma_{ij}c_i^+C_{ij}c_j}\}$$
$$\equiv\det[1+e^{-A}e^{-B}e^{-C}], \tag{B1}$$

and of its generalization to more than three matrices. Equation (B1) is easily derived using the rules of Gaussian integration for Grassmann variables, and a very instructive elementary derivation can be found in (Hirsch, 1985). The equivalence of $\det\mathcal{O}_{s_1,\ldots,s_L}$ with the Blanckenbeckler, Scalapino, and Sugar formula Eq. (139) can then be shown by Gaussian elimination (replacing successively the first row of $\mathcal{O}$ by multiples of rows $L,L-1,\ldots,1$, $\{\mathcal{O}_{1i}\}_{i=1,\ldots,L}\to\{\mathcal{O}_{1i}-B_LB_{L-1}\cdots B_{L-k+1}\times\mathcal{O}_{L-k+1,i}\}_{i=1,\ldots,L}$ for $k=0,1,\ldots,L-1$).

The identity $g^{\Delta\tau}_{s_1,\ldots,s_L} = \mathcal{O}^{-1}_{s_1,\ldots,s_L}$ is easily established in a similar way. It is quite useful to consider the simple example of a 3×3 matrix (of *matrices* B_i), for which we explicitly write down the inverse.

$$\mathcal{O}=\begin{pmatrix} 1 & 0 & B_3 \\ -B_1 & 1 & 0 \\ 0 & -B_2 & 1 \end{pmatrix}, \tag{B2}$$

$$\mathcal{O}^{-1}=\begin{pmatrix} \{1+B_3B_2B_1\}^{-1} & -B_3B_2\{1+B_1B_3B_2\}^{-1} & -B_3\{1+B_2B_1B_3\}^{-1} \\ B_1\{1+B_3B_2B_1\}^{-1} & \{1+B_1B_3B_2\}^{-1} & -B_1B_3\{1+B_2B_1B_3\}^{-1} \\ B_2B_1\{1+B_3B_2B_1\}^{-1} & B_2\{1+B_1B_3B_2\}^{-1} & \{1+B_2B_1B_3\}^{-1} \end{pmatrix}. \tag{B3}$$

The reader will easily be able to verify Eq. (B3) and to generalize it for arbitrary L. Manifestly, Eq. (B3) reproduces Eq. (140).

To derive the Dyson equation it is useful to consider the matrix $\mathcal{O}\exp(-V)$ with the $Ln_s\times Ln_s$ matrix

$$e^{-\tilde{V}}_{s_1,\ldots,s_L}=\begin{pmatrix} e^{-V(s_1)} & \cdot & \cdot & 0 \\ \cdot & e^{-V(s_2)} & \cdot & \cdot \\ \cdot & \cdot & \cdot & \cdot \\ 0 & \cdot & \cdot & e^{-V(s_L)} \end{pmatrix}; \tag{B4}$$

$\mathcal{O}\exp(-\tilde{V})$ is therefore a matrix which depends on $(s_1,\ldots,s_L)$ only in the space- and time-diagonal elements

$$\mathcal{O}_{s_1,\ldots,s_L}e^{-\tilde{V}}_{s_1,\ldots,s_L}-\mathcal{O}_{s'_1,\ldots,s'_L}e^{-\tilde{V}}_{s'_1,\ldots,s'_L}=e^{-\tilde{V}}_{s_1,\ldots,s_L}-e^{-\tilde{V}}_{s'_1,\ldots,s'_L}. \tag{B5}$$

Abbreviating $g \equiv g_{s_1,\ldots,s_L}$ and $g' \equiv g_{s'_1,\ldots,s'_L}$, etc., and using $\mathcal{O}=g^{-1}$, it is very easy to see that Eq. (B5) leads to $\exp(V'-V)g'-g=g[\exp(V'-V)-1]g'$, which is equivalent to Eq. (125).

2. Numerical implementation of the QMC and Gray code enumeration

As described in the main body of the paper, the Monte Carlo procedure consists of two independent parts (single impurity problem, self-consistency). This structure is mirrored in the setup of our numerical program, which consists of two parts: LISAQMC.F and LISASELF.F. The programs communicate with each other via files that contain the current values of $G(\tau_i)$ and $\mathcal{G}_0(\tau_i)$.

In the program LISAQMC.F, the different parts of the algorithm are distributed over a few subroutines, in a way explained in the following table:

function	purpose	Equation
DETRAT	calculate determinant ratio	Eq. (131)
INITIAL	initialize ($\mathcal{G}_0^{\Delta\tau}(\tau)\rightarrow\mathcal{O}^{-1}_{0,\ldots,0}(\tau,\tau')$)	–
RECORD	perform fast update	Eq. (130)
UPDATE	compute $G^{\Delta\tau}_{s_1,\ldots,s_L}$ from $\mathcal{G}_0^{\Delta\tau}$	Eq. (128)

Besides the Monte Carlo update, the program LISAQMC.F also allows one to compute physical Green's functions by *complete enumeration* using the Gray code. In this method, *all* possible configurations of Ising spins are visited in an order in which every configuration of spins $(s_1,\ldots,s_L)$ differs from the following one $(s'_1,\ldots,s'_L)$ in a single index only ($s_i = s'_i$, except for a single value of i). More precisely, the configurations are enumerated by flipping the spin s_i with the largest possible value of i, provided that this flip does not yield a previously visited configuration. As an example, let us give the first steps of a Gray code enumeration for L=5:

Gray code	standard
+ + + + +	+ + + + +
+ + + + −	+ + + + −
+ + + − −	+ + + − +
+ + + − +	+ + + − −
+ + − − +	+ + − + +
+ + − − −	+ + − + −
+ + − + −	+ + − − +
+ + − + +	+ + − − −
⋮	⋮

(B6)

This algorithm can be simply programmed (cf. Press *et al.*, 1991). By doing this, we can again compute the Green's function $G^{\Delta\tau}_{s_1,\ldots,s'_k,\ldots,s_L}$ from $G^{\Delta\tau}_{s_1,\ldots,s_k,\ldots,s_L}$ by the fast update RECORD [in $O(L^2)$ steps], rather than having to compute it from $\mathcal{G}_0^{\Delta\tau}$ in $O(L^3)$ steps (using UPDATE). Naturally, the averages must now be computed by including the determinant in the statistical weight. Furthermore, the normalization needs also be calculated. Further details can be found in the program LISAQMC.F.

Both the Monte Carlo and the exact enumeration include checks to avoid loss of precision. In the Monte Carlo algorithm, this is done from time to time by confronting the result of subroutine UPDATE with the single spin-flip updates. In the exact enumeration calculation, the precision can be evaluated simply by restarting the Gray code with an initial spin configuration $(s_1,\ldots,s_L)$ different from (1,...,1).

Finally, we briefly discuss the discretization error in $\Delta\tau$ which is introduced by the Trotter breakup. Let us first

note the remarkable fact that besides this error—i.e., the passage from Z [Eq. (116)] to $Z^{\Delta\tau}$ [Eq. (120)]—*no* other systematic error is introduced. Due to the cyclic nature of the fermion trace

$$\mathrm{Tr}\,\exp(-\tau\mathscr{H}_0)\exp(-\tau\mathscr{H}_1)$$
$$=\mathrm{Tr}\,\exp(-\tau\mathscr{H}_0/2)\exp(-\tau\mathscr{H}_1)\exp(-\tau\mathscr{H}_0/2), \quad \text{(B7)}$$

Eq. (120) can be obtained from Eq. (116) using the third-order approximation in $\Delta\tau$:

$$e^{-\Delta\tau(\mathscr{H}_0+\mathscr{H}_1)}=e^{-\Delta\tau\mathscr{H}_0/2}e^{-\Delta\tau\mathscr{H}_1}e^{-\Delta\tau\mathscr{H}_0/2}+O(\Delta\tau^3), \quad \text{(B8)}$$

which results in an $O(\Delta\tau^2)$ discretization error for $Z^{\Delta\tau}=Z+O(\Delta\tau^2)$. An important point is that in order to keep the systematic errors introduced by the Trotter breakup under control, one should not use a value of the argument that is too large for the exponential in Eq. (119). As a working rule one may use $\Delta\tau U/2<1$, but this depends of course on the quantity considered.

Regarding the Green's function, it has been established that the error committed when solving the Anderson impurity model with the Hirsch-Fye algorithm is also of order $\Delta\tau^2$ (Fye, 1986). In the LISA context (i.e., with the additional complication of the self-consistency condition), this observation still appears to hold empirically (see, e.g., the inset of Fig. 14).

3. Numerical implementation of the self-consistency condition

As indicated in the main text, the Fourier transform of the discretized $G^{\Delta\tau}(\tau)$ is not calculated by a straightforward fast Fourier transform. Rather, it is an interpolation of $G(\tau)$ which is Fourier transformed. In the program FOURIER, a (natural) spline interpolation

$$G^{\mathrm{interpol}}(\tau)=\alpha_i+\beta_i(\tau-\tau_i)+\gamma_i(\tau-\tau_i)^2+\delta_i(\tau-\tau_i)^3,$$
$$\tau_i<\tau<\tau_{i+1}, \quad \text{(B9)}$$

is computed. The coefficients $\alpha_i,\beta_i,\gamma_i,\delta_i$ are analytically calculated from the $G^{\Delta\tau}(\tau_i)$ such that $G^{\mathrm{interpol}}(\tau)$ is a twice continuously differentiable function (cf. Stoer and Bulirsch, 1980). From $G^{\mathrm{interpol}}(\tau)$ it is a simple matter to calculate the piecewise integral $\int_{-\beta}^{\beta}d\tau G^{\mathrm{interpol}}(\tau)\exp(i\tau\omega_n)$, which yields $G(i\omega_n)$. Explicit formulas can be found in the subroutine FOURIER.

APPENDIX C: DETAILS OF THE EXACT DIAGONALIZATION ALGORITHM

In this appendix, we assemble a few details on the exact diagonalization algorithms and make contact with the programs LISADIAG.F and LISALANC.F. Both programs split up into three main parts, of which the first and the third are identical.

(i) The construction of $\mathscr{H}$ (or of the nonzero elements of the matrix) is achieved by the subroutine BUILDBASIS, which constructs the vectors $|i\rangle$ defined in Eq. (143), for each of the sectors $(n^{\uparrow},n^{\downarrow})$ at a time. After construction of the Hilbert space, the Hamiltonian is built with the subroutines ADAG and A, which allow the computing of the vectors $a_j^{+}|i\rangle$ and $a_j|i\rangle$. In the exact diagonalization program, the matrix $\mathscr{H}$ is then diagonalized exactly (subroutine DIAG), using the QL algorithm (Stoer and Bulirsch, 1980). For reasons of simplicity, the eigenvectors (which are later needed for the calculation of Green's functions) are then dumped onto file storage.

In the Lanczos procedure, the ground-state eigenvalues for *all* sectors are calculated by diagonalizing $\mathscr{H}$ in an (approximately) invariant subspace spanned by vectors $\mathscr{H}^n|p_0\rangle$, $n=0,\ldots,n_L$. The power of the Lanczos algorithm stems from the fact that usually a small number of vectors ($n_L\sim100$, largely independent of the dimension of $\mathscr{H}$) allows an extremely precise computation of the ground-state eigenvalue and eigenvector—cf. Lin and Gubernatis (1993) for a practical introduction to the Lanczos method, and Golub and Van Loan (1983) for a thorough discussion. The diagonalization of $\mathscr{H}$, restricted to the indicated subspace, is again performed using the QL algorithm. This first Lanczos procedure is coded in the subroutine FINDGROUNDSTATE1. A simple iterative scheme (vector iteration) then verifies (in the routine FINDGROUNDSTATE), that the ground state has indeed been found to machine precision.

(ii) The calculation of the Green's function is done in a straightforward manner in the case of the exact diagonalization algorithm: to calculate $\langle i|d^{+}|j\rangle$, the corresponding vectors are fetched from disk storage and computed. In the case of the Lanczos procedure, the vector $d^{+}|\mathrm{g.s.}\rangle$ is initially formed, where $|\mathrm{g.s.}\rangle$ is the overall ground state of the Hamiltonian (the lowest of the sector-wise ground states computed being FINDGROUNDSTATE1). The procedure has to be generalized in the case of a ground-state degeneracy (several sectors with the same ground-state eigenvalue). The Green's function can then be calculated from a *second* Lanczos procedure, with initial vector $|p_0\rangle=d^{+}|gs\rangle$ (cf. Haydock *et al.*, 1975). It is straightforward to determine the parameters of the continuous fractions Eq. (146):

$$a_i^{\alpha}=\langle p_i^{\alpha}|H|p_i^{\alpha}\rangle, \quad b_i^{\alpha 2}=\frac{\langle p_i^{\alpha}|p_i^{\alpha}\rangle}{\langle p_{i-1}^{\alpha}|p_{i-1}^{\alpha}\rangle}, \quad \text{(C1)}$$

where $\alpha=\rangle,\langle$ and $|p_0^{>}\rangle=d^{\dagger}|\mathrm{g.s.}\rangle$, $|p_0^{<}\rangle=d|\mathrm{g.s.}\rangle$ and

$$|p_{i+1}^{\alpha}\rangle=H|p_i^{\alpha}\rangle-a_i^{\alpha}|p_i^{\alpha}\rangle-b_i^{\alpha 2}|f_{i-1}^{\alpha}\rangle \quad \text{(C2)}$$

and $b_0^{\alpha}=0$. The construction of the $|p_i^{\alpha}\rangle$ is done in the subroutine LANCZOS. The evaluation of the continued fractions is programmed in the subroutine COMPUTEGREEN. Again, care has to be taken in the case of a degenerate ground state.

(iii) After computing the Green's function, we are able to iterate once through the self-consistency loop. The projection of the "new" bath Green's function $\mathscr{G}_0\rightarrow\mathscr{G}_0^{ns}$ can be easily assembled from a routine, CALCG0, which evaluates $\mathscr{G}_0^{ns}$ for a given set of parameters $V,\tilde{\epsilon}$, another one, ENERGY, which calculates the mismatch between $\mathscr{G}_0^{ns}$ and $\mathscr{G}_0$, and a minimization rou-

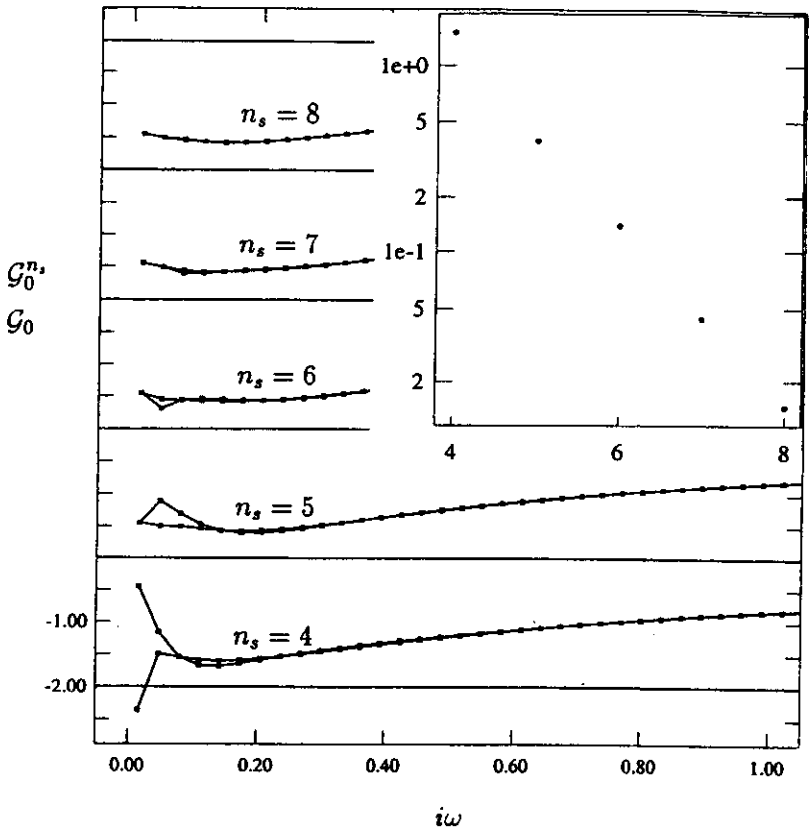

FIG. 87. Effective bath Green's functions $\mathcal{G}_0$ and $\mathcal{G}_0^{n_s}$ at self-consistency for the half-filled Hubbard model at $U=3D/\sqrt{2}$, $\beta D/\sqrt{2}=200$ for $n_s=4,\ldots,8$. Curves labeled $n_s=4,\ldots,6$ are for the exact diagonalization algorithm at finite temperature β. The curves at $n_s=7$ and 8 were obtained by the Lanczos algorithm, in which β only serves as a discretization parameter defining the grid of imaginary frequencies. The inset shows the maximum difference between $\mathcal{G}_0$ and $\mathcal{G}_0^{n_s}$ as a function of n_s (note the semilogarithmic scale).

tine, (conjugate-gradient routine MINIMIZE), which determines the optimal function $\mathcal{G}_0^{n_s}$.

In Fig. 87, we give an example of the comparison between $\mathcal{G}_0^{n_s}(i\omega)$ and $\mathcal{G}_0(i\omega)$, again for the half-filled Hubbard model at $U/t=3$ for $n_s=3,\ldots,8$ and at $\beta D\sqrt{2}=200$. Naturally, the agreement between the two quantities is the least acceptable at *small* frequencies, closest to the real axis. However, at larger frequencies, $\mathcal{G}_0^{n_s}$ and $\mathcal{G}_0$ agree for all intents and purposes. For example, at $\omega=0.1$, the two solutions differ by less than 10^{-5}, and there is virtually *no* detectable dependence on n_s. The precision obtained is thus quite spectacular. The mismatch between $\mathcal{G}_0$ and $\mathcal{G}_0^{n_s}$ decreases nicely by a constant factor as n_s is incremented by one, as shown in the inset of the figure. This scaling of the "discretization" error with the number of sites is an empirical fact, but a highly plausible one: In increasing the number of sites, the Hilbert space of the Hamiltonian increases exponentially, and there is a much larger number of basis vectors, of which the function $\mathcal{G}_0^{n_s}$ can be constructed. This scaling would not be observed if the positions of the conduction electrons were taken fixed.

It is very interesting to compare the full diagonalization algorithm with the Lanczos procedure, and the interesting reader is invited to perform such a comparison. The full diagonalization program contains an option which allows computing zero-temperature Green's functions (and other response functions), which (should) agree to machine precision with the ones of the Lanczos algorithm. The zero-temperature Green's functions, and other response functions may however appreciably differ from the (self-consistent) results at very small finite temperatures. This is as it should be, and translates the importance of low-temperature scales, for example, in the vicinity of the Mott transition. Notice that most of the low-temperature variability is brought in through the self-consistency condition: at a *given* $\mathcal{G}_0^{n_s}$, the calculated Green's functions almost coincide, but are driven apart under repeated iterations. As was mentioned in several places throughout the article, the impurity model is usually uncritical, and the critical effects are brought in by the lattice, i.e., by the self-consistency condition.

APPENDIX D: ACCESS TO FORTRAN PROGRAMS

The programs described in this section may be obtained by ANONYMOUS FTP, or in the WWW.

To access the programs by ftp, you should log on to ftp.lps.ens.fr. Register as "anonymous," and give your complete electronic address as the password. You should first retrieve a file called HOW-TO-GET-SOFTWARE, which will inform you about the availability of codes. This file also points you to the necessary auxiliary files and provides further information. Suppose your username is username@usernode.univ.edu. To retrieve the above file (and any other), you should proceed as follows:

ftp ftp.lps.ens.fr
Username: anonymous
Password: username@usernode.univ.edu
cd pub/users/lisa
ls
get HOW-TO-GET-SOFTWARE

The WWW access is via http://www.lps.ens.fr/~krauth

A short synopsis of the available programs is given in the following table:

Program	Purpose	Section
QMCEXAMPLE.F	small example by Blanckenbecler, Scalapino, and $\mathcal{G}^{-1}$, Hirsch-Fye algorithm	VI.A.1.e
LISAQMC.F	Hirsch-Fye algorithm	VI.A.1.c
LISASELF.F	Fourier transforms $\tau \rightarrow i\omega$, self-consistency	VI.A.1.d
LISADIAG.F	exact diagonalization, finite temperature	VI.A.2. C
LISALANC.F	Lanczos algorithm (zero temperature)	VI.A.2. C
LISAIPT0.F	iterated perturbation theory approximation (zero temperature)	VI.B.2
LISAIPT.F	iterated perturbation theory approximation (finite temperature)	VI.B.2

REFERENCES

[Preprint numbers refer to the archives cond-mat@babbage.sissa.it]

Abramowitz, M., and I. A. Stegun, 1972, *Handbook of Mathematical Functions* (Dover, New York).

Abrikosov, A. A., L. P. Gorkov, and I. E. Dzialoshinski, 1965, *Methods of Quantum Field Theory in Statistical Physics* (Pergamon, Elmsford, New York).

Affleck, I., and A. W. W. Ludwig, 1991, Nucl. Phys. B **352**, 849; **360**, 641.

Anders, F. B., 1995, Preprint No. cond-mat/9502020 (unpublished).

Anderson, P. W., 1961, Phys. Rev. **124**, 41.

Anderson, P. W., 1970, J. Phys. C **3**, 2439.

Anderson, P. W., G. Yuval, and D. R. Hamann, 1970, Phys. Rev. B **1**, 4464.

Andrei, N., K. Furuya, and J. H. Lowenstein, 1983, Rev. Mod. Phys. **55**, 331.

Anisimov, V. I., J. Zaanen, and O. K. Andersen, 1991, Phys. Rev. B **44**, 943.

Appelbaum, J. A., and D. R. Penn, 1969, Phys. Rev. **188**, 874.

Balatsky, A. V., and E. Abrahams, 1992, Phys. Rev. B **45**, 13125.

Bang, Y., C. Castellani, M. Grilli, G. Kotliar, R. Raimondi, and Z. Wang, 1992, Int. J. Mod. Phys. **6**, 531.

Beni, G., P. Pincus, and J. Kanamori, 1974, Phys. Rev. B **10**, 1896.

Berezinskii, V. L., 1974, JETP Lett. **20**, 287.

Bhatt, R. N., and D. S. Fisher, 1992, Phys. Rev. Lett. **68**, 3072.

Bickers, N. E., 1987, Rev. Mod. Phys. **59**, 845.

Blankenbecler, R., D. J. Scalapino, and R. L. Sugar, 1981, Phys. Rev D **24**, 2278.

Brandt, U., and C. Mielsch, 1989, Z. Phys. **75**, 365.

Brandt, U., and C. Mielsch, 1990, Z. Phys. **79**, 295.

Brandt, U., and C. Mielsch, 1991, Z. Phys. **82**, 37.

Brandt, U., and R. Schmidt, 1986, Z. Phys. **63**, 45.

Brandt, U., and R. Schmidt, 1987, Z. Phys. **67**, 43.

Brandt, U., and M. P. Urbanek, 1992, Z. Phys. **89**, 297.

Brinkman, W. F., and T. M. Rice, 1970, Phys. Rev. B **2**, 4302.

Bucher, B., Z. Schlesinger, P. C. Canfield, and Z. Fisk, 1994, Phys. Rev. Lett. **72**, 522.

Burley, D. M., 1972, in *Phase Transitions and Critical Phenomena*, edited by C. Domb and M. Green (Academic, New York), Vol. II.

Caffarel, M., and W. Krauth, 1994, Phys. Rev. Lett. **72**, 1545, and unpublished.

Cardy, J. L., 1981, J. Phys. A **14**, 1407.

Carter, S. A., T. F. Rosenbaum, J. M. Honig, and J. Spalek, 1992, Phys. Rev. Lett. **67**, 3440.

Carter, S. A., T. F. Rosenbaum, P. Metcalf, J. M. Honig, and J. Spalek, 1993, Phys. Rev. B **48**, 16841.

Castellani, C., C. DiCastro, D. Feinberg, and J. Ranninger, 1979, Phys. Rev. Lett. **43**, 1957.

Castellani, C., M. Grilli, and G. Kotliar, 1991, Phys. Rev. B **43**, 8000.

Castellani, C., G. Kotliar, R. Raimondi, M. Grilli, Z. Wang, and M. Rozenberg, 1992, Phys. Rev. Lett. **69**, 2009.

Castellani, C., C. R. Natoli, and J. Ranninger, 1978, Phys. Rev. B **18**, 4945.

Cava, R. J., B. Batlogg, J. J. Krajewski, R. Farrow, L. W. Rupp, A. E. White, K. Short, W. F. Peck, and T. Kometani, 1988, Nature **332**, 814.

Chakravarty, S., and J. Hirsch, 1982, Phys. Rev. B **25**, 3273.

Chen, 1994, Phys. Rev. Lett. **73**, 1982.

Ciuchi, S., F. de Pasquale, and D. Feinberg, 1995, Europhys. Lett. **30**, 151.

Ciuchi, S., F. de Pasquale, C. Masciovecchio, and D. Feinberg, 1993, Europhys. Lett. **24**, 575.

Clarke D. G., T. Giamarchi, and B. Shraiman, 1993, Phys. Rev. B **48**, 7070.

Coleman, P., 1987, Phys. Rev. B **35**, 5072.

Compte, C., and P. Nozieres, 1982, J. Phys. (Paris) **43**, 1069.

Costi, T. A. and A. C. Hewson, 1990, Physica B **163**, 179.

Cox, D. L., 1994, Physica B (to be published).

Cox, D. L., and A. E. Ruckenstein, 1993, Phys. Rev. Lett. **71**, 1613.
Cyrot, M., 1972, J. Phys. (Paris) **33**, 125.
Cyrot, M., and C. Lyon-Caen, 1975, J. Phys. (Paris) **36**, 253.
Dagotto, E., 1994, Rev. Mod. Phys. **66**, 763.
de Dominicis, C., I. Kondor, and T. Temesvari, 1991, J. Phys. A **24**, L301.
Dobrosavljević, V., T. R. Kirkpatrick, and G. Kotliar, 1992, Phys. Rev. Lett. **69**, 1113.
Dobrosavljević, V., and G. Kotliar, 1993, Phys. Rev. Lett. **71**, 3218.
Dobrosavljević, V., and G. Kotliar, 1994, Phys. Rev. B **50**, 1430, and Acta Physica Polonica **85**, 21.
Doniach, S., 1977, Physica B **91**, 231.
Dworin, L., and A. Narath, 1970, Phys. Rev. Lett. **25**, 1287.
Economou, E. N., 1983, *Green's Functions in Quantum Physics* (Springer-Verlag, Berlin).
Edwards, D. M., 1993, J. Phys. Cond. Mat. **5**, 161.
Elliott, R. J., J. A. Krumhansl, and P. L. Leath, 1974, Rev. Mod. Phys. **46**, 465.
Emery, V., 1987, Phys. Rev. Lett. **58**, 2794.
Emery, V., and S. Kivelson, 1992, Phys. Rev. B **46**, 10812.
Emery, V., and S. Kivelson, 1993a, Physica C **209**, 597.
Emery, V., and S. Kivelson, 1993b, in *Strongly Correlated Electronic Materials*, edited by K. Bedell, Z. Wang, A. Balatzky and E. Abrahams (Addison-Wesley, Reading, MA).
Emery V., and S. Kivelson, 1995, unpublished.
Emery, V., S. Kivelson, and Q. Lin, 1990, Phys. Rev. Lett. **64**, 475.
Falicov, L. M., and J. C. Kimball, 1969, Phys. Rev. Lett. **22**, 997.
Fetter, A. L., and J. D. Walecka, 1971, *Quantum Theory of Many-Particle Systems* (McGraw-Hill, New York).
Finkelshtein, A. M., 1987, Sov. Phys. JETP **46**, 407.
Fisher, D. S., G. Kotliar, and G. Moeller, 1995, Phys. Rev. B **52**, 17112.
Fortin E., S. Fafard, and A. Mysyrowicz, 1993, Phys. Rev. Lett **70**, 3951.
Freericks, J. K., 1993a, Phys. Rev. B **47**, 9263.
Freericks, J. K., 1993b, Phys. Rev. B **48**, 14797.
Freericks, J. K., 1993c, Phys. Rev. B **48**, 3881.
Freericks, J. K., 1994, Phys. Rev. B **50**, 403.
Freericks, J. K., and M. Jarrell, 1994a, Phys. Rev. B **50**, 6939.
Freericks, J. K., and M. Jarrell, 1994b, in *Computer Simulations in Condensed Matter Physics*, edited by D. P. Landau, K. K. Mon, and H.-B. Schüttler (Springer, Berlin).
Freericks, J. K., and M. Jarrell, 1995a, Phys. Rev. Lett. **74**, 186.
Freericks, J. K., and M. Jarrell, 1995b, Phys. Rev. Lett. **75**, 2570.
Freericks, J. K., M. Jarrell, and D. J. Scalapino, 1993, Phys. Rev. B **48**, 6302.
Freericks, J. K., M. Jarrell, and D. J. Scalapino, 1994, Europhys. Lett. **25**, 37.
Freericks, J. K., and D. J. Scalapino, 1994, Phys. Rev. B **49**, 6368.
Fresard, R., and P. Wölfle, 1992, Int. J. Mod. Phys. B **6**, 685; **6**, 3087(E).
Frota, H. O., and L. N. Oliveira, 1986, Phys. Rev. B **33**, 7871.
Fu, C., and S. Doniach, 1994, Phys. Rev. B **49**, 2219.
Fu, C., and S. Doniach, 1995, Phys. Rev. B **51**, 17 439.
Fujimori, A., I. Hase, H. Namatame, Y. Fujishima, Y. Tokura, H. Eisaki, S. Uchida, K. Takegahara, and F. M. F. de Groot, 1992, Phys. Rev. Lett. **69**, 1796.
Fujimori, A., F. Minami, and S. Sugano, 1984, Phys. Rev. B **29**, 5225.
Fujimori, A., *et al.*, 1992, Phys. Rev. B **46**, 9841.
Furukawa, N., 1994, J. Phys. Soc. Jpn. **63**, 3214.
Furukawa, N., 1995, unpublished.
Furukawa, N., 1995a, J. Phys. Soc. Jpn. **64**, 2754.
Furukawa, N., 1995b, in *Proceedings of the 17th Taniguchi International Conference*, edited by (Springer Verlag, Berlin).
Furukawa, N., 1995c, J. Phys. Soc. Jpn. **64**, 2734.
Furukawa, N., 1995d, J. Phys. Soc. Jpn. **64**, 3164.
Furukawa, N. and M. Imada, 1993, Physica B **186-188**, 931.
Fye, R. M., 1986, Phys. Rev. B **33**, 6271.
Gagliano, E. R., E. Dagotto, A. Mereo, and F. C. Alcaraz, 1986, Phys. Rev. B **34**, 1677.
Georges, A., and G. Kotliar, 1992, Phys. Rev. B **45**, 6479.
Georges, A., G. Kotliar, and W. Krauth, 1993, Z. Phys. B **92**, 313.
Georges, A., G. Kotliar, and Q. Si, 1992, Int. J. Mod. Phys. B **6**, 705.
Georges, A., and W. Krauth, 1992, Phys. Rev. Lett. **69**, 1240.
Georges, A., and W. Krauth, 1993, Phys. Rev. B **48**, 7167.
Georges, A. and A. Sengupta, 1995, Phys. Rev. Lett. **74**, 2808.
Georges, A., and J. S. Yedidia, 1991, Phys. Rev. B 43, 3475.
Golub, G. H., and C. F. Van Loan, 1983, *Matrix Computations* (Baltimore University Press, Baltimore, MD).
Goodenough, J. B., 1968, Phys. Rev. **171**, 466.
Grilli, M., and G. Kotliar, 1990, Phys. Rev. Lett. **64**, 1170.
Gros, C., 1994, Phys. Rev. B **50**, 7295.
Gros, C., W. Wenzel, R. Valenti, G. Hülsenbeck, and J. Stolze, 1994, Europhys. Lett. **27**, 299.
Gubernatis, J. E., M. Jarrell, R. N. Silver, D. S. Sivia, 1991, Phys. Rev. B **44**, 6011.
Gubernatis, J. E., T. C. Olson, D. J. Scalapino, and R. L. Sugar, 1986, J. Stat. Phys. **43**, 831.
Gunnarson, O., and K. Schönhammer, 1983a, Phys. Rev. Lett. **50**, 604.
Gunnarson, O., and K. Schönhammer, 1983b, Phys. Rev. B **28**, 4315.
Gutzwiller, M. C., 1965, Phys. Rev. **137**, A1726.
Haldane, F. D. M., 1978a, Phys. Rev. Lett. **40**, 416 (Ph.D thesis, Univ. of Cambridge).
Haldane, F. D. M., 1978b, J Phys. C **11**, 5015.
Halvorsen, E., G. S. Uhrig, and G. Czycholl, 1994, Z. Phys. B **94**, 291.
Haydock, R., 1985, *The Recursion Method and Its Applications* (Springer-Verlag, Heidelberg).
Haydock, R., V. Heine, and M. J. Kelly, 1975, J. Phys. C **8**, 2591.
Held, K., M. Ulmke, and D. Volhardt, 1995, Preprint No. cond-mat/9505147.
Hewson, A. C., 1993, *The Kondo Problem to Heavy Fermions*, Cambridge Studies in Magnetism Vol. 2 (Cambridge University Press, Cambridge, England).
Hirsch, J. E., 1983, Phys. Rev. B **28**, 4059.
Hirsch, J. E., 1985, Phys. Rev. B **31**, 4403.
Hirsch, J. E., 1988, Phys. Rev. B **38**, 12 023.
Hirsch, J. E., and E. Fradkin, 1982, Phys. Rev. Lett. **49**, 402.
Hirsch, J. E., and E. Fradkin, 1983, Phys. Rev. B **27**, 4302.
Hirsch, J. E., and R. M. Fye, 1986, Phys. Rev. Lett. **56**, 2521.
Holstein, T., 1959, Ann. Phys. (N.Y.) **8**, 325.
Hong, J., and H. Y. Kee, 1995a, Phys. Rev. B **52**, 2415.
Hong, J., and H. Y. Kee, 1995b, Europhys. Lett. (to be published).

Hubbard, J., 1964, Proc. Roy. Soc. (London) A **281**, 401.
Hubbard, J., 1979, Phys. Rev. B **19**, 2626.
Hüfner, S., 1994, Adv. Phys. **43**, 183.
Hülsenbeck, G., and F. Stephan, 1994, Z. Phys. B **94**, 281.
Hwang, H. Y., S. W. Cheong, P. G. Radaelli, M. Morezio, and B. Batlogg, 1995, Phys. Rev. Lett. **75**, 914.
Iga, F., T. Nishiguchi, N. Shirakawa, K. Murata, Y. Nishihara, T. Ishii, Y. Uwatoko, and G. Oomi, 1995, Bull. Electrotechn. Lab. **59**, 459.
Imada, M., 1994, J. Phys. Soc. Jpn. **63**, 3059.
Ingersent, K., B. A. Jones, and J. W. Wilkins, 1992, Phys. Rev. Lett. **69**, 2594.
Inoue, I. H., I. Hase, Y. Aiura, A. Fujimori, Y. Haruyama, T. Maruyama, and Y. Nishihara, 1995, Phys. Rev. Lett. **74**, 2539, and private communication.
Jaccarino, V. G., K. Wertheim, J. H. Wernick, L. R. Walker, and S. Arajs, 1967, Phys. Rev. **160**, 476.
Janiš, V., 1986, Czech. J. Phys. B **36**, 1107.
Janiš, V., 1989, Phys. Rev. B **40**, 11331.
Janiš, V., 1991, Z. Phys. B **83**, 227.
Janiš, V., 1993, J. Phys Cond. Matter **5**, L425.
Janiš, V., 1994, Phys. Rev. B **49**, 1612.
Janiš, V., M. Ulmke, and D. Vollhardt, 1993, Europhys. Lett. **24**, 287.
Janiš, V., and D. Vollhardt, 1992a, Int. J. Mod. Phys. B **6**, 731.
Janiš, V., and D. Vollhardt, 1992b, Phys. Rev. B **46**, 15712.
Jarrell, M., 1992, Phys. Rev. Lett. **69**, 168.
Jarrell, M., 1995, Phys. Rev. B **51**, 7429.
Jarrell, M., H. Akhlaghpour, and Th. Pruschke, 1993a, Phys. Rev. Lett. **70**, 1670.
Jarrell, M., H. Akhlaghpour, and Th. Pruschke, 1993b, in *Quantum Monte Carlo Methods in Condensed Matter Physics*, edited by M. Suzuki (World Scientific, Singapore).
Jarrell, M., J. K. Freericks, and Th. Pruschke, 1995, Phys. Rev. B **51**, 11704.
Jarrell, M., and J. Gubernatis, 1996, Phys. Rep. (in press).
Jarrell, M., and T. Pruschke, 1993a, Z. Phys. B **90**, 187.
Jarrell, M., and T. Pruschke, 1993b, Phys. Rev. B **49**, 1458.
Jin, S., T. H. Tiefel, M. McCormack, R. A. Fastnacht, R. Ramesh, and L. H. Chen, 1994, Science **264**, 413.
Jones, B., C. M. Varma, and J. W. Wilkins, 1988, Phys. Rev. Lett. **61**, 125.
Kajueter, H., and G. Kotliar, 1995, Preprint No. cond-mat/9509152.
Kajueter, H., G. Kotliar, and G. Moeller, 1995, unpublished.
Kakehashi, Y., 1992, Phys. Rev. B **45**, 7196.
Kanamori, J., 1959, J. Phys. Chem. Solids **10**, 87.
Kane, C. L., P. A. Lee, and N. Read, 1989, Phys. Rev. B **39**, 6880.
Kee, H. Y., and J. Hong, 1995, Preprint No. cond-mat/9508096.
Kennedy, T., and E. H. Lieb, 1986, Physica **138A**, 320.
Khomskii, D., 1979, Sov. Phys. Usp. **22**, 879.
Khurana, A., 1990, Phys. Rev. Lett. **64**, 1990.
Kikuchi, R., 1951, Phys. Rev. **81**, 988.
Kim, C. I., Y. Kuramoto, and T. Kasoya, 1990, J. Phys. Soc. Jpn. **59**, 2414.
Kohn, W., 1964, Phys. Rev. **133**, A171.
Kohno, H., and K. Yamada, 1988, Prog. Theor. Fiz. **80**, 623.
Kopietz, P., 1994, J. Phys. Cond. Matter **6**, 4885; Physica B **194-196**, 271.
Kotliar, G., 1993a, in *Correlated Electron Systems*, edited by V. J. Emery (World Scientific, Singapore).
Kotliar, G., 1993b, in *Strongly Correlated Electronic Materials*, edited by K. Bedell, Z. Wang, D. Meltzer, A. Balatzky, and E. Abrahams (Adison-Wesley, Reading, MA).
Kotliar, G., 1994, in *Strongly Interacting Fermions and High T_c Superconductivity*, edited by B. Doucot and J. Zinn-Justin (Elsevier Science, New York).
Kotliar, G., and J. Liu, 1988, Phys. Rev. Lett. **61**, 1784.
Kotliar, G., and M. Rozenberg, 1995, in *The Hubbard Model*, Proceedings of the Conference on the Mathematics and Physics of the Hubbard model (San Sebastian), edited by D. Bareswyl, D. Campbell, J. Carmelo, and F. Guinea (Plenum, New York).
Kotliar, G., and A. Ruckenstein, 1986, Phys. Rev. Lett. **57**, 1362.
Kotliar, G., and Q. Si, 1993, Physica Scripta **49**, 165.
Kotliar, G., and Q. Si, 1995, Preprint No. cond-mat/9508112.
Krishnamurthy, H. R., J. W. Wilkins, and K. G. Wilson, 1980, Phys. Rev. B **21**, 1003, 1044.
Kugel, K., and D. Khomskii, 1973, Sov. Phys. JETP **37**, 725.
Kugel, K., and D. Khomskii, 1982, Sov. Phys. Usp. **25**, 231.
Kuramoto, Y., 1985, Springer Series in Sol. State. Science Vol. 62, pp. 152–162.
Kuramoto, Y. and T. Watanabe, 1987, Physica B **148**, 80.
Kuwamoto, H., J. M. Honig, and J. Appel, 1980, Phys. Rev. B **22**, 2626.
Kutzelnigg, W., 1982, J. Chem. Phys. **77**, 3081.
Kutzelnigg, W., and S. Koch, 1983, J. Chem. Phys. **79**, 4315.
Laad, M., 1994, Phys. Rev. B **49**, 2327.
Lacroix, C., 1981, J. Phys. F **11**, 2389.
Laloux, L., 1995, private communication.
Laloux, L., A. Georges, and W. Krauth, 1994, Phys. Rev. B **50**, 3092.
Langer, W., M. Plischke, and D. Mattis, 1969, Phys. Rev. Lett. **23**, 1448.
Langreth, D., 1966, Phys. Rev. **150**, 516.
Lelievre, F., G. Misguich, and A. Georges, 1995, unpublished.
Li, Y. M., and d'Ambrumenil, 1992, Mod. Phys. Lett. B **6**, 1827.
Lieb, E. H., 1986, Physica **140A**, 240.
Lin, J. L., and J. P. Wolfe, 1993, Phys. Rev. Lett. **71**, 1222.
Lin, H. Q., and J. E. Gubernatis 1993, Comput. Phys. **7**, 400.
Luttinger, J. M., and J. C. Ward, 1960, Phys. Rev. **118**, 1417.
Majumdar, P., and H. R. Krishnamurthy, 1994, Phys. Rev. Lett. **73**, 1525.
Majumdar, P., and H. R. Krishnamurthy, 1995a, Phys. Rev. B **52**, R5479.
Majumdar, P., and H. R. Krishnamurthy, 1995b, Preprint No. cond-mat/9512151.
Maple, M. B., C. L. Seaman, D. A. Gajewski, Y. Dalichaouch, V. B. Barbetta, M. C. de Andrade, H. A. Mook, H. G. Lukefahr, O. O. Bernal, and D. E. MacLaughlin, 1994, J. Low Temp. Phys. **95**, 225.
Matsuura, A., Z. X. Shen, D. S. Dessau, C. H. Park, T. Thio, J. W. Bennett, and O. Jepsen, 1994, unpublished.
Mattheiss, L., F., 1994, J. Phys. Condens. Matter **6**, 6477.
McWhan, D. B., J. P. Remeika, T. M. Rice, W. F. Brinkman, J. P. Maita, and A. Menth, 1971, Phys. Rev. Lett. **27**, 941.
McWhan, D. B., A. Menth, J. P. Remeika, W. F. Brinkman, and T. M. Rice, 1973, Phys. Rev. B **7**, 1920.
Menge, B., and E. Müller-Hartmann, 1991, Z. Phys. B **82**, 237.
Metzner, W., 1989, Z. Phys. B **77**, 253.
Metzner, W., 1991, Phys. Rev. B **43**, 8549.
Metzner, W., and D. Vollhardt, 1989, Phys. Rev. Lett. **62**, 324.

Mezard, M., G. Parisi, and M. A. Virasoro, 1987, *Spin Glass Theory and Beyond* (World Scientific, Singapore).
Micnas, R., J. Ranninger, and S. Robaszkiewicz, 1990, Rev. Mod. Phys. **62**, 113.
Millis, A., P. B. Littlewood, and B. I. Shraiman, 1995, Phys. Rev. Lett. **74**, 5144.
Millis, A., B. I. Shraiman, and R. Mueller, 1995, Preprint No. cond-mat/9507084.
Milovanović, M., S. Sachdev, and R. N. Bhatt, 1989, Phys. Rev. Lett. **63**, 82.
Möbius A., 1989, Phys. Rev. B **40**, 4194.
Möbius A., 1990, Z. Phys. B **80**, 213.
Moeller, G., V. Dobrosavljević, and A. Ruckenstein, 1995, unpublished.
Moeller, G., A. Ruckenstein, and S. Schmitt-Rink, 1992, Phys. Rev. B **46**, 7427.
Moeller, G., Q. Si, G. Kotliar, M. J. Rozenberg, and D. S. Fisher, 1995, Phys. Rev. Lett., **74**, 2082.
Möller, B., and Wölfle, P., 1993, Phys. Rev. B **48**, 10320.
Morita, T., 1990, J. Stat. Phys. **59**, 819.
Mott, N. F., 1949, Proc. Phys. Soc. A **62**, 416.
Mott, N. F., 1956, Can. J. Phys. **34**, 1356.
Mott, N. F., 1961, Philos. Mag. **6**, 287.
Mott, N. F., 1990, *Metal Insulator Transitions* (Taylor and Francis, London).
Müller-Hartmann, E., 1984, Z Phys. B **57**, 281.
Müller-Hartmann, E., 1989a, Z Phys. B **74**, 507.
Müller-Hartmann, E., 1989b, Z. Phys. B **76**, 211.
Müller-Hartmann, E., 1989c, Int. J. Mod. Phys. B **3**, 2169.
Newns, D. M., and N. Read, 1987, Adv. Phys. **36**, 799.
Nishino, T., and K. Ueda, 1993, Phys. Rev. B **47**, 12451.
Nozieres P., and A. Blandin, 1980, J. Phys. (Paris) **41**, 193.
Nozieres P., and S. Schmitt-Rink, 1985, J. Low. Temp. Phys. **59**, 195.
Ohkawa, F. J., 1991a, J. Phys. Soc. Jpn. **60**, 3218.
Ohkawa, F. J., 1991b, Prog. Theor. Phys. (Suppl.) **106**, 95.
Okimoto, Y., T. Katsufuji, T. Ishikawa, A. Urushibara, T. Arima, and Y. Tokura, 1995, Phys. Rev. Lett. **75**, 109.
Onsager, L., 1936, J. Am. Chem. Soc. **58**, 1486.
Park, C. H., Z. X. Shen, A. G. Loeser, D. S. Dessau, D. G. Mandrus, A. Migliori, J. Sarrao, and Z. K. Fisk, 1994, unpublished.
Park, J. H., L. H. Tjeng, J. W. Allen, P. Metcalf, and C. T. Chen, 1994, AT&T Bell Labs Report.
Pei, S., J. D. Jorgensen, B. Dabrowski, D. G. Hinks, D. R. Richards, A. W. Mitchell, J. M. Newsam, S. K. Sinha, D. Vaknin, and A. J. Jacobson, 1990, Phys. Rev. B **41**, 4126.
Penn, D. R., 1966, Phys. Rev. **142**, 350.
Press, W. H., S. A. Teukolsky, W. T. Vetterling, and B. P. Flannery, 1991, *Numerical Recipes*, 2nd ed. (Cambridge University Press), Cambridge, England.
Pruschke, T., D. L. Cox, and M. Jarrell, 1993a, Europhys. Lett. **21**, 593.
Pruschke, T., D. L. Cox, and M. Jarrell, 1993b, Phys. Rev. B **47**, 3553.
Pruschke, T., and N. Grewe, 1989, Z. Phys. B **74**, 439.
Pruschke, T., and M. Jarrell, 1994, Physica B **199**, 217.
Pruschke, T., M. Jarrell, and J. K. Freericks, 1995, Adv. Phys. **44**, 187.
Qin, Q., and G. Czycholl, 1994, Physica B **199-200**, 219.
Quirt, J. D., and J. R. Marko, 1972, Phys. Rev. Lett. **26**, 318.
Raimondi, R., and C. Castellani, 1993, Phys. Rev. B **48**, 11453.
Randeria, M., J. Duan, and L. Shieh, 1989, Phys. Rev. Lett. **62**, 981.
Randeria, M., J. Duan, and L. Shieh, 1990, Phys. Rev. B **41**, 327.
Randeria, M., N. Trivedi, A. Moreo, and R. T. Scalettar, 1992, Phys. Rev. Lett. **69**, 2001.
Read, N., D. M. Newns, and S. Doniach, 1984, Phys. Rev. B **30**, 3841.
Rice, T. M., and K. Ueda, Phys. Rev. B **34**, 6420.
Rozenberg, M. J., 1995, Phys. Rev. B **52**, 7369.
Rozenberg, M. J., I. H. Inoue, H. Makino, F. Iga, and Y. Nishihara, 1996, Preprint No. cond-mat/9603051.
Rozenberg, M. J., G. Kotliar, and H. Kajueter, 1995, Preprint No. cond-mat/9509182.
Rozenberg, M. J., G. Kotliar, H. Kajueter, G. A. Thomas, D. H. Rapkine, J. M. Honig, and P. Metcalf, 1995, Phys. Rev. Lett. **75**, 105.
Rozenberg, M. J., G. Kotliar, and X. Y. Zhang, 1994, Phys. Rev. B **49**, 10181.
Rozenberg, M. J., G. Moeller, and G. Kotliar, 1994, Mod. Phys. Lett. B **8**, 535.
Rozenberg, M., X. Y. Zhang, and G. Kotliar, 1992, Phys. Rev. Lett. **69**, 1236.
Sachdev, S., and A. Georges, 1995, Phys. Rev. B **52**, 9520.
Sachdev, S., N. Read, and R. Oppermann, 1995, Phys. Rev. B **52**, 10 286.
Saitoh, T., A. E. Bocquet, T. Mizokawa, H. Namatame, A. Fujimori, M. Abbate, Y. Takeda, and M. Takano, 1995, Phys. Rev. B **51**, 13942.
Sakai, O. and Y. Kuramoto, 1994, Solid State Commun. **89**, 307.
Sakai, O., Y. Shimizu, and T. Kasuya, 1989, J. Phys. Soc. Jpn. **58**, 162.
Salomaa, M., 1981, Solid State Commun. **38**, 815.
Sanchez, J. M., F. Ducastelle, and D. Gratias, 1984, Physica **128A**, 334.
Santoro, G., M. Airoldi, S. Sorella, and E. Tosatti, 1993, Phys. Rev. B **47**, 16216.
Sarma, D. D., S. Barman, H. Kajueter, and G. Kotliar, 1995, unpublished.
Saso, T., and M. Itoh, 1995, Preprint No. cond-mat/9512094.
Schiller, A., and Ingersent, K., 1995, unpublished.
Schlesinger, Z., Z. Fisk, H. T. Zhang, M. B. Maple, J. F. DiTusa, and G. Aeppli, 1993, Phys. Rev. Lett. **71**, 1748.
Schmalian, J., P. Lombardo, M. Avignon, and K. H. Bennemann, 1995, Physica B (to be published).
Schotte, K. D., and U. Schotte, 1969, Phys. Rev. **182**, 479; Phys. Rev. **185**, 509.
Schrieffer, J. R., and P. A. Wolf, 1966, Phys. Rev. **149**, 491.
Schwartz, L., and E. Siggia, 1972, Phys. Rev. B **5**, 383.
Schweitzer, H., and G. Czycholl, 1989, Solid State Commun. **69**, 171.
Schweitzer, H., and G. Czycholl, 1990a, Z. Phys B **79**, 377.
Schweitzer, H., and G. Czycholl, 1990b, Solid State Commun. **74**, 735.
Schweitzer, H., and G. Czycholl, 1991a, Z. Phys B **83**, 93.
Schweitzer, H., and G. Czycholl, 1991b, Phys. Rev. Lett. **67**, 3724.
Sengupta, A. M., and A. Georges, 1995, Phys. Rev. B **52**, 10 295.
Shimizu, Y., and O. Sakai, 1995, J. Phys. Soc. Jpn. (to be published).

Si, Q., and G. Kotliar, 1993, Phys. Rev. Lett. **70**, 3143; Phys. Rev. B **48**, 13 881.
Si, Q., K. Kotliar, and A. Georges, 1992, Phys. Rev. B **46**, 1261.
Si, Q., M. J. Rozenberg, K. Kotliar, and A. E. Ruckenstein, 1994, Phys. Rev. Lett. **72**, 2761.
Sire, C., C. M. Varma, and H. R. Krishnamurthy, 1993, Phys. Rev. B **48**, 13833.
Slater, J. C., 1951, Phys. Rev. **82**, 538.
Spalek, J., A. Datta, and J. M. Honig, 1987, Phys. Rev. Lett. **59**, 728.
Spalek, J., 1990, J. Sol. St. Chem. **88**, 70.
Strack, R., and D. Vollhardt, 1992, Phys. Rev. B **46**, 13852.
Stoer, J., and Bulirsch, R., 1980, *Introduction to Numerical Analysis* (Springer-Verlag, New York).
Sugiyama, G., S. E. Koonin, 1986, Ann. Phys. **168**, 1.
Sun, S. J., M. F. Yang, and T. M. Hong, 1993, Phys. Rev. B **48**, 16127.
Suzuki, M., 1988, J. Stat. Phys. **53**, 483, and references therein.
Theumann, A., 1969, Phys. Rev. **178**, 978.
Thomas, G. A., D. H. Rapkine, S. A. Carter, A. J. Millis, T. F. Rosenbaum, P. Metcalf, and D. F. Honig, 1994, Phys. Rev. Lett. **73**, 1529.
Thomas, G. A., D. H. Rapkine, S. A. Carter, T. F. Rosenbaum, P. Metcalf, and D. F. Honig, 1994, J. Low Temp. Phys. **95**, 33.
Thouless, D. J., P. W. Anderson, and R. G. Palmer, 1977, Philos. Mag. **35**, 593.
Tokura, Y., Y. Taguchi, Y. Okada, Y. Fujishima, T. Arima, K. Kumagai, and Y. Iye, 1993, Phys. Rev. Lett. **70**, 2126.
Tokura, Y., A. Urushibara, Y. Morimoto, T. Arima, A. Asamitsu, G. Kido, and N. Furukawa, 1994, J. Phys. Soc. Jpn. **63**, 3931.
Torrance, J. B., P. Lacorre, and A. I. Nazzal, 1992, Phys. Rev. B **45**, 8209.
Toulouse, G., 1970, Phys. Rev. B **2**, 270.
Treglia, G., F. Ducastelle, and D. Spanjaard, 1980, Phys. Rev. B **21**, 3729.
Tsuda, N., K. Nasu, A. Yanase, and K. Siratori, 1991, *Electronic Conduction in Oxides*, Springer Series in Solid State Sciences Vol. 94 (Springer-Verlag, Berlin).
Tsvelick, A. M., and P. B. Wiegmann, 1983, Adv. Phys. **32**, 453.
Turov, E., and V. Grebenikov, 1988, Physica B **149**, 150.
Uhrig, R. S., and R. Vlaming, 1993, Phys. Rev. Lett. **71**, 271.
Ulmke, M., 1995, Preprint No. cond-mat/9512044.
Ulmke M., V. Janiš, and D. Vollhardt, 1995, Phys. Rev. B **51**, 10 411.
Urushibara, A., Y. Moritome, T. Arima, A. Asamitso, G. Kido, and Y. Tokura, 1995, Phys. Rev. B **51**, 14103.
Valenti, R., and C. Gros, 1993, Z. Phys. B **90**, 161.
van Dongen, P. G. J., 1991a, Mod. Phys. Lett. B **5**, 861.
van Dongen, P. G. J., 1991b, Phys. Rev. Lett. **67**, 757.
van Dongen, P. G. J., 1992, Phys. Rev. B **45**, 2267.
van Dongen, P. G. J., 1994, Phys. Rev. B **49**, 7904.
van Dongen, P. G. J., 1995, Phys. Rev. Lett. **74**, 182.
van Dongen, P. G. J., and D. Vollhardt, 1990, Phys. Rev. Lett. **65**, 1663.
Varma, C. M., 1976, Rev. Mod. Phys. **48**, 219.
Varma, C. M., and T. Giamarchi, 1994, in "Strongly Interacting Fermions and High-T_c Superconductivity," edited by B. Doucot and J. Zinn-Justin (Elsevier, New York).
Varma, C. M., S. Schmitt-Rink, and E. Abrahams, 1987, Solid State Commun. **62**, 681.
Vekič M., J. W. Cannon, D. J. Scalapino, R. T. Scalettar, and R. L. Sugar, 1995, Phys. Rev. Lett. **74**, 2367.
Vidberg, H. J., and J. W. Serene, 1977, J. Low Temp. Phys. **29**, 179.
Visscher, P. B., 1974, Phys. Rev. B **10**, 943.
Vlaming, R., G. S. Uhrig, and D. Vollhardt, 1992, J. Phys. C **4**, 7773.
Vlaming, R., and D. Vollhardt, 1992, Phys. Rev. B **45**, 4637.
Vollhardt, D., 1984, Rev. Mod. Phys. **56**, 99.
Vollhardt, D., 1991, Physica B **169**, 277.
Vollhardt, D., 1993, in *Correlated Electron Systems*, edited by V. J. Emery (World Scientific, Singapore).
Vollhardt, D., 1994, in Proceedings of the Enrico Fermi School, Course CXXI, edited by Broglia and Schrieffer (North-Holland, Amsterdam).
von Helmolt, R., J. Wecker, B. Holzapfel, L. Schultz, and K. Samwer, 1993, Phys. Rev. Lett. **71**, 2331.
Wang, S. Q., W. E. Evenson, and J. R. Schrieffer, 1969, Phys. Rev. Lett **23**, 92.
Wegner, F., 1976, Z. Phys. B **25**, 327.
White, J. A., 1992, Phys. Rev. B **45**, 1100.
White, S. R., D. J. Scalapino, R. L. Sugar, E. Y. Loh, J. E. Gubernatis, R. T. Scalettar, 1989, Phys. Rev. B **40**, 506.
White, S. R., R. L. Sugar, and R. T. Scalettar, 1988, Phys. Rev. B **38**, 11665.
Wilson, K. G., 1975, Rev. Mod. Phys. **47**, 773.
Withoff, D., and E. Fradkin, 1990, Phys. Rev. Lett. **64**, 1835.
Wolff, P. A., 1961, Phys. Rev. **124**, 1030.
Wortis, M., 1974, in *Phase Transitions and Critical Phenomena*, edited by C. Domb and M. Green (Academic, London), Vol. 3.
Yamada, K., 1975, Prog. Theor. Phys. **53**, 970.
Yokoyama, H., and H. Shiba, 1987, J. Phys. Soc. Jpn. **56**, 3582.
Yosida, K., and K. Yamada, 1970, Prog. Theor. Phys. **46**, 244.
Yosida, K., and K. Yamada, 1975, Prog. Theor. Phys. **53**, 1286.
Yu, C. C., and P. W. Anderson, 1984, Phys. Rev. B **29**, 6165.
Zaanen, J., and G. A. Sawatzky, 1987, Can. J. Phys. **65**, 1262.
Zaanen, J., and G. A. Sawatzky, 1990, Prog. Theor. Phys. (Suppl.) **101**, 231.
Zaanen, J., G. A. Sawatzky, and J. W. Allen, 1985, Phys. Rev. Lett. **55**, 418.
Zang, J., A. Bishop, and H. Roder, 1995, Preprint No. cond-mat/9507097.
Zhang, X. Y., M. J. Rozenberg, and G. Kotliar, 1993, Phys. Rev. Lett. **70**, 1666.
Zlatić, V., B. Horvatić, and D. Sokcević, 1985, Z. Phys. B **59**, 151.
Zlatić, V., and B. Horvatić, 1990, Solid State Commun. **75**, 263.